Rio de Janeiro, Rio de Janeiro

October 10, 2020

Numerical Simulations using COMSOL, of Superconducting Circuits for Quantum Information Processing

Arthur C. M. Rebello

Orientadores

João Paulo Sinnecker

Ivan S. Oliveira

Contents

List of Figures

Acknowledgement

I would like to think my coordinators João Paulo Sinnecker and Ivan S. Oliveira for sharing their enthusiasm and support during this work. My family for inconditional support. Furthermore I would like to think the institue, which I felt at all times welcomed in, Center of Brazilian Physics Research. I would also like to thank the Ministry of Science, Technology and Innovations. Furthermore I would like to thank PETROBRAS for sponsoring this incredibly fascinating field of research which is cavity quantum electrodynamics.

Abstract

This work is aimed at creating useful simulations to aid laboratory fabrication of superconducting qubits. First we make a description of the physics involved in superconducting qubit state preparation and control. Superconducting qubits are coupled and controlled via superconducting microwave transmission lines. Through the numerical simulation software COMSOL multiphysics, we aim at designing superconducting transmission lines, to attempt to gain insight on qubit cavity coupling. The interaction occurs via the vacuum state electric field E_0 of cavity with island of superconducting material placed in it. This island is connected to the rest of the circuit using Josephson Junctions. These special connections can be described as a quantum anharmonic oscillators. This kind of system is of special interest to Quantum Computing, as this serves as a scalable quantum chips.

Furthermore Josephson Junctions are incredibly rich objects, phenomenologically speaking. Having a wide range of applicability from academic research to industrial purposes. With emphasis on the known uses of Josephson Junctions such as highly sensitive metrology devices, rapid single flux quantum digital electronics and quantum-mechanical circuits. In the light of these significant applicabilities, the main purpose of this work is to decide if COMSOL Multiphysics is an appropriate tool to set a north for the creation of superconducting qubits. Since this is a preliminary study, we aim to bring to surface the underlying mechanisms that drive superconducting qubits. Therefore, we will simulate known Superconducting circuits, as opposed to making a hypothetical model.

A simulation is not the real experiment. If it was possible to recreate the experiment to its full extent, the experiment itself would turn obsolete. Thus the structure of this work begins by trying to elucidate the basic principles behind the overall physics processes. In the following chapter, we describe some possible simulation setups. We conclude by contrasting our results to the available experimental data.

1 Introduction

Quantum processors promise to complement the classical computer and revolutionize the now available computational power. Harnessing the power of quantum mechanics for computational purposes was first suggested in 1959, during a lecture at Caltech, by renowned physicist Richard P. Feynman [8]. He proposed the idea of manipulating individual atoms as the building blocks of a quantum processor. To Feynman, using classical physics to simulate quantum systems was not possible. Over half a century has passed and scientists were finally able to create a quantum computer capable of outperforming a classical one [1]. A huge milestone has been reached as the Noisy Intermediate-Scale Quantum era is now emerging. NISQ for short, it is known as the time when quantum processing relies on noisy processors, these will only be able to handle very specific tasks. Industrial giants, such as Google and IBM, are betting on superconducting circuits for scalable quantum processors.

Classical computers have changed the world we live in. They have been around for nearly a century, and scientists have pushed their computing power to fascinating limits. Both in the scalability of transistors in computer chips and in the sofistication of software. Classical processors have as a basic building block, a circuit element called transistor. Current flowing through the transistor codes for a 1 and its absence for 0. Transistors are still used to this day, furthermore it made viable modern computing by being the physical entity that represents the classical states of 0 and 1.

Transistors have been shrinking ever since they were invented in Bells lab 1947, resulting in enormous gains in computational power. In 1965, Gordon Moore wrote a paper describing how the number of transistors per processor chip would grow exponentially with time. Today Moore's law is near to its limit as transistors reach the atomic scale, challenging the continuous scalability of computational power in classical processors.

Regardless the size, the fundamental nature of quantum and classical information processing is different. The building block of the quantum processor is the qubit which is a general name for a quantum object with 2 distinct energy levels. Instead of the logical gates applied to classical bits, quantum bits are subjected to quantum interaction. This means operations which affect the state of the qubit, a quantum algorithm transforms the state of your qubit performing a series of reversible operations to it. Unlike the classical computer where the value stored indefinetly, in quantum computing the value of the qubits are not defined until they are measured, the measurement is an irreversible process therefore the calculation or experiment is over.

One major issue is having enough time to run the algorithms before the qubit simply changes its state. This could happen for various reasons, it can't be said enough how delicate this system is to any stray form of energy. While quantum objects such as europium ion dopants in yttrium orthosilicate have measurements of the ground-state hyperfine transition with coherence times of 6 hours [30], these are not suitable for qubits. These quantum states have long coherence due to how well they are shielded from the rest of the world. In this case the electrons measured are shielded by other electron shells. This means that entangling this quantum object to another, will be dificult, so scalling this system is not discussed. Instead it can be used for quantum information storage.

It is relevant to stress how extraordinary it is to imagine how far science has come, ever since Stern-Gerlach first measured a quantum fenomena on a bulk sample of ions [20], to the control of a single quantum object with extreme precision. The latter work earned the 2012 nobel prize award to both David J. Wineland (US-NIST) and Serge Haroche (College of France). Both scientists were able to control and individual quantum system, and exercise all quantum functionability. That means they were able to completly manipulate the quantum state of the object. The difference is Serge Heroche used a photon in a cavity [12] and David J. Wineland manipulation ions with lasers [29]. The frontier now is to have an ensemble of perfectly working qubits which promisses to serve as a "strong arm" for certain problems.

Quantum mechanics predicts entangling of quantum systems and the superposition of states. While classical bits are held in a fixed state as 0 or 1, qubits are prepared in a certain state which has a well defined evolution in time given by the Schrodinger Equation as long as it remains isolated from its environment. These properties are exploited by quantum algorithms to process information. Furthermore the information you can store in N entangled quantum bits is 2^N, which overcasts the information density growth on its classical 2N counterpart.

Peter Shor and Grover from $AT\&T$ Bell Labs, were pioneers in creating powerful quantum algorithms that could be used to solve problems of significant interest. In 1994 Peter Shor developed an algorithm for factoring large numbers [23]. In 1996, Grover created one for finding an item in a random list. A classical computer needs to check N/2 entries to have a 50% chance of finding item in a list with N items, Grover's algorithm reduces the steps to $O\sqrt{N}$ [10]. These, among other results showed how quantum computing could be a powerful tool and spurred the search for quantum systems that could be manipulated with extreme precision and scaled up to form quantum processors. Much speculation on whether it was possible to be done and weather the gains would be worth cost. Nonetheless Google was able to build a processor and run an algorithm which creates large reliable random numbers in record time. The Sycamore chip consisting of 53 working qubits was able to outperform the largest computer working today. It ran the algorithm significantly faster then the largest classical computer available today. According to Google [1] it is estimated that Google Cloud servers performing the same task with 0.1% fidelity using the SFA algorithm would cost 50 trillion core-hours and consume 1 petawatt hour of energy. To put this in perspective, it took 600 seconds to sample the circuit on the quantum processor 3 million times.

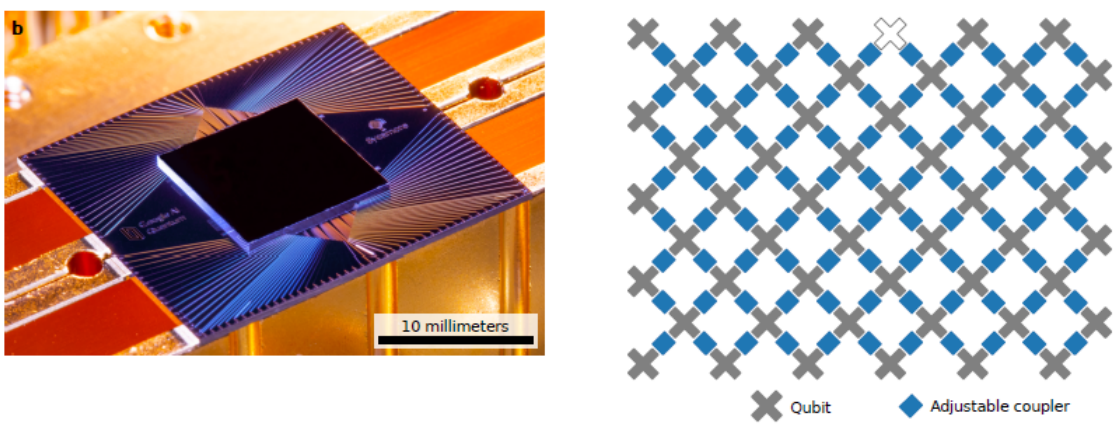

Figure 1: On the left Google's Sycamore processor and on the right a map of the qubits in the chip. Notice that the white colored qubit is faulty, there are 86 couplers and 53 working qubits.

In circuit quantum electrodynamics (cQED), microwave waveguides are used to prepare and manipulate quantum states. In other words, these circuits are a real life representation of the preparation of an arbitrary initial wave function which will be eventually subjected to unitary quantum operators. Quantum computing is the process of applying transformations to individual or multiple qubits. These operations inherently introduce error which is a major concern of modern research. Error naturally arises from the difficulty of the task at hand, which is the necessary isolation of the qubits from the environment to maintain coherent states. Furthermore, the qubit needs to be accessible in order to be manipulated and read, which contradicts the first necessity of isolating it. Therefore the great challenge in building a quantum computer is creating perfectly isolated accessible qubits. To put this into perspective, given a certain operation on a qubit has 99.9% accuracy, there will still be an error every one thousand calculations on average. Qubits need to be extremely coherent to make quantum information processing a viable resource, this is due to the large number of transformations they must withstand for quantum computing to be an effective tool. Quantum decoherence as the name suggests is when the phase difference between states is not well defined. Another way to interpret this process is the loss of information contained in a quantum system, naturally it is desired that information and energy are conserved during quantum information processing. Otherwise quantum information being processed would not be stable and it would dissipate. This is a major challenge for modern quantum computing.

This research aims to describe and simulate the behavior of superconducting waveguides, as well as the interaction with qubits placed within. This interaction is mediated through dipole-photon coupling. To understand this process we must look into superconducting qubits which involve superconductors and Josephson Junctions. Type I superconductors which are well described by the BCS theory, can be described by a macroscopic wave function. The superconducting properties are observed due to the formation of Cooper pairs. These are formed when electrons are at the lowest energy state, the fermion finds an opposite spin counterpart and joins it to form a bosonic pair. These electrons can be centimeters apart, and since all the pairs in a superconductor can be in the same state, they can all be described by a single wave function. This stands out as one of the few if not the only example of a macroscopic quantum object.

Josephson Junctions are nonlinear potential barriers obtained by separating superconductors with a non-superconducting potential barrier, or simply a gap in the order of 10 Angstrom. Josephson predicted that Cooper Pairs would tunnel from superconductor to the other, with no current applied. The dimensions of the superconducting chunks and barrier will define specific Josephson Inductance and capacitance. Manipulating these variables, it's possible to create an artificial atom. This is due to the nonlinear inductance which causes the energy levels accessible to the cooper pair to be nonlinear and harmonic. There are different ways to exploit these properties and different qubits can be created using Josephson Junctions. In essence there are 3 types, charge, phase and flux qubits.

The charge qubit is composed of a small superconducting island with on average 10^9 electrons separated from a much larger reservoir by a Josephson Junction. The state of this quantum bit is defined by the absence or presence of an extra Cooper pair in the island. This can be measured using a very sensitive electrometer such as a radio frequency single electron transistor. But also by placing this island in a cavity, it will disturb the cavity and this excitation can be measured in this manner. This was done by A. Wallraff et al. (2004), by coupling a resonator to a superconducting charge qubit via single photon interaction [28]. The cavity is fabricaded using a 24 mm strip of superconducting material capacitively coupled to an oscillating frequency of 6.044 GHz. The first step in our research aims to understand the physics involved which is presented in second chapter called Theoretical background. Next, on Chapter 3 we show the methodology used for the simulations through COMSOL Multiphysics. This is done by first simulating a transmission line, in order to create the cavity conditions seen in the experiment. Next we attempt to introduce methods that could potentially be used to simulate qubit cavity interaction. On chapter 4 we will discuss the results obtained through these simulations.

2 Theoretical background

This chapter summarizes the information necessary to understand the physics of superconducting qubits. First we will discuss the basic differences between classic and quantum computing. Next we will describe the physics behind superconductors and how it's possible to create artificial atoms from these materials.

2.1 Quantum Information Processing

In this section the goal is to condense the current state of quantum information processing. By stating the fundamental differences between classical and quantum computing, this discussion is aimed at situating the reader to go further into the fundamental building block of the quantum processor, the qubit.

2.1.1 Quantum Computing

Quantum computing is fundamentally different from classical. For a quantum processor to be called universal it must be able to implement a universal set of quantum gates. This translates to being able manipulate a binary quantum system completely. In 1981 Feynman predicted that a computer that could use this for computational purposes would outperform classical computers. At the third quarter of the year 2019, Google the information giant, has claimed to have demonstrated quantum supremacy[1] . They used superconducting quantum circuits to perform a calculation which presumably would take the IBM summit 10,000 years, The summit is the most powerful classical computer available today.

Quantum computing was not of broad interest until Shor's algorithm was created in 1994. Peter Shor discovered a way to use quantum interference to improve a known algorithm for factoring a large number [23]. Shor's algorithm made evident that quantum computers could have an impact on economy and in people's lives. As we know, cyber security is based on the difficulty of factoring large prime numbers. This sparked enthusiasm into the quantum computing field, and other applications followed, such as a $\sqrt{n}$ gain in finding a listing in an list containing n randomly ordered items. This was accomplished by Lov Grover with a quantum algorithm published in 1996 [10].

Another realistic advantage a quantum computer could have over a classical one is calculating quantum interaction between molecules. This could revolutionize biology and chemistry having an significant impact on drug development.

2.1.2 Quantum Annealing

In metallurgy annealling is the process of slow cooling metal. The bonds formed during the heating process are slowly cooled to organize themselves in the lowest energy state. The latter will maximize the strength of the alloy. However if there was to be an imperfection in the bulk material, it would mean that it did not reach the lowest energy state. Quantum Annealing works the same way. After a problem is mapped to fit the Ising Hamiltonian seen on Equation 1, it is ran on a quantum annealer. This process consists of addressing the initial wave function to physical qubits and allow them to evolve over some time and measure its final state. The system should evolve statistically to the lowest energy state more frequently then others. The lowest energy state then is translated to the optimization of the initial function.

$$H(\sigma) = -\mu \sum_{j=1}^{\infty} h_j \sigma_j - \sum_{i,j}^{\infty} J_{ij} \sigma_j \sigma_i \tag{1}$$

The Ising Model was essentially created to solve the problems of interacting spins. The first term is equivalent to the systems energy and the second corresponds to the energy of a spin's interaction with its immediate neighbor. Here h_j represents value of an external magnetic field. And J_{ij} is the strength of the interaction of two neighboring spins. The magnetic moment is given by μ.

Since the Ising Model is essentially an optimization problem, a wide range of problems can be adapted to fit this model. This turns out to be important as classical computers calculation times grow exponentially for minimization problems. Quantum computers's advantage is essentially in how information is processed. There is debate as to whether a quantum annealer is a universal quantum computer or not. It harnesses the natural evolution of a quantum state to map certain types of problems, such as optimization and sampling problems [5]. The most successful quantum annealing machines are created by D-Wave. Their machines have qubit networks described by the Ising model [5] seen in Equation 1.

2.1.3 Qubit candidates

To perform universal quantum operations, it is necessary to have a controllable two level quantum object. It is necessary to entangle an arbitrary number of qubits and create superposition of states to any proportion from 0 to 1 with a controllable relative phase. The most promising candidate systems which can be used to perform these operations are displayed in Figure 2. For example the electrons in atoms are trapped in potential wells with discrete energy levels. Successfully controlling transition of the electron within two energy levels makes it a candidate for a qubit [11].

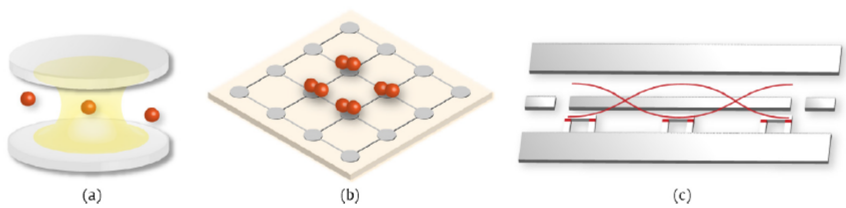

Table 1
Comparison between natural atoms and artificial atoms based on superconducting circuits and their interaction with quantized bosonic modes.

	Natural atoms		Artificial atoms
	Neutral atoms	Trapped ions	Superconducting qubits
Qubits	Atoms	Ions	Josephson-junction devices
Dimensions	$\sim 10^{-10}$ m	$\sim 10^{-10}$ m	$\sim 10^{-6}$ m
Energy gap	$\sim 10^{14}$ Hz (optical), GHz (hyperfine)	$\sim 10^{14}$ Hz (optical), GHz (hyperfine)	$\sim$1–10 GHz
Quantized bosonic modes	Photons	Collective vibration modes of ions (phonons)	*LC* circuits (photons), surface acoustic waves (phonons)
Frequency range	Microwave, optical	Microwave, optical	Microwave
Controls	Lasers	Lasers, electric/magnetic fields	Microwave pulses, voltages, currents
Components	Mirrors Optical and microwave cavities Optical fibers Beam-splitters	Electrodes Optical cavities, vibration modes Optical fibers Beam-splitters	Capacitors *LC* and transmission-line resonators, 3D cavities Transmission lines Hybrid couplers, Josephson mixers
Temperature	nK–μK	μK–mK	$\sim$10 mK
Advantages	Homogeneous (parameters set by nature)	Long coherence times	Strong and controllable coupling, tunable in situ, fabricated on chip

Figure 2: On top from left to right, (a) Neutral atoms, (b) Two dimensional Ion trap and (c) Superconducting qubits interacting with electric fields. On the bottom table of natural and artificial atoms that can be used as qubits. Adapted from Xiu Gu, et aliae. [11]

Atoms are good candidates for storing quantum information. Neutral atoms or ions can be isolated and controlled by either lasers or creating impurities in diamonds or Si. This can be used to perform quantum operations, naturally the parameters involved are predetermined by natural characteristics and can not be changed. Superconducting qubits however are labboratory engineered and can be seen as artificial atoms. The fabrication of these superconducting circuits requires state of the art technology and creating identical chips is a daunting task due to extreme precision necessary to do so.

Although trapped ions have particularly long coherence times which translate to less errors, they have a limit on how fast you can apply quantum gates to them [22]. Since this is a natural system there is no way around it. Superconducting circuits however are constantly evolving to meet the needs of quantum computation. The gate speed is about 1000 times greater than trapped ions and although they are still noisy and faulty circuits, improvements are constantly made. In Figure 3 the most prominent qubit candidates are compared. While natural systems have limited mobility in this graph, superconducting qubits are flexible and evolving towards the ideal qubit.

Low error and high calculation speed are the qualities scientists look for when searching for useful qubits. The quantum realm is in constant change, which makes the coherence time of a quantum state generally very short. Too short to perform calculations with. Scientists are constantly trying to make qubits that hold states for a long time and take very little time to manipulate. These aspects are sometimes defined by the fundamental nature of the system or engineered in the case of artificial atoms. Trapped ions naturally have slow calculation speed, and since this can not be changed these make bad candidates for quantum bits, superconducting qubits perform calculations about 1000 times faster, as can be seen in the graph in Figure 3.

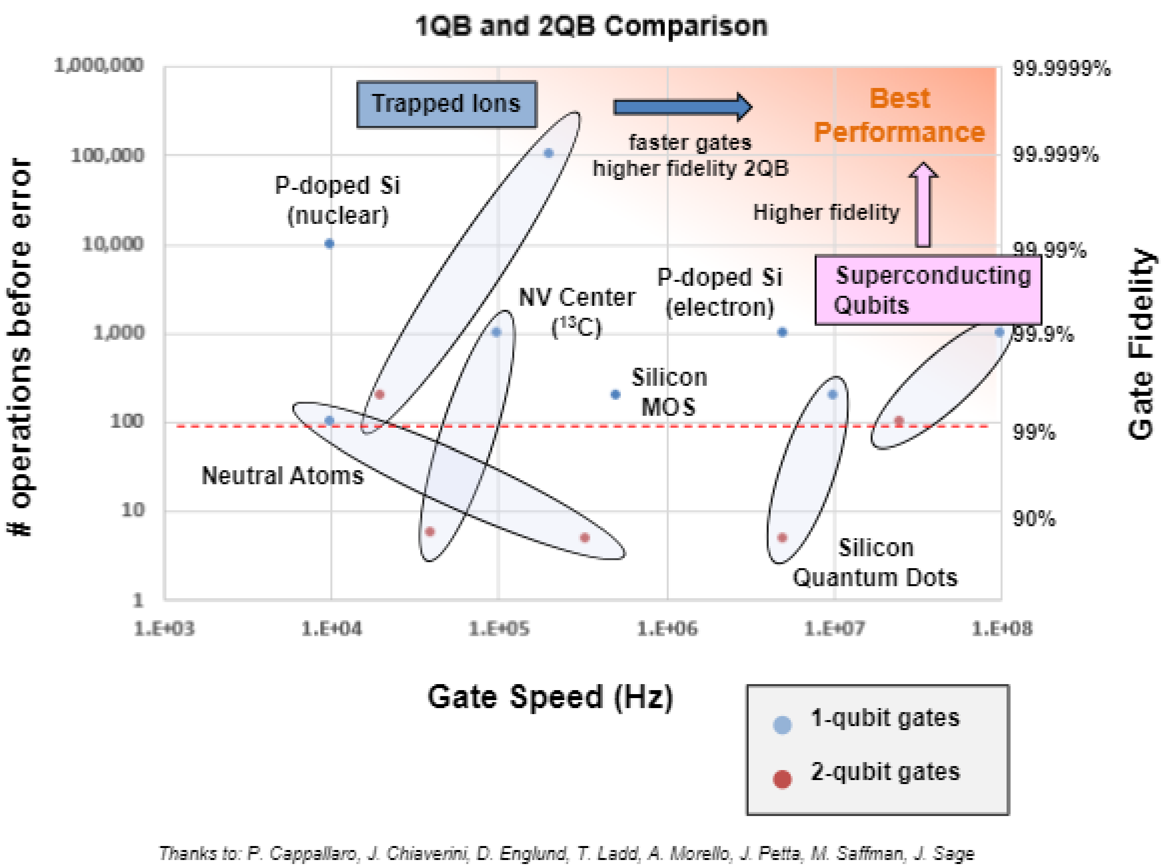

Figure 3: One and two qubit fidelity and gate speed. Image extracted from Live MIT xPRO Program: Quantum Computing Fundamentals lecture on August 26, 2019 [2]

2.1.4 Classical Gates

Classical computing began with an idealization by Alan Turing in 1936 [27]. The Turing Machine is abstract, it can be thought of as a tape with symbols on it. A device is attached to this tape, and is able to go forward or backwards reading the symbols and manipulating them according to preset rules that are decided prior to the reading. This opened way for the creation of classical algorithms and their physical implementation by the creation of the computer. The process of reading and analyzing the symbols on the tape is done by what is known as logical gates. Using a handful of specific one and two bit logical gates, one can implement any classical algorithm. This is known as an universal set of gates. Meaning they are able to exploit all degrees of freedom available for the particular method of calculation. The classical information processing is based on going from one state to the next. It will be shown in the quantum gates section that quantum states can hold more information, as they can be represented by different proportions of 1 and 0 and have a phase attribute.

A universal set of classical gates is described as a set of basic operations that can describe any arbitrary complex operation. For example, the set $F = \{AND, XOR\}$ is an universal set [15], thus combinations of those two gates can execute any classical computation. Certain sets of classical gates are more efficient for certain tasks, and computer chips have these gates in different proportions to optimize processing speed. On the right side of Figure 4 there are some examples of most common one and two bit classical gates. The truth table in Figure 4 shows the value of the bit before and after the applied gate. There is also a symbol used for electronic circuit representation.

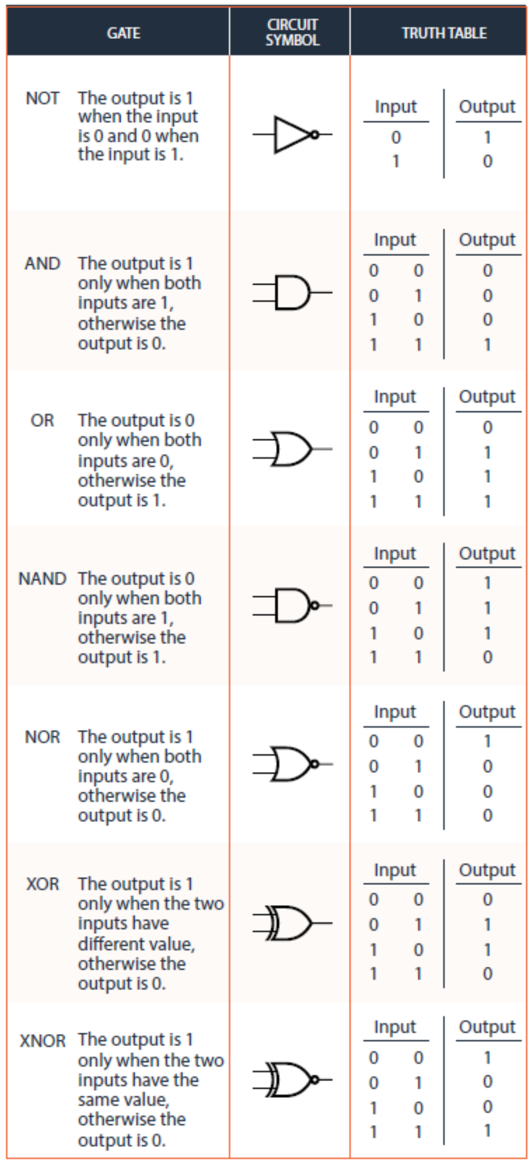

GATE		CIRCUIT SYMBOL	TRUTH TABLE Input	TRUTH TABLE Output
NOT	The output is 1 when the input is 0 and 0 when the input is 1.		0 1	1 0
AND	The output is 1 only when both inputs are 1, otherwise the output is 0.		0 0 0 1 1 0 1 1	0 0 0 1
OR	The output is 0 only when both inputs are 0, otherwise the output is 1.		0 0 0 1 1 0 1 1	0 1 1 1
NAND	The output is 0 only when both inputs are 1, otherwise the output is 1.		0 0 0 1 1 0 1 1	1 1 1 0
NOR	The output is 1 only when both inputs are 0, otherwise the output is 0.		0 0 0 1 1 0 1 1	1 0 0 0
XOR	The output is 1 only when the two inputs have different value, otherwise the output is 0.		0 0 0 1 1 0 1 1	0 1 1 0
XNOR	The output is 1 only when the two inputs have the same value, otherwise the output is 0.		0 0 0 1 1 0 1 1	1 0 0 1

Figure 4: Description of single and two bit classical gates. Image extracted and modified from P. Krantz, et al. [15]

2.1.5 Bloch Sphere Representation of States

The Bloch Sphere is used to describe all possible states of a two level quantum system. Notice the states are described using two variables. In this representation, each possible state is represented by a vector beginning at the origin reaching out to the surface if its a pure state and a point within the sphere for mixed states.

A Bloch vector can bex described by

$$\left|\psi(t)\right\rangle = \alpha\left|0\right\rangle + \beta\left|1\right\rangle = \cos\frac{\theta}{2}\left|0\right\rangle + \sin\frac{\theta}{2}\, e^{-i\phi}\left|1\right\rangle \tag{2}$$

Here α and β are complex numbers. As it can be seen in Figure 5, the north pole would be a classic 1 state and the south the 0 state. At the equator of the sphere the states 1 and 0 are superpositioned in equal amounts. If the vector is dragged up or down while bound to the ZY plane, this represents a shift in the amplitude of probability. Furthermore a rotation about the Z-axis represents a change in the gauge invariant phase.

By analyzing the density matrix $\rho = |\Psi\rangle\langle\Psi|$ it can be concluded that a pure state $|\Psi\rangle$ is given by

$$\rho = \frac{1}{2}(I + \vec{a}\cdot\vec{\sigma}) = \tag{3}$$

$$\frac{1}{2}\begin{bmatrix} 1 & 0 \\ 0 & 1 \end{bmatrix} + \frac{a_x}{2}\begin{bmatrix} 0 & 1 \\ 1 & 0 \end{bmatrix} + \frac{a_y}{2}\begin{bmatrix} 0 & -i \\ i & 0 \end{bmatrix} + \frac{a_z}{2}\begin{bmatrix} 1 & 0 \\ 0 & -1 \end{bmatrix} =$$

$$\frac{1}{2}\begin{bmatrix} 1+\cos\theta & \sin\theta\ e^{-i\phi} \\ \sin\theta\ e^{i\phi} & 1+\sin\theta \end{bmatrix} = \begin{bmatrix} \cos^2\frac{\theta}{2} & \cos\frac{\theta}{2}\sin\frac{\theta}{2}\ e^{-i\phi} \\ \cos\frac{\theta}{2}\sin\frac{\theta}{2}e^{i\phi} & \sin^2\frac{\theta}{2} \end{bmatrix} =$$

$$\begin{bmatrix} \alpha^2 & \alpha\beta^* \\ \alpha^*\beta & \beta^2 \end{bmatrix}$$

Here $\sigma = [\sigma_x, \sigma_y, \sigma_z]$ and $\vec{a} = (\sin\theta\cos\phi, \sin\theta\sin\phi, \cos\theta)$ is a Bloch vector in the unit sphere $\in \mathbb{R}^3$.

If $\vec{a}$ is unitary then ρ represents a pure state ψ and $Tr(\rho^2) = 1$. More generally, the Bloch sphere can be used to represent mixed sates, for which $|\vec{a}| < 1$; in this case, the Bloch vector terminates at points inside the unit sphere, and $0 \leq Tr(\rho^2) < 1$.

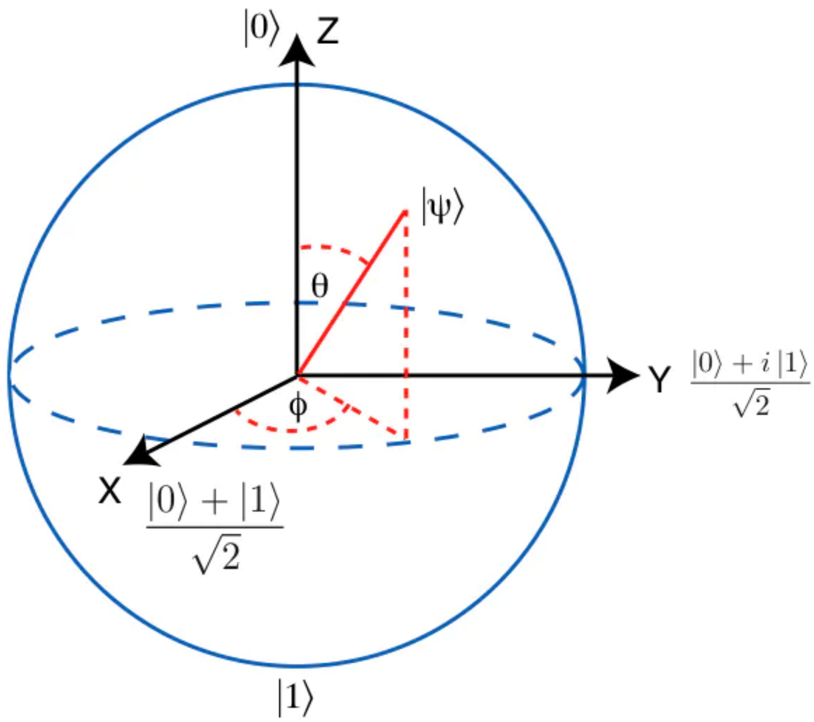

Figure 5: All possible states of a qubit can be represented on the Bloch sphere. At the north pole the 0 stat and on the south the 1 state. At the equator the states are perfectly balanced superposition of sates. Rotations about the Z axis a represented by a change in the relative phase. Bloch sphere courtesy of http://www.laborsciencenetwork.com

2.1.6 Quantum Gates

Different from quantum annealing, quantum gate based algorithms have more similarities to classical computing. This system relies on a sequence of operators being applied to one or more qubits. These operators apply reversible transformations to the Bloch vector. A universal quantum computer is one which can apply any desired rotation to the Bloch vector. Quantum gates implement changes to the state of qubits, which have states described by $\left|\psi(t)\right\rangle = \cos\frac{\theta}{2}\left|0\right\rangle + \sin\frac{\theta}{2}\, e^{-i\phi}\left|1\right\rangle$. Quantum gates apply changes in θ and ϕ. Since each gate is an operator it has a matrix representation, some examples can be seen on Figure 6.

A quantum algorithm is created by finding a useful sequence of quantum gates. In practice, performing quantum gates depends on the hardware available. Therefore for a quantum computer to be said universal, it needs to be able to apply a universal set of quantum gates to its qubits. This way it can process any quantum algorithm. For example, the following set is an universal set of quantum gates.

$$G = \{X, Y, Z, T, CNOT\} \tag{4}$$

These gates are defined in Figures 6 and 7, furthermore this is not a unique set. Other sets of gates may form a universal set. Particularly this is an important set for superconducting qubits. A superconducting quantum processor naturally has the X, Y, Z gates while the other necessary gates necessary to form a universal set can be created through combinations of the native gates, more information on this can be found in [15].

In Figure 6 the most common 1 bit quantum gates are shown. There is a circuit representation for quantum algorithms and a matrix representation which can be applied to states. As can be seen in the Bloch sphere representation, quantum gates in general are rotations about a certain axis. I will single out here the Hadamard gate which is used to set the qubit to a superposition of states. This is a clear example of how quantum computing is different from classic.

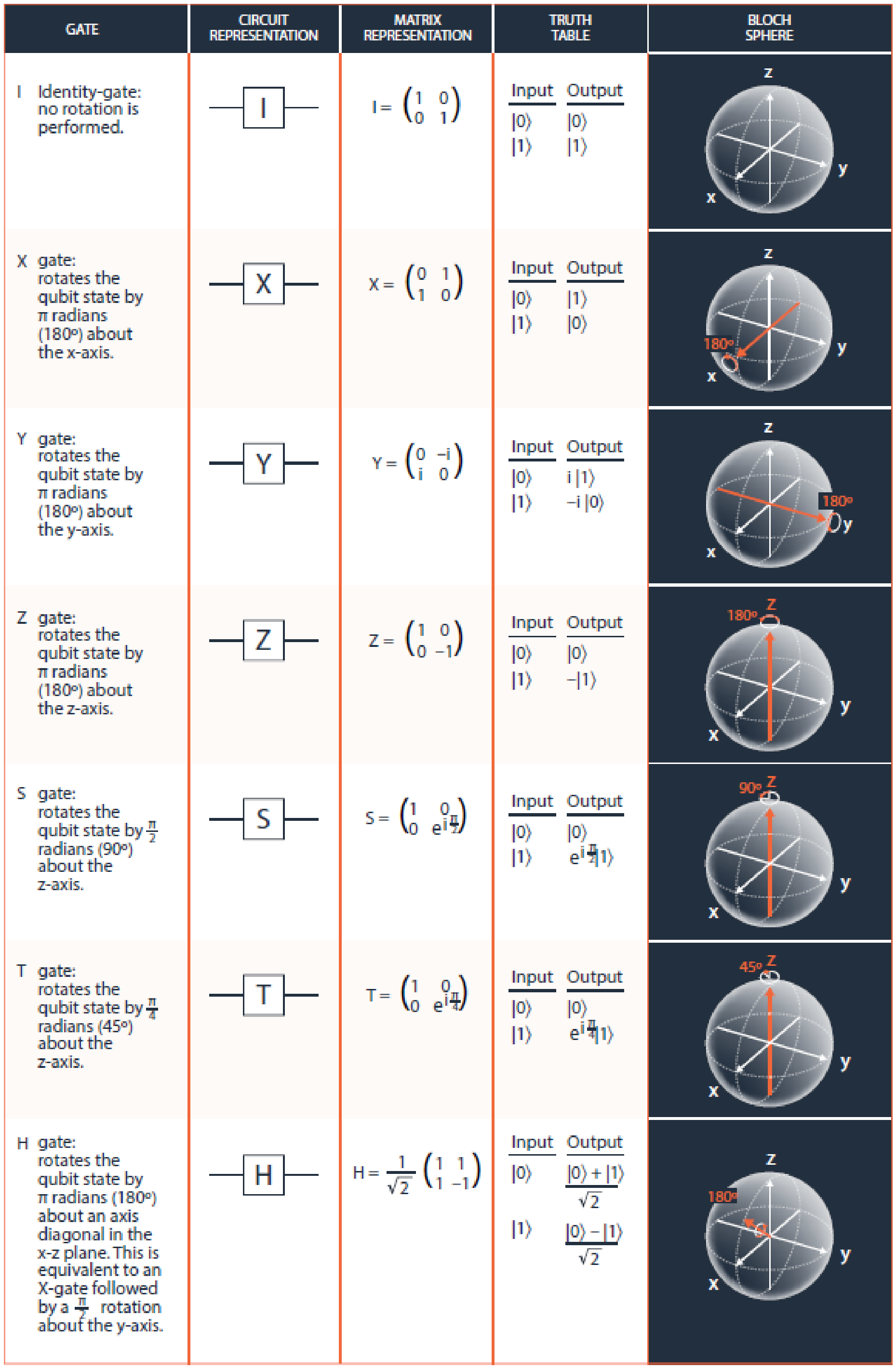

GATE	CIRCUIT REPRESENTATION	MATRIX REPRESENTATION	TRUTH TABLE	BLOCH SPHERE
I Identity-gate: no rotation is performed.	I	$I = \begin{pmatrix} 1 & 0 \\ 0 & 1 \end{pmatrix}$	Input / Output $\|0\rangle$ / $\|0\rangle$ $\|1\rangle$ / $\|1\rangle$	z, y, x
X gate: rotates the qubit state by π radians (180°) about the x-axis.	X	$X = \begin{pmatrix} 0 & 1 \\ 1 & 0 \end{pmatrix}$	Input / Output $\|0\rangle$ / $\|1\rangle$ $\|1\rangle$ / $\|0\rangle$	z, 180°, y, x
Y gate: rotates the qubit state by π radians (180°) about the y-axis.	Y	$Y = \begin{pmatrix} 0 & -i \\ i & 0 \end{pmatrix}$	Input / Output $\|0\rangle$ / $i\|1\rangle$ $\|1\rangle$ / $-i\|0\rangle$	z, 180°, y, x
Z gate: rotates the qubit state by π radians (180°) about the z-axis.	Z	$Z = \begin{pmatrix} 1 & 0 \\ 0 & -1 \end{pmatrix}$	Input / Output $\|0\rangle$ / $\|0\rangle$ $\|1\rangle$ / $-\|1\rangle$	180°, Z, y, x
S gate: rotates the qubit state by $\frac{\pi}{2}$ radians (90°) about the z-axis.	S	$S = \begin{pmatrix} 1 & 0 \\ 0 & e^{i\frac{\pi}{2}} \end{pmatrix}$	Input / Output $\|0\rangle$ / $\|0\rangle$ $\|1\rangle$ / $e^{i\frac{\pi}{2}}\|1\rangle$	90°, Z, y, x
T gate: rotates the qubit state by $\frac{\pi}{4}$ radians (45°) about the z-axis.	T	$T = \begin{pmatrix} 1 & 0 \\ 0 & e^{i\frac{\pi}{4}} \end{pmatrix}$	Input / Output $\|0\rangle$ / $\|0\rangle$ $\|1\rangle$ / $e^{i\frac{\pi}{4}}\|1\rangle$	45°, Z, y, x
H gate: rotates the qubit state by π radians (180°) about an axis diagonal in the x-z plane. This is equivalent to an X-gate followed by a $\frac{\pi}{2}$ rotation about the y-axis.	H	$H = \frac{1}{\sqrt{2}} \begin{pmatrix} 1 & 1 \\ 1 & -1 \end{pmatrix}$	Input / Output $\|0\rangle$ / $\frac{\|0\rangle + \|1\rangle}{\sqrt{2}}$ $\|1\rangle$ / $\frac{\|0\rangle - \|1\rangle}{\sqrt{2}}$	z, 180°, y, x

Figure 6: Description of single bit Quantum gates. Image extracted from P. Krantz, et al. [15]

In Figure 7 there are representations of 2 qubit gates.Two qubit gates perform an operation on one qubit based on the state of another. The control qubit which is represented as a black dot in Figure 7 is measured and in the case of the CNOT gate, the X-gate is applied to the the second qubit according to the state of a control qubit.

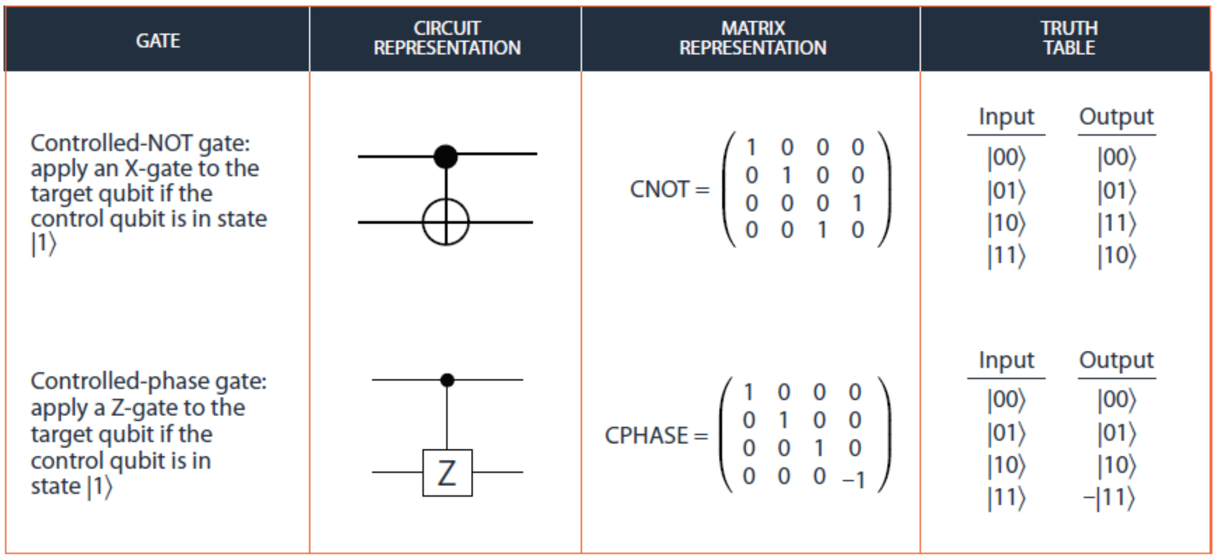

GATE	CIRCUIT REPRESENTATION	MATRIX REPRESENTATION	TRUTH TABLE
Controlled-NOT gate: apply an X-gate to the target qubit if the control qubit is in state $\|1\rangle$		$\text{CNOT} = \begin{pmatrix} 1 & 0 & 0 & 0 \\ 0 & 1 & 0 & 0 \\ 0 & 0 & 0 & 1 \\ 0 & 0 & 1 & 0 \end{pmatrix}$	Input / Output: $\|00\rangle \to \|00\rangle$, $\|01\rangle \to \|01\rangle$, $\|10\rangle \to \|11\rangle$, $\|11\rangle \to \|10\rangle$
Controlled-phase gate: apply a Z-gate to the target qubit if the control qubit is in state $\|1\rangle$	Z	$\text{CPHASE} = \begin{pmatrix} 1 & 0 & 0 & 0 \\ 0 & 1 & 0 & 0 \\ 0 & 0 & 1 & 0 \\ 0 & 0 & 0 & -1 \end{pmatrix}$	Input / Output: $\|00\rangle \to \|00\rangle$, $\|01\rangle \to \|01\rangle$, $\|10\rangle \to \|10\rangle$, $\|11\rangle \to -\|11\rangle$

Figure 7: Description of two bit Quantum gates. Image extracted from ref [15]

2.2 Working principles of Superconducting Qubits

In this section we will discuss the physics that enables the creation of artificial atoms from superconductors. First we will discuss the quantum nature of these materials and next describe how they can be used for binary quantum information processing.

2.2.1 Superconductors

Some metals such and Pb, Al under very low temperatures exhibit superconducting properties, which enables current to flow with no resistance. This state of matter was only successfully described using quantum mechanics in the BCS theory [17]. John Bardeen, Leon Cooper, and John Robert Schrieffer won the Nobel prize in 1973 for this work which theorized that condensates of Cooper pairs were responsible for the properties of these materials. For quantum computing purposes this means that superconductors have wave functions and display all other natural quantum mechanical properties. In 1961, Deaverand and Fairbank performed experiments with tiny superconducting cylinders and discovered the unitary flux value $\Phi_0 = \frac{hc}{2e} = 2 \times 10^{-15} \quad Tm^2$ [6]. The quantization of current in superconductors was evidence that this is a a quantum system.

Superconducting materials are only successfully explained through quantum mechanics. And the quantum mechanical description of a superconductor consists of a condensate of bosonic particles called Cooper pairs, after Brian Cooper, who was one of the authors of the BCS theory which correctly describes type I superconductors [17]. Cooper pairs are composed of two electrons, fermions of opposing or parallel spin orientation, logically their spin sum up to 0 or 1 [9]. Each Cooper pair is individually described by a wave function

$$\Psi(\vec{r},t) = \psi_0 e^{-i\theta(\vec{r},t)} = \psi_0 e^{i(\vec{k_s}\cdot\vec{r}-\omega t)}.$$

Where $k = |\vec{k_s}| = 2\pi/\lambda$; $\lambda =$ wavelength and therefore k is the wavenumber. Here $\theta(\vec{r},t)$ is a phase attributed to the Cooper pair which depends on space and time. It follows that the Cooper particle has momentum $\hbar\vec{k_s}$ and velocity $\vec{v_s} = \hbar\vec{k_s}/m$. Cooper pairs can have wave equations spanning out from 10 to 1000 nm [18]. They can all be in the same energy state as they are bosons. Thus the whole ensemble of Cooper pairs can be treated by one wave function which describes the entire system determined by only two variables, $n_s(\vec{r},t)$ and $\theta(\vec{r},t)$ the number of Cooper pairs and a phase respectively. This has been observed in macroscopic range, around 10^{13} times bigger then the atomic scale where quantum mechanics phenomena are customary. These are so called mesoscopic objects.

$$\Psi(\vec{r},t) = \sqrt{n_s(\vec{r},t)}\psi_0 e^{-i\theta(\vec{r},t)} \tag{5}$$

The charged super-fluid is described by only two variables. A phase which is coherent and measurable, having influence on frequency and momentum and the time dependent density of Cooper pairs. The fact that this charged super-fluid is explained through quantum mechanics results in the discretion of voltage and super-current as will be shown here.

The motion of electrons can be described by the Schrodinger equation:

$$i\hbar \frac{\partial \Psi_1}{\partial t} = \hat{H}\Psi_1 \tag{6}$$

$$\hat{H}\Psi_1 = \left(-\frac{\hbar^2}{2m}\nabla^2 + V(\vec{r},t)\right)\vec{\Psi}(\vec{r},t) \tag{7}$$

From quantum mechanics $|\psi|^2$ can be interpreted as the probability density of the particle. I if we picture a stationary system, with a finite number of particles we can assume that $|\Psi_1|^2$ is constant and therefore does not vary with time. In a stationary system $\hat{H}$ is constant and can be interpreted simply as the energy E, therefore we are left with the partial time derivative with respect to θ :

$$\hbar \frac{\partial \theta}{\partial t} = -E \tag{8}$$

This does not work for normal metals, since the electrons in normal metals obey fermi-dirac statistics which prohibits two electrons from having exactly the same energy. In superconductors however the bosonic cooper pairs can occupy the same energy level and become phase-locked state described by a single wave funcion Ψ [9]. Lets examine some consequences of postulating that one wave function describes a whole ensemble of Cooper pairs. From quantum mechanics we get that for a particle $|\Psi(\vec{r},t)|^2 = \rho(\vec{r},t)$ is the density of probability of finding this particle at position r, at a time t. The normalization rule $\int \Psi^*\Psi dV = 1$ imposes that if you integrate over all of space you have a 100% probability of finding the particle. For the ensemble of Cooper pairs we have

$$\int \Psi^*(\vec{r},t)\Psi(\vec{r},t)dV = 1 \tag{9}$$

$$|\Psi(\vec{r},t)|^2 = \Psi^*(\vec{r},t)\Psi(\vec{r},t) = \rho(\vec{r},t) \tag{10}$$

Here we have the integration of $\Psi(\vec{r},t)$ time its conjugate over all space equal to 1 which is the probabily that a quantum object will be at position $\vec{r}$ at time t. This Equation represents the normalization condition, since we must be able to find the particle somewhere in space at all times. As for the square module of $\Psi(\vec{r},t)$ equal to $\rho(\vec{r},t)$ the local particle density. In order to understand how $\rho(\vec{r},t)$ evolves in time we must follow three steps.

- First multiply the Schrödinger equation from the left side by $\Psi^*(\vec{r},t)$.
- Next multiply the complex conjugate of the Schrödinger equation from the left side by $\Psi(\vec{r},t)$.
- We then subtract both equations from each other.

After these steps we end up with

$$\frac{\partial}{\partial t}\Psi^*\Psi + \frac{\hbar}{2mi}(\Psi^*\nabla^2\Psi - \Psi\nabla^2\Psi^*) = 0 \tag{11}$$

But since del obeys the following product rule

$$\nabla\cdot(f\vec{v}) = f\nabla\cdot\vec{v} + \vec{v}\cdot\nabla f \tag{12}$$

Equation 11 can be further simplified to

$$\frac{\partial}{\partial t}\Psi^*\Psi + \nabla\left[\frac{\hbar}{2mi}(\Psi^*\nabla\Psi - \Psi\nabla\Psi^*)\right] = 0. \tag{13}$$

Which is analogous to the conservation law for currents. Equation 14 implies that there is a quantity we define as J_s which is related to the change in the probability density.

$$\frac{\partial\rho}{\partial t} - \nabla\cdot J_s = 0 \tag{14}$$

Therefore a change of ρ in time is equal to the gradient of a probability current J_s. We can express the probability current in terms of the momentum operator $\hat{p} = -i\hbar\frac{\partial}{\partial t}$

$$\vec{J}_s \equiv \frac{\hbar}{2mi}(\Psi^* \nabla \Psi - \Psi \nabla \Psi^*) = Re(\Psi^* \frac{\hbar}{2mi} \nabla \Psi) = Re(\Psi^* \frac{\hat{p}}{m} \Psi) \tag{15}$$

From Equation 15 we can see that a quantum object can not simply change its position. In other words ρ needs to change continuosly in time.

If we extend these notion to a system such that N_s^* is the total number of superconducting particles. As for $n_s^*(\vec{r}, t)$ equals to the local particle density.

$$\int \Psi^*(\vec{r}, t)\Psi(\vec{r}, t) dV = N_s^* \tag{16}$$

$$|\Psi(\vec{r}, t)|^2 = \Psi^*(\vec{r}, t)\Psi(\vec{r}, t) = n_s^*(\vec{r}, t) \tag{17}$$

Considering a vector field $\vec{A}(\vec{r}, t)$, we can then arrive at an expression for the supercurrent in superconductors,

$$\vec{J}_s = q^* n_s^*(\vec{r}, t) \left\{ \frac{\hbar}{m^*} \nabla \Theta(\vec{r}, t) - \frac{q^*}{m^*} \vec{A}(\vec{r}, t) \right\} \tag{18}$$

This equation describes the supercurrent present in superconductors. From this we can also extract group velocity and a simplified form of the current. A more in depth review can be seen in Reference [18]. We can simplify Equation 18 defining the group velocity as

$$v_s = \left\{ \frac{\hbar}{m^*} \nabla \Theta(\vec{r}, t) - \frac{q^*}{m^*} \vec{A}(\vec{r}, t) \right\},$$

and therefore the supercurrent is defined as

$$\vec{J}_s = q^* n_s^* v_s.$$

2.2.2 Hamiltonian of an ensemble of Cooper pairs

A good starting point is the Hamiltonian for a chunk of superconducting material. Let's begin with the general classical equation of motion:

$$\frac{d}{dt}\,\vec{p} = -\vec{\nabla} V \tag{19}$$

For a particle with charge q immersed in an electromagnetic field the Lorentz's equation applies.

$$m\frac{d}{dt}\,\vec{v} = q\,[\vec{E}\,+\,(\vec{v}\,\times\,\vec{B})] \tag{20}$$

For Lorentz's equation to be useful it needs to be in potential form. For this we will use Gauss's law and Faraday's law which are respectively.

$$\vec{B}\ =\ \vec{\nabla}\times\vec{A}\ ;\ \ \vec{\nabla}\times\vec{E} = -\frac{\partial\vec{B}}{\partial t} \tag{21}$$

By substituting Gauss into Faraday

$$\vec{\nabla}\times\vec{E} = -\frac{\partial(\vec{\nabla}\,\times\,\vec{A})}{\partial t} = -\vec{\nabla}\,\times\,\frac{\partial\vec{A}}{\partial t} \tag{22}$$

And finally

$$\vec{\nabla}\,\times\,\left(\vec{E}\,+\,\frac{\partial\vec{A}}{\partial t}\right) = 0 \tag{23}$$

Taking into consideration that the curl of the gradient of any single valued scalar field ϕ is also zero $(\vec{\nabla}\,\times\,(\vec{\nabla}\,\phi)\,=\,0)$.

Evidently

$$\vec{E}\ =\ -\frac{\partial\vec{A}}{\partial t}\ -\ \vec{\nabla}\phi \tag{24}$$

Now, take this result and rewrite Lorentz's equation in terms of these potentials.

$$m\frac{d}{dt}\,\vec{v} = q\,[\,-\,\frac{\partial\vec{A}}{\partial t}\;-\;\vec{\nabla}\phi\;+\;(\vec{v}\;\times\;\vec{\nabla}\;\times\;\vec{A}\;\;)] \tag{25}$$

Next we must use the chain rule of differentiation to group all time derivatives together

$$\frac{d\vec{A}}{dt}\;=\;\frac{\partial\vec{A}}{\partial t}\;+\;(\vec{v}\;\cdot\;\vec{\nabla})\;\vec{A} \tag{26}$$

This yields

$$m\frac{d}{dt}\,\vec{v} = q\,[\,-\,\frac{d\vec{A}}{dt}\;-\;(\vec{v}\;\cdot\;\vec{\nabla})\;\vec{A}\;\;-\;\vec{\nabla}\phi\;+\;(\vec{v}\;\times\;\vec{\nabla}\;\times\;\vec{A}\;\;)] \tag{27}$$

then

$$\frac{d}{dt}(\;m\vec{v}\;+\;q\vec{A}\;) = q\,[\,-\;(\vec{v}\;\cdot\;\vec{\nabla})\;\vec{A}\;\;-\;\vec{\nabla}\phi\;+\;(\vec{v}\;\times\;\vec{\nabla}\;\times\;\vec{A}\;\;)] \tag{28}$$

From here we can guess that the canonical momentum is given by

$$\vec{p} = \frac{d}{dt}(\;m\vec{v}\;+\;q\vec{A}\;) \tag{29}$$

To verify this we must be able to express the right hand side of the function as the gradient of a scalar. To do this we will rewrite the function in terms of the canonical momentum

$$\frac{d}{dt}\vec{p} = -q\vec{\nabla}\phi\;+\frac{q}{m}(\vec{p}\;\cdot\;\vec{\nabla})\;\vec{A}\;\;-\frac{q^2}{m}(\vec{A}\;\cdot\;\vec{\nabla})\;\vec{A}+\frac{q}{m}\;\;\vec{p}\;\times\;(\vec{\nabla}\;\times\;\vec{A}\;)\;-\frac{q^2}{m}\vec{A}\;\times\;(\vec{\nabla}\;\times\;\vec{A}\;\;) \tag{30}$$

To simplify this equation two vectorial identities below will be used

$$\vec{a}\;\times\;(\vec{\nabla}\;\times\;\vec{b}) = \vec{\nabla}(\vec{a}\;\cdot\;\;\vec{b}) - (\vec{a}\;\cdot\;\vec{\nabla})\;\vec{b} - (\vec{b}\;\cdot\;\vec{\nabla})\;\vec{a} - \vec{b}\;\times\;(\vec{\nabla}\;\times\;\vec{a}) \tag{31}$$

$$\vec{a}\;\times\;(\vec{\nabla}\;\times\;\vec{a}) = \frac{1}{2}\vec{\nabla}(\vec{a}\;\cdot\;\;\vec{a}) - (\vec{a}\;\cdot\;\vec{\nabla})\;\vec{a} \tag{32}$$

Applying these to Equation 30 we come to:

$$-\frac{q^2}{m}(\vec{A}\cdot\vec{\nabla})\,\vec{A}-\frac{q^2}{m}\vec{A}\times(\vec{\nabla}\times\vec{A}\,)=-\frac{q^2}{2m}\vec{\nabla}(\vec{A}\cdot\ \vec{A})$$

$$\frac{q}{m}(\vec{p}\cdot\vec{\nabla})\,\vec{A}\ +\frac{q}{m}\ \vec{p}\times(\vec{\nabla}\times\vec{A}\,)\ =\ +\frac{q}{m}[\vec{\nabla}(\vec{p}\cdot\ \vec{A})-(\vec{p}\cdot\vec{\nabla})\,\vec{A}-(\vec{A}\cdot\vec{\nabla})\,\vec{p}]$$

$$\frac{d}{dt}\vec{p}=-q\vec{\nabla}\phi\ -\frac{q^2}{2m}\vec{\nabla}(\vec{A}\cdot\ \vec{A})\ +\frac{q}{m}[\vec{\nabla}(\vec{p}\cdot\ \vec{A})-(\vec{p}\cdot\vec{\nabla})\,\vec{A}-(\vec{A}\cdot\vec{\nabla})\,\vec{p}] \tag{33}$$

The spatial derivatives of the canonical momentum is zero because we are using a set of independently specified variables $(\vec{r},\vec{p})$. And finally we arrive at the Lorentz's equation in potential form

$$\frac{d}{dt}\vec{p}=-\vec{\nabla}[q\phi\ -\frac{q^2}{2m}(\vec{A}\cdot\ \vec{A})\ +\frac{q}{m}(\vec{p}\cdot\vec{A})] \tag{34}$$

From equation 19 we see that the potential V is

$$V=q\phi\ -\frac{q^2}{2m}(\vec{A}\cdot\ \vec{A})\ +\frac{q}{m}(\vec{p}\cdot\vec{A}) \tag{35}$$

Next step is to write the total classical energy

$$E\ =\ E_{kin}\ +\ E_{pot}\ =\ \frac{\vec{p}\cdot\vec{p}}{2m}\ +\ \{q\phi\ -\frac{q^2}{2m}(\vec{A}\cdot\ \vec{A})\ +\frac{q}{m}(\vec{p}\cdot\vec{A})\} \tag{36}$$

This can be simplified to

$$E\ =\ \frac{1}{2m}(\vec{p}\ -\ q\vec{A})\cdot(\vec{p}\ -\ q\vec{A})\ +\ q\phi \tag{37}$$

To transform this into the Schrödinger equation we will introduce the quantum mechanical operators in the place of energy and momentum.

$$E\ =\ i\hbar\frac{\partial}{\partial t}\qquad\qquad \vec{p}=-i\hbar\vec{\nabla} \tag{38}$$

Therefore the quantum form of the Lorentz's Law is expected to be

$$i\hbar\frac{\partial\vec{\psi}}{\partial t}=\frac{1}{2m}\left(\frac{\hbar}{i}\vec{\nabla}\ -\ q\vec{A}\right)^2\ \vec{\psi}\ +\ q\phi\,\vec{\psi} \tag{39}$$

With this result we have a Hamiltonian for an ensemble of Cooper Pairs.

2.2.3 Josephson Junction (JJ)

Josephson Junctions have a wide variety of applications in precise measurement tools, such as squids andqubits. There is a rich phenomenological background which will not be seen here in depth. However we will discuss the basic behavior when applying voltages and currents are applied and their expected behavior.

The wave function which describes the behavior of the collective of Cooper pairs is contained by the boundaries of the superconductor [18]. The walls being a potential barrier that keeps the charged super-fluid confined. Due to the quantum nature of this charged super-fluid, it has a nonzero probability of being beyond the limiting volume. Taking two superconducting materials and placing them close enough so that the wave functions overlap, Cooper pairs have a nonzero probability of tunneling from one side of the material to the other. This may also be achieved by placing a layer of non superconducting metal or insulating barrier with the right dimensions to form the proper potential barrier. Another possibility is tunneling through a weak link. This tunneling process was first envisioned by Brian Josephson in 1962 [13]. Here we will discuss three basic experiments:

i The non driven state

ii The DC driven JJ

iii The AC driven JJ

First we will look at the zero voltage state of the Josephson effect from which we can derive the Josephson equations which govern the other two states. In this state the system is isolated, two superconductors separated by a potential barrier.

We begin by defining the amplitude of probability to find a cooperpair on one side Ψ_1 and the amplitude to find it on the other Ψ_2. The wave function amplitudes of each superconductor overlap at the junction, the Cooper pairs will have a non-zero probability of tunneling [18].

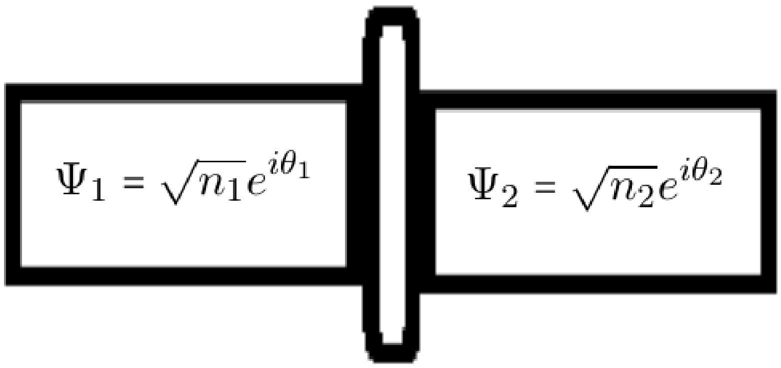

Figure 8: Idealization of a Josephson Junction.

$$\begin{aligned} n_1\, is\, the\, Cooper\, pair\, density\, of\, \Psi_1 \\ n_2\, is\, the\, Cooper\, pair\, density\, of\, \Psi_2 \\ \theta_1\, is\, the\, phase\, of\, \Psi_1 \\ \theta_2\, is\, the\, phase\, of\, \Psi_2 \end{aligned} \tag{40}$$

This wave equation assigns each superconductor a particle density (n_1, n_2) and a phase (θ_1, θ_2). Applying the time dependent Hamiltonian to each wave equation:

$$\begin{aligned} i\hbar\frac{\partial \Psi_1}{\partial t} = U_1\Psi_1 + K\Psi_2 \\ i\hbar\frac{\partial \Psi_2}{\partial t} = U_2\Psi_2 + K\Psi_1 \end{aligned} \tag{41}$$

If we picture the system in an initial configuration where we have a voltage V applied to the superconductors, such that $U_2 - U_1 = V$:

$$
\begin{aligned}
i\hbar\frac{\partial\Psi_1}{\partial t} &= \frac{qV}{2}\Psi_1 + K\Psi_2 \\
i\hbar\frac{\partial\Psi_2}{\partial t} &= \frac{-qV}{2}\Psi_2 + K\Psi_1
\end{aligned}
\tag{42}
$$

The constant K is a characteristic of the junction. It indicates the amplitude of the coupling between the two superconductors. If it were zero then there would be no coupling and the superconducting metals would describe the lowest energy state with energies If a Cooper pair leaves one superconducting material it will be accounted for in the other. Therefore there needs to be total Cooper pair conservation $\hbar\frac{\partial n_1}{\partial t} = -\hbar\frac{\partial n_2}{\partial t}$. If we take Equation 5 and plug it into Equation 42. Next we equate the real and imaginary parts in each case. Letting $\theta_2 - \theta_1 = \delta$ we get :

$$
\begin{aligned}
\dot{n}_1 &= \frac{2}{\hbar}K\sqrt{n_2 n_1}\sin\delta, \\
\dot{n}_2 &= -\frac{2}{\hbar}K\sqrt{n_2 n_1}\sin\delta,
\end{aligned}
\tag{43}
$$

$$
\begin{aligned}
\dot{\theta}_1 &= -\frac{K}{\hbar}\sqrt{\frac{\rho_2}{\rho_1}}\cos\delta - \frac{qV}{2\hbar}, \\
\dot{\theta}_2 &= -\frac{K}{\hbar}\sqrt{\frac{\rho_1}{\rho_2}}\cos\delta + \frac{qV}{2\hbar}.
\end{aligned}
\tag{44}
$$

From Equation 43 we see that $\dot{n}_1 = -\dot{n}_1$, physically this translates to the notion that if a Cooper pair leaves one superconductor is will arrive at the other.

$$
\hbar\dot{n}_1 \quad = \quad -\hbar\dot{n}_2 \quad = \quad 2K\sqrt{n_1 n_2}\, sin(\delta) \tag{45}
$$

Now taking into account that $\frac{\partial n_1}{\partial t} = I$ and defining the critical current $I_c = 2K\sqrt{n_1 n_2}/\hbar$ we get the Josephson equations

$$
I = I_c sin(\delta), \tag{46}
$$

$$\frac{\partial\delta}{\partial t} = \frac{2eV}{\hbar}. \tag{47}$$

From these equations it is evident that in the absence of any electrical field a direct current will cross the insulating layer. The maximum current is limited by the phase difference across the JJ as seen in Equation 46. Thus it can take values ranging from I_o to $-I_o$.

2.2.4 The DC driven state of the Josephson Junction

The AC voltage state of JJ is caused by the application of a fixed DC voltage V. Equation 48 describes how the phase δ evolves with time t. By taking the second Josephson equation and plugging into the first we can see that applying a DC voltage V produces a modulated current given by

$$I(t) = I_0 sin(\frac{2eV}{\hbar}t) \tag{48}$$

Therefore the frequency is

$$\nu = \frac{2eV_0}{\hbar} \tag{49}$$

$$\frac{2e}{\hbar} = \frac{2 \times 1,6021766 \times 10^{-19} C}{4,1356676 \times 10^{-15} eVs} = \frac{483,5978 \times 10^{9}}{mV \cdot s} = 483,6\frac{GHz}{mV} \tag{50}$$

$$1\frac{eV}{C} = 1,60217662 * 10^{-19}V$$

In this regime the Josephson Junction acts like a perfect Voltage to frequency converter.

2.2.5 The AC driven state of the Josephson Junction

This effect is of interest to us. It deals with the application of microwave frequency electromagnetic radiation on JJ. This will induce DC voltages across the JJ. Therefore the Junction acts like a perfect frequency-to-voltage converter, according to Equation 51. This means that the resonators used to create the cavity induce tunneling in the JJ. V_n is the DC voltage across the junction for a certain microwave radiation with frequency ω. The energy of the incident foton is evidently $\hbar\omega$, furthermore n is the number of incident photons. This number is divided by the charge of the cooper pair which is 2e. More about this can be seen in Levinsen, M. T. [16].

$$V_n = \frac{n\hbar\omega}{2e} \tag{51}$$

2.2.6 The Nonlinear Josephson Inductance

The nonlinear inductance L_J is what makes Josephson junctions specially useful for quantum computing. This nonlinear inductance results in shifts to the spacing between energy levels breaking the degeneracy. We will start at Ohm's Law for an inductor given by Equation 52. Next we will write the Josephson Equations in similar form. Looking back to the Josephson equations (Equations 46 and 47), take the first and differentiate with respect to time then substitute the result into the second, this yields

$$\frac{dI}{dt}L = V \tag{52}$$

$$\frac{dI_J}{dt} = I_0 cos(\delta \frac{\Phi_0}{2\pi I_0} V) \tag{53}$$

$$\frac{dI_J}{dt} L_J = V \tag{54}$$

$$L_J = \frac{\Phi_0}{2\pi I_0 cos(\delta)} \tag{55}$$

2.2.7 Josephson Tunneling Hamiltonian

The Hamiltonian for the superconducting qubit is similar to that of a quantum harmonic oscillator (QHO). Here, we will begin with a linear LC resonant circuit and adapt it to describe superconducting qubits. We will start by defining the Lagrangian of the QHO then move on to the Hamiltonian. By arbitrarily associating the electrical energy with the "kinetic energy" and the magnetic energy with the "potential energy" of the oscillator. The instantaneous, time dependent energy in each element is derived from its current and voltage.

We will start with the classical harmonic oscillator shown in Figure 9. The cycle begins when the capacitor is fully charged and no energy is flowing. We have that the "kinetic energy" is $E = \frac{1}{2}CV^2$. And the "potential energy" will correspond to the energy stored in the magnetic field around the coil $E = \frac{LI^2}{2}$.

$$E(t) = \int_{-\infty}^{t} V(t')I(t')dt' \tag{56}$$

$$\Phi(t) = \int_{-\infty}^{t} V(t`)dt` \tag{57}$$

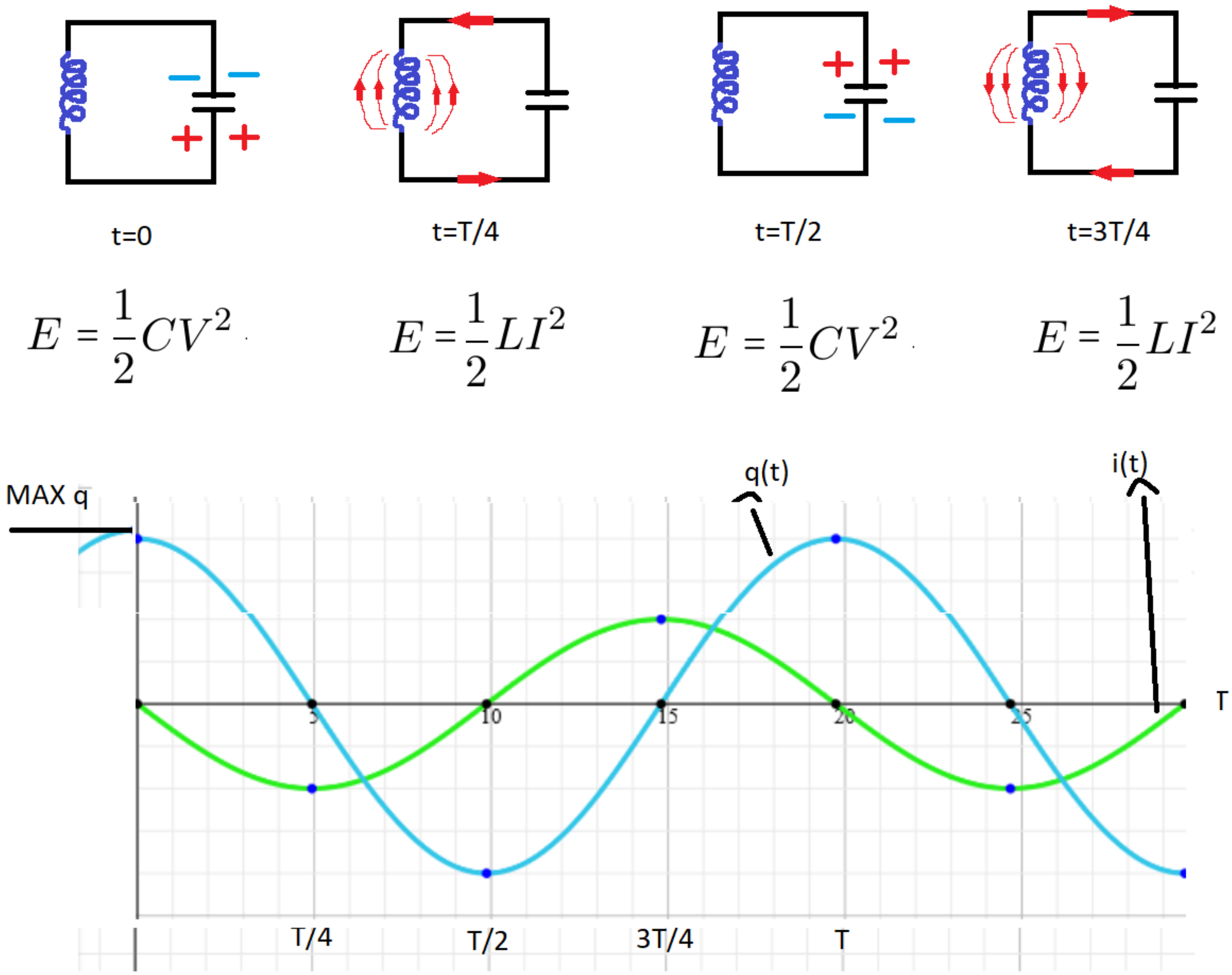

Figure 9: This image portrays a LC circuit whose circuit is closed and currents starts to flow from the charged capacitor at $t = 0$. T is the period and we analyze this system at intervals of T/4. When the capacitor is fully charged (t=0 and t=T/2) the energy is given by . When the energy is trapped in the field ($t = T/4$ and $t = 3T/4$)created by the coil we have energy equal to $E = \frac{LI^2}{2}$.

Using $V = LdI/dt$, $I = CdV/dt$ and the integration by parts formula $dx = d(uv)/dx = udv/dx + vdu/dx$. We obtain the Langragian seen in Equation 58

$$L = T_c - U_L = \frac{1}{2}C\dot{\Phi}^2 - \frac{1}{2L}\Phi^2 \tag{58}$$

$$Q = \frac{\partial L}{\partial \dot{\Phi}} = C\dot{\Phi} \tag{59}$$

The Hamiltonian of the system is now defined as

$$H = Q\dot{\Phi} - L = \frac{Q^2}{2C} + \frac{\Phi^2}{2L} \equiv \frac{1}{2}CV^2 + \frac{LI^2}{2} \tag{60}$$

Notice that this Hamiltonian is analogous to the mechanical harmonic oscillator expressed in momentum p and position x. By making $m = C$ and $\omega = 1/\sqrt{LC}$, we recover $H = p^2/2m + m\omega^2 x^2/2$. In order to go from a classical description to a quantum mechanical one the Poisson brackets must be verified.

$$\left\{ f \, , \, g \right\} = \frac{\delta f}{\delta \Phi}\frac{\delta g}{\delta Q} - \frac{\delta g}{\delta \Phi}\frac{\delta f}{\delta Q} \tag{61}$$

$$\left\{ Q \, , \, \Phi \right\} = \frac{\delta g}{\delta \Phi}\frac{\delta f}{\delta Q} - \frac{\delta f}{\delta \Phi}\frac{\delta g}{\delta Q} = 1 - 0 = 1 \tag{62}$$

The quantum operators also satisfy the commutation relationship.

$$[\hat{\phi}, \hat{Q}] = \hat{\phi}\hat{Q} - \hat{Q}\hat{\phi} = i\hbar \tag{63}$$

Therefore we can make the canonical transformation and arrive at the Hamiltonian of the quantum harmonic oscillator by defining $\phi \equiv 2\pi\Phi/\phi_0$ and $n = Q/2e$. To simplify the expression we have the charging energy $E_C = e^2/(2C)$ and the Josephson energy $E_J = (\Phi_0/2\pi)^2/L$.

$$H = E_C n^2 + \frac{1}{2}E_J\phi^2 \tag{64}$$

Quantum mechanically, the solution to $H\left|\psi(t)\right\rangle$ yields a discrete infinite eingenvector series $\left|k\right\rangle = \left\{\left|0\right\rangle, \left|1\right\rangle, \left|2\right\rangle, ...\right\}$ The eigenenergies are all evenly spaced $E_{k+1} - E_k = \hbar\omega_r$ where $\omega_r = \sqrt{8E_L E_C}/\hbar = 1/\sqrt{LC}$. Taking this solution into consideration a second quantization can be made.

$$H = \hbar\omega_r\left(a^\dagger a + \frac{1}{2}\right) \tag{65}$$

The original number and phase operators can be expressed as $n = [E_L/(32E_C)]^{1/4} \times i(\hat{a} - \hat{a}^\dagger)$ and $\phi = (2E_C/E_L)^{1/4} \times (\hat{a} + \hat{a}^\dagger)$.

These evenly spaced energy levels makes them indistinguishable. The physical quantity that solves this problem is nonl inear Josephson Inductance seen on Equation 55. In theory the larger anharmonicity the better, but the mechanisms that are used to create distinguishable energy levels also limit the processing speed of the qubit [15].

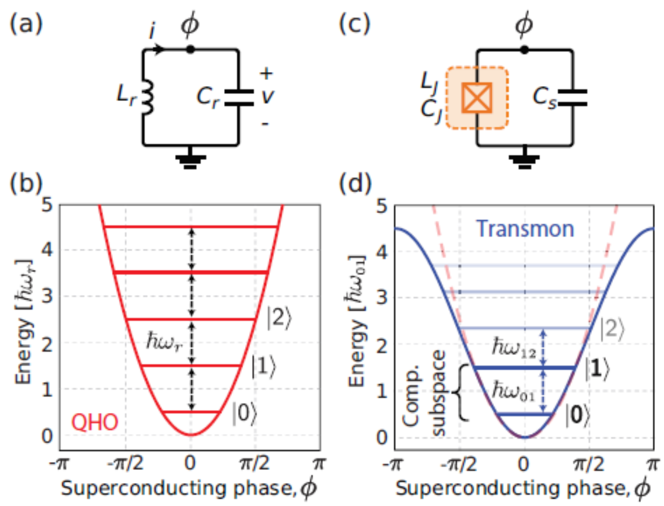

Figure 10: On the left we have a quantum harmonic oscilatore with fixed capacitanc C and Inductance L, on the right is the anharmonic oscillator produced by the nonlinear Josephson Junction in the circuit (box with x inside). Image extraced from P. krantz, et al. [15].

Introducing the nonlinear phase dependent Josephson inductance. seen on Equation 55. we get

$$H = E_C n^2 + E_J\, cos(\phi) \tag{66}$$

Here $E_J = I_c\Phi_0/2\pi$ is the Josephson energy, where Ic is the critical current, and $E_C = e^2/(2C_s+C_J)$, which means E_C is a combination of the junction capacitance C_J and shunt capacitance C_S.

The E_C/E_J ratio plays an important role in noise reduction, there is noise associated with the charging of the qubit. In the transmon regime, $E_J >> E_C$ thus the noise atributed to E_C reduces exponentially. However the anharmonicity also decreases as E_J is increased but in a much slower algebraic pace, therefore a optimization is needed to find the best configuration [14].

2.3 Superconducting Qubits

Superconducting qubits are microscopic circuits with built in Josephson Junctions, which are equivalent to nonlinear inductors [11]. Combining JJ with classical capacitors, inductors and resistors, artificial atoms can be made with distinguishable energy levels. Since superconducting qubits can be engineered to modify its characteristics, there is constant research to improve the performance of these devices.

The two main charecteristics determining the working regime of qubits is the Josephson energy E_J and Charging Energy E_C. E_C is proportional to the charging energy, its a measure of how much the electric field of one superconductor acts on the other. The total resistance of the barrier on the other hand has a direct effect on the Josephson energy [28]. Therefore the ratio of E_J to E_C show what the necessary energy is for one cooper pair to charge the total capacitance of the circuit. When the ratio is very large macroscopic currents tunnel through the junction, and it can be so small that only one cooper pair tunnels throught at a time. This relationship characterizes a qubit. Furthermore the room temperature resistance of the JJ can be used to determine the Josephson energy E_J [19].

Although there are many different types of superonducting qubits, the three main types are charge, phase and flux. The main scope of this study is the transmon, since this is the one used by A. Wallraff et al [28]. The charge qubit has $E_C/E_J > 1$ this makes E_C the dominant term in the Hamiltonian. The transmon is a special type of charge qubit, it naturally has low charging energy due to shunt capacitance and can have this ratio in the order of 10 100.This means charge fluctuations create distinct energy levels as seen in Figure 11. The Flux and Phase qubit on the other Hand $E_C/E_J < 1$ which translates to a phase dominant term in the Hamiltonian. As can be seen in Figure 11 the energy levels fluctuate acording to phase instead of charge. The phase is closely related to the flux, which is quantized when you make a loop out of superconducting material. From the uncertainty principle $\Delta N \Delta \phi \approx 2\pi$ the uncertainties of the number of Cooper pairs and phase difference are made evident. The superconducting qubits take advantage of either superposition of phase or number of Cooper pairs to create superpositioned states.

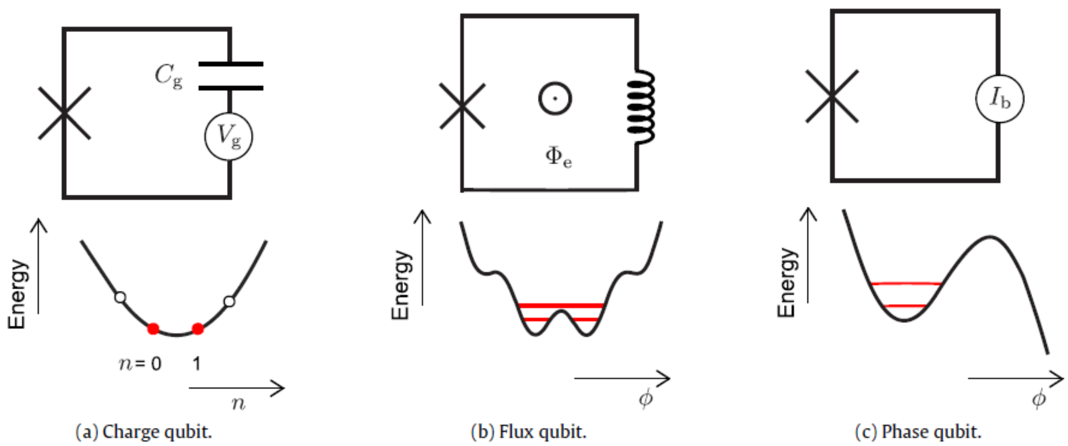

Figure 11: Three different types of superconducting qubits. This image was extracted from Xiu Gu, et al [11]

From the experimental point of view qubits are two level systems, therefore we can extend the formalism used to describe spins. A qubit that is in the higher energy level can be said to be precessing around the north pole. Some qubits like the one we wish to study are controlled via microwave signals which are either used to set the states of individual qubits or force the wave functions to collapse.

2.3.1 Charge Qubit

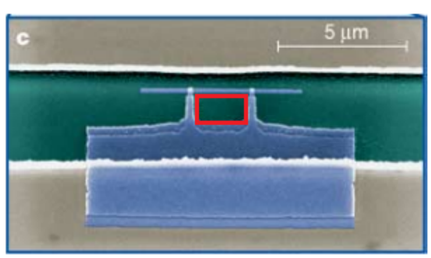

Figure 12: This is a false colour electron micrograph of a Cooper pair box, the bar looking structure is the island while the reservoir is connected via two Josephson Junctions. This image is extracted from A. Aalraff, et al. [28].

The charge qubit is composed of an island of Cooper pairs connected to a large reservoir. This qubit works by measuring an absence or excess of cooper pairs. Usually charge qubits are measured using a Single Electron Transistor, which detects charge differences of one electron as the name suggests. Since this work is focused in the coupling of a charge qubit to a resonator. Lets look closer at the qubit from A. Walraff, et al [28] seen in Figure 12. This technique uses a resonator to set and probe the states of the qubit. The island is the thin line isolated in the cavity, connected to the large reservoir via two Josephson Junctions. The Hamiltonian of the Cooper pair box is given by Equation 67 which is a slight variation of Equation 64. There are two forms of controlling the parameters of this Hamiltonian. The first by applying an electric field perpendicular to the island in order to control the electric potential on the barriers, this affects $E_{el} = 4E_C(1 - n_g)$ directly. Here $n_g = C_g V_g/(2e)$ is the gate charge number, being that E_C is the total capacitance from the feed to the island and V_g is the induced gate charge from the port. The other term in the hamiltonian can be controled by the Josephson energy being that $E_J = E_{J,max} cos(\pi \Phi_b)$. More specifically $\Phi_b = \Phi/\phi_0$ is the flux accounted by the qubit, which is applied through the red rectangular loop highlighted in Figure 12.

$$\mathscr{H}_a = -4E_C(n - n_g)^2 - E_J \cos\phi \tag{67}$$

The charge qubit works at $E_C/E_J \approx 10$, in general the energy scales are $\Delta E \gg E_C \gg E_J \gg k_B T$. Given these conditions and taking into account that $e^{\pm i\hat{\theta}}|n\rangle = |n \pm 1\rangle$ the Hamiltonian can be expressed as:

$$\mathscr{H}_a = -4E_C(n - n_g)^2 |n\rangle\langle n| - E_J(|n+1\rangle\langle n| + |n\rangle\langle n+1|) \tag{68}$$

To diagonalize this hamiltonian we must truncate the infinite series at some n_{max} number of cooper pairs on the island. This is not a plroblem since we are interested in the lowest everny level which we drift away from as we increase the number of excess or missing cooper pairs. Lets switch to the matrix representation:

$$\mathscr{H}_a = \begin{pmatrix} 4E_C(-n_{max} - n_g)^2 & -E_J & 0 & \cdots & \cdots & \cdots & 0 \\ -E_J & 4E_C(-n_{max} + 1 - n_g)^2 & -E_J & 0 & \ddots & \ddots & \vdots \\ 0 & -E_J & \ddots & \ddots & 0 & \ddots & \vdots \\ \vdots & 0 & \ddots & \ddots & \cdots & -E_J & 0 \\ \vdots & \ddots & 0 & \vdots & -E_J & 4E_C(n_{max} - 1 - n_g)^2 & -E_J \\ 0 & \cdots & \cdots & \cdots & 0 & -E_J & 4E_C(n_{max} - n_g)^2 \end{pmatrix}$$

To evaluate how this Hamiltonian serves as a qubit lets analyse the energy graph taken from the article A. Wallraff [28] seen in Figure 13. . Lets tune the magnetic field so that $E_J = 0$, starting with $n_i = 0$ which is represented by the solid black line, we travel down to $n_g = -1$. This is a degenerate point because its energy is the same as $n_i = -2$ (black line, short dashes). A two level configuration is a requisite for a working qubit, depicted by the solid blue and red lines. To lift the degeneracy a magnetic flux is applied to the circuit. Manipulating the E_J term in Equation 70, distinguishable energy levels are created thus having a working qubit.

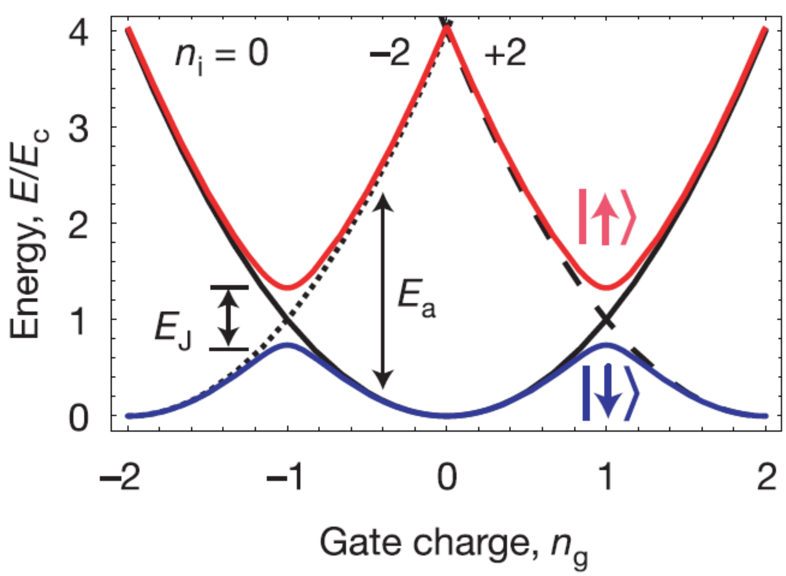

Figure 13: This image shows how degeneracy is lifted and a two level system created by manipulating the Josephson energy. Image extracted from from the A. Wallraff, et al. [28].

For a little deeper understanding lets look at Figure 13 and fix our system at $n_g = 1$ and $E_J \neq 0$. for this "sweet spot" as it's commonly called, we can reduce the hamiltonian to:

$$\mathscr{H}_a = -4E_C(n - n_g)\hat{\sigma_z} - E_J\hat{\sigma_x}) \tag{69}$$

in which $\hat{\sigma_z} = |0\rangle\langle 0| - |1\rangle\langle 1|$ and $\hat{\sigma_x} = |0\rangle\langle 1| - |1\rangle\langle 0|$ are the Pauli spin matrices. Therefore the energy values for this two level system can be found by diagonalizing the matrix

$$\mathscr{H}_a = \begin{pmatrix} 4E_C(-n_{max} + 1 - n_g) & -E_J \\ -E_J & 4E_C(n_{max} - 1 - n_g) \end{pmatrix}$$

in this way the energy values are

$$E\pm = \pm\sqrt{16E_C^2(n - n_g)^2 + E_J^2} \tag{70}$$

2.3.2 Flux Qubit

Flux qubits are also known as continuous current qubits, they are loop shaped. The direction of current flow determines the state is the direction of current flow or by the magnetic flux direction inside the loop. Being this a quantum system the flux is quantized and it can be set up in a way that the lowest energy state is a superposition of clockwise and counterclockwise currents. To create the potential seen in the figure 11 the loop must have 1, 3 or more Josephson Junctions. The flux qubit works at $E_J/E_C \approx 10$ to 100 [15]. This means a large number of Cooper pairs tunnel through the junction, forming mesoscopic supercurrents. These qubits are used the type used in the D-Wave quantum computer.

2.3.3 Phase Qubit

The phase qubit works at $E_J/E_C \approx 10^6$ The phase qubit is subjected to a potential of the type:

$$U(\phi) = \frac{\hbar}{2e}(-I_b \cos\phi - I\phi) \tag{71}$$

This potential has a tilted washboard characteristic. It is controlled through dc bias current $|I| < I_b$, operated in the zero voltage state. The absolute value of the current must be smaller then critical current, with sufficiently high resistance and small capacitance Josephson junction, quantum energy levels become detectable in the quantum minima of the washboard potential. These can be detected using microwave signals embedded in the current bias. Transitions from the zero voltage state to the voltage state were measured by monitoring the voltage across the junction. Clear resonances at certain frequencies were observed, which corresponded well with the quantum transition energies obtained by solving the Schrödinger equation [7] for the local minimum in the washboard potential.

2.4 Quantum description of cavity qubit coupling

The coupling of the cavity and qubit in the article of interest is correctly described by quantum mechanics. This is due to successfully populating the cavity with exactly one photon. One of the requirements is to guarantee that the energy of the photon is much larger then the energy in its eviroment. The wave guide is in a thermally isolated system kept at 20mK since the energy of the photon is $\hbar\omega_r/k_B \approx 300mK$, this guarantees the system is in it's ground state. It can be tuned to produce a single photon that interacts with the cooper pair island. In these conditions the resonator is found in the its ground state and produces a vacuum state field according to the following hamiltonian.

$$\mathscr{H}_r = \hbar\omega_r(\hat{a}^\dagger\hat{a} + 1/2) \tag{72}$$

Taking into account that $\langle\hat{a}^\dagger\hat{a}\rangle = \langle\hat{n}\rangle = n$ we see that the resonator has energy equal to $E_r = \hbar\omega_r(n+1/2)$. As for the Hamiltonian that describes the Cooper Pair Box $\mathscr{H}_a$ please turn to Equation 66.

The strength of the coupling depends predominantly on matching the frequency of the cavity and qubit. For the coupling to be successful the energy of the photons emitted by the wave guide must equal the energy gaps of the qubit. Also there must be only one photon as discussed earlier, strong coupling occurs when the cavity and CPB exchange energy many times before this energy dessipates into the enviroment. One could think of rock skipping, with each bounce, energy is dissipated when this necessity is met via an applied magnetic field and a gate charge, the qubit starts oscillate between its two possible states. In this regime its possible to know when the qubit will be in a desired state. Another way of looking at the same problem is that the microwave radiated from the resonator controls creation and annihilation of Cooper pairs in the island. This process is described by the James Cummings Hamiltonian [28]:

$$\mathscr{H}_{JC} = \mathscr{H}_a + \mathscr{H}_r + \hbar g(\hat{a}^\dagger \hat{\sigma^-} + \hat{a}\hat{\sigma^+}) \tag{73}$$

Now we will overlook the experimental process that involves the coupling of the qubit to a photon in the cavity. To begin lets observe that the cavity and qubit exchange energy at a rate of $g/2\pi$, to measure the qubit states this time must be a lot larger than the decoherence times for the cavity and qubit. This is to ensure the qubit and cavity exchange energy several times before decaying into the continuum degrees of freedom of the electric field [26]. To set up the experiment, n_g is set to 1. By doing this the gaps in qubit states are separated an ammount proportional to E_J, which is controled by the flux Φ_b. The system is tuned so that $n_g = 1$ and $E_a = \hbar\omega_r(n + 1/2) = E_r$. To ensure that $\Delta = \omega_r - \omega_a = 0$, which will cause strong coupling. The resonator and cavity are cooled until both are in the ground state, next the cavity is populated with average photon number of one, the electric field interacts with the cooper pair box. Causing it to couple, the strength of the coupling is proportional to g. The state of this quantum system is defined as the superposition of one photon in the cavity with the qubit in the down state or a empty cavity and qubit in the up state. More information on this experiment can be seen in A. Wallraff, et al. [28].

3 Methodology

The purpose of this work is to simulate superconducting qubits. Superconducting transmission lines are the means of controlling these superconducting circuits containing JJ. For this, the software COMSOL Multiphysics was chosen as the tool for achieving the objective. In Section 3.1 there is a brief disscussion about Numerical Analysis via The Finite Element Method. An attempt here is made to show that the Radio Frequency Module (Frequency Domain) can be used as a tool to aid the production of qubits. The Radio Frequency Module will be looked at in Section 3.2. Once a transmission line is created and mapped, the goal then became to study how can the interactions with qubits could be modeled. The basic interaction is of the vacuum state energy produced by the resonator and the qubit dipole moment. There are two main strategies, the most successful one consists in applying a qubit size parallel LC circuit, and the latter is to add a terminal to drive a qubit state and study the properties of this system. and the circuit schematics on Figure 14.

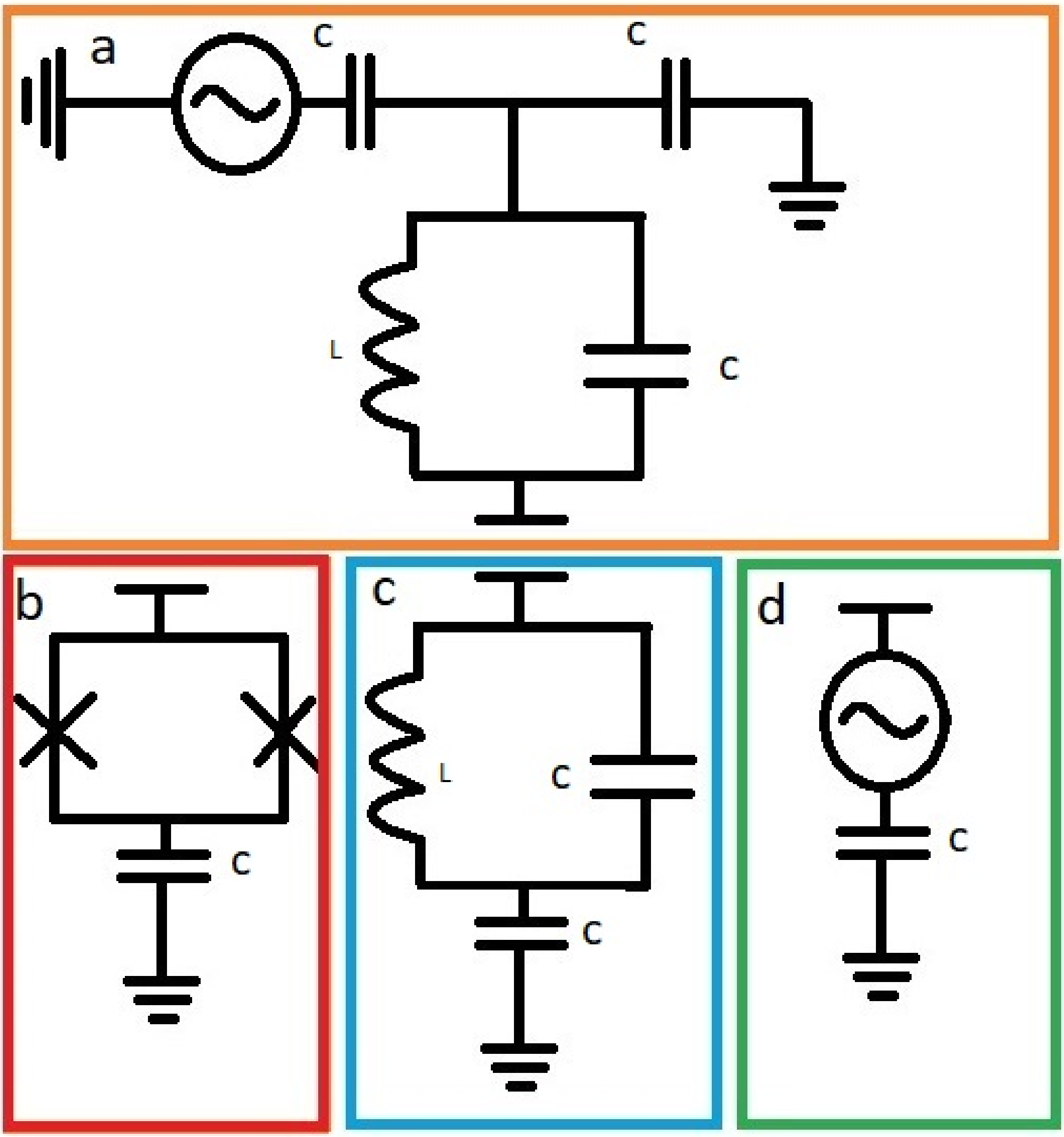

Figure 14: The orange box (a) at the top represents the wave guide. In the red box (b) is the circuit representation of the real qubit used in experiment by A. Wallraf [28]. In the blue box (c) a coupled inductor capacitor (LC) circuit. In the green box (d) is the representation of an induced voltage via a terminal, used to reproduce a dipole in the cavity.

The software chosen to create these simulations was COMSOL Multiphysics software which offers a user friendly interface to solve PDEs via finite element method. The module at interest here is the Radio Frequency Electromagnetic Waves, Frequency Domain. Which is used to solve for time-harmonic electromagnetic field distributions. [4]

3.1 Finite Element Method (FEM)

FEM is a the mathematical technique used to solve differential equations. It works by dividing a certain geometry in descrete small partitions which are easier to solve. Then an overall solution is found if the solver can minimize an associated error function. COMSOL Multiphysics presents a user friendly interface with modules that solve specific differential equations. For example, in this work we will use the Radio frequency Module (Frequency Domain) which solves Equation 79. There are also modules that solve arbitrary differential equations, here there will be a brief discussion about the Partial Differential Equation Module on section 3.6.

3.2 Electromagnetic wave package (frequency domain) - COMSOL Multiphysics

The physics applied to the geometry, was preset the COMSOL Radio Frequency module, which features an Electromagnetic wave package (frequency domain). This package solves a particular set of Maxwell equations in the frequency domain. Consider the following Maxwell's equations.

$$
\begin{aligned}
\frac{\partial \mathcal{D}}{\partial t} + \vec{J} &= \nabla \times \vec{H}, && \text{(Ampère's Law)} \\
\frac{\partial \mathcal{B}}{\partial t} &= -\nabla \times \vec{E}, && \text{(Faraday's Law)} \\
\nabla \cdot \mathcal{B} &= 0, && \text{(Gauss' Law for magnetism)} \\
\nabla \cdot \mathcal{D} &= \rho. && \text{(Gauss' Law)}
\end{aligned}
\tag{74}
$$

Taking Maxwell's equations and considering we are looking for harmonic fields of the type: $E = E_0\, e^{iwt-k\vec{r}}$ and $H = H_0\, e^{iwt-k\vec{r}}$

$$\begin{aligned} \vec{J} + i\omega\vec{D} &= \nabla \times \vec{H}, \qquad \text{(Ampère's Law)} \\ -i\omega\vec{B} &= \nabla \times \vec{E}, \qquad \text{(Faraday's Law)} \end{aligned} \tag{75}$$

Using :

$$\begin{gathered} \vec{J} = \sigma\vec{E} \\ \vec{B} = \mu\vec{H} \\ \vec{D} = \epsilon\vec{E} \end{gathered} \tag{76}$$

Ampère's Law and Faraday's Law come out to:

$$\begin{aligned} \sigma\vec{E} + i\omega\epsilon\vec{E} &= \nabla \times \vec{H}, \qquad \text{(Faraday's Law)} \\ \vec{H} &= \frac{\nabla \times \vec{E}}{-i\omega\mu}, \qquad \text{(Ampère's Law)} \end{aligned} \tag{77}$$

Now combining these two equations

$$\sigma\vec{E} + i\omega\epsilon_r\vec{E} = \nabla \times \frac{\nabla \times \vec{E}}{-i\omega\mu_r} \tag{78}$$

Rearranging the variables

$$\vec{\nabla} \times \mu_r^{-1}(\vec{\nabla} \times \vec{E}) - k_0^2(\epsilon_r - \frac{i\sigma}{\omega\epsilon_0})\vec{E} = \vec{0} \tag{79}$$

This equation yields the Electric field $\vec{E}$ for a frequency ω applied to the system. Each domain needs to be attributed a material, whose properties of interest are the material's relative permittivity ϵ_r, permeability μ_r and conductivity σ.

3.2.1 Perfect Electric Conductor - PEC

The PEC boundary condition was applied to simulate the properties of superconducting surfaces. This condition is applied via $\vec{n} \times \vec{E} = \vec{0}$. This equation sets the tangential vector of the Electric field to zero, confining the electric field instead of scattering it. In other words this represents a lossless surface which is suitable for a ground plane or the conductive properties of superconducting materials.

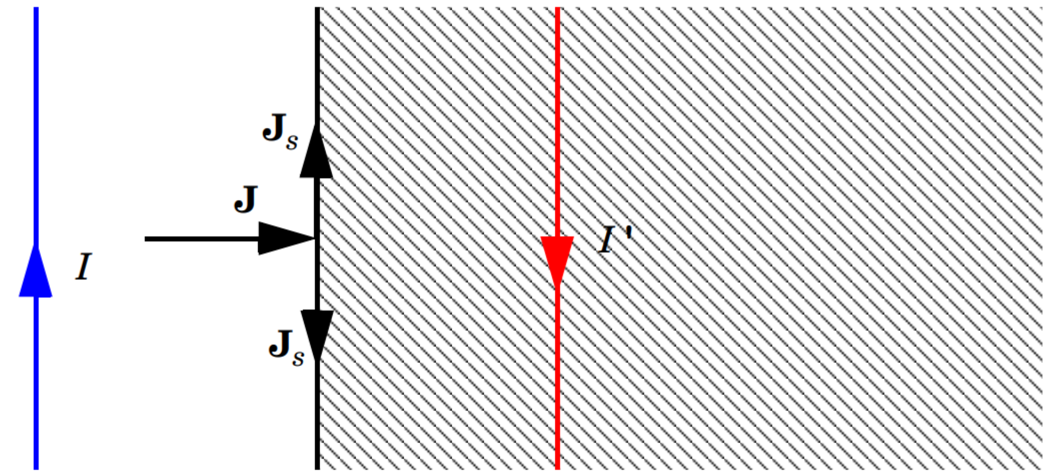

Figure 4-2: The perfect electric conductor boundary condition is used on exterior and interior boundaries representing the surface of a lossless metallic conductor or (on exterior boundaries) representing a symmetry cut. The shaded (metallic) region is not part of the model but still carries effective mirror images of the sources. Note also that any current

Figure 15: This image was extracted from the RF Module User's Guide [4]

3.2.2 Lumped Port

The lumped port is a condition that can be applied to a boundary. The port boundary condition can only be applied to an external boundary in the model. The Lumped Port is easier to work within the domain of a model. In the following image extracted from the COMSOL RF Module User's Guide [4], the set up for the port is illustrated. A surface current J_S that goes from ground to the +V node. The total port height can be adjusted by the h Parameter. When working in the RF Module - Frequency Domain the lumped ports are used to excite a conductor with alternating current.

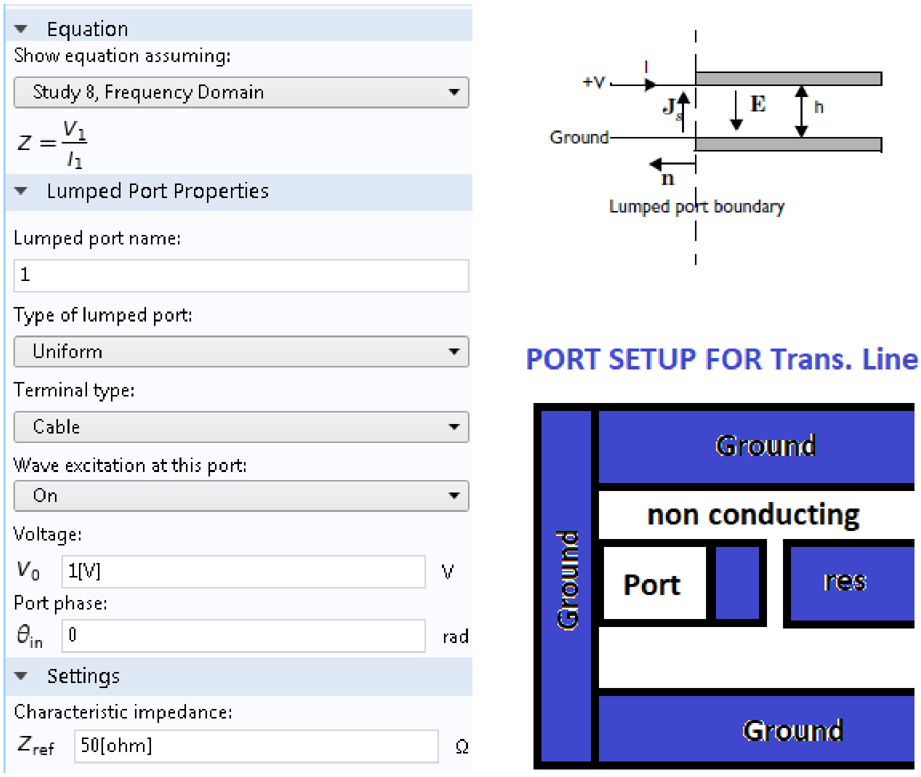

Figure 16: On the left is the user interface for setting up terminals within the geometry. The top right shows the working mechanisms of the lumped ports, this image was adapted from the RF Module User's Guide [4]. The bottom right is a diagram for the port setup of the Transmission Line Ressonators.

3.2.3 Data Analysis

The COMSOL RF module used in the Frequency Domain can be solved by applying different frequencies or searching for modes. To apply frequencies the frequency study is chosen and the user can input one or a sequence of frequencies to be studied. The eigenfrequency solver will find the natural modes of your system. These are complementary studies, the frequency spectrum will show the overall behavior of the transmission line. The eigenfrequency solver will provide information about specific modes, such as the Q factor atributed to a certain mode.

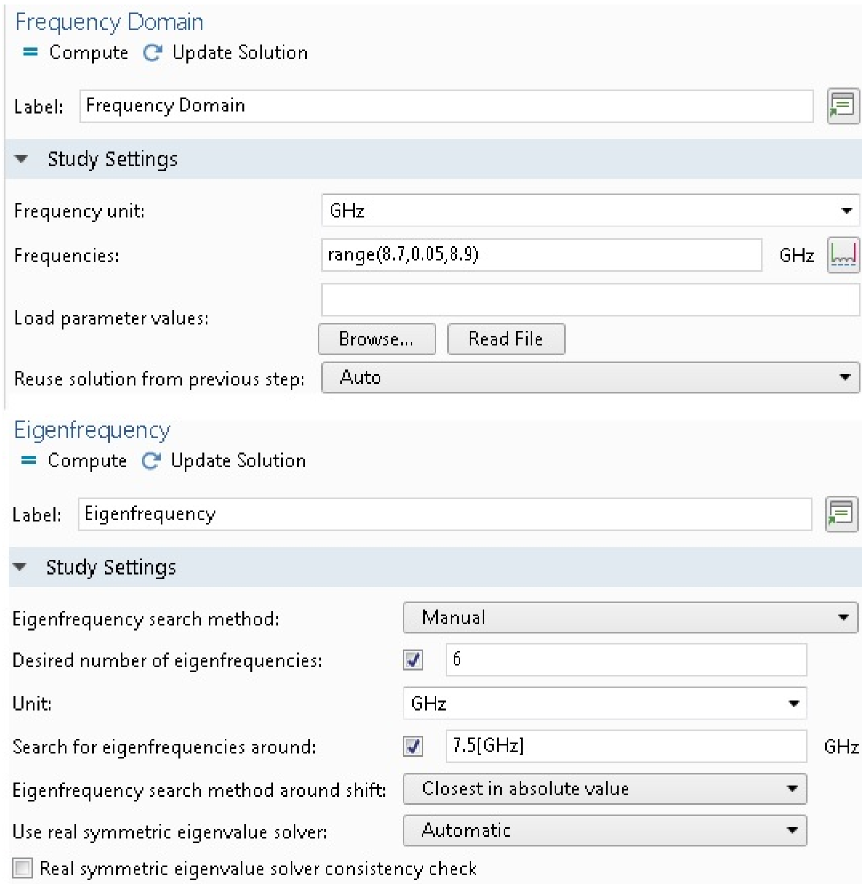

Figure 17: Screen shots of the interface, used in Frequency Domain and Eigenfrequency Study.

3.3 Transmission Line Resonators

Superconducting transmission lines are essentially filaments capacitively coupled to an input feed and detection port. These are used to control and create coherent electric field modes that enable photon-qubit coupling. Resonant modes are useful to us because they are fixed at a specific frequency and information from the qubit can be obtained when the qubit disturbs these delicate modes. There is a way to qualify these modes as being better or worse for our applications purposes. These quality factors will be disscussed in Section 3.3.5. This Q-factor is a measurement of how much energy the cavity loses to the external enviroment. In Figure 18 (top) we have a generic representation of the components of the transmission line. The feed is responsible for applying alternating current that excites the system. The resonator creates an electric field on the circuit plane. The field around the resonator is illustrated on Figure 18 (bottom). The radio frequency electric field E_{RF} interacts with the dipole moment of the Cooper pair island and allows for manipulation of the tunneling of Cooper pairs.

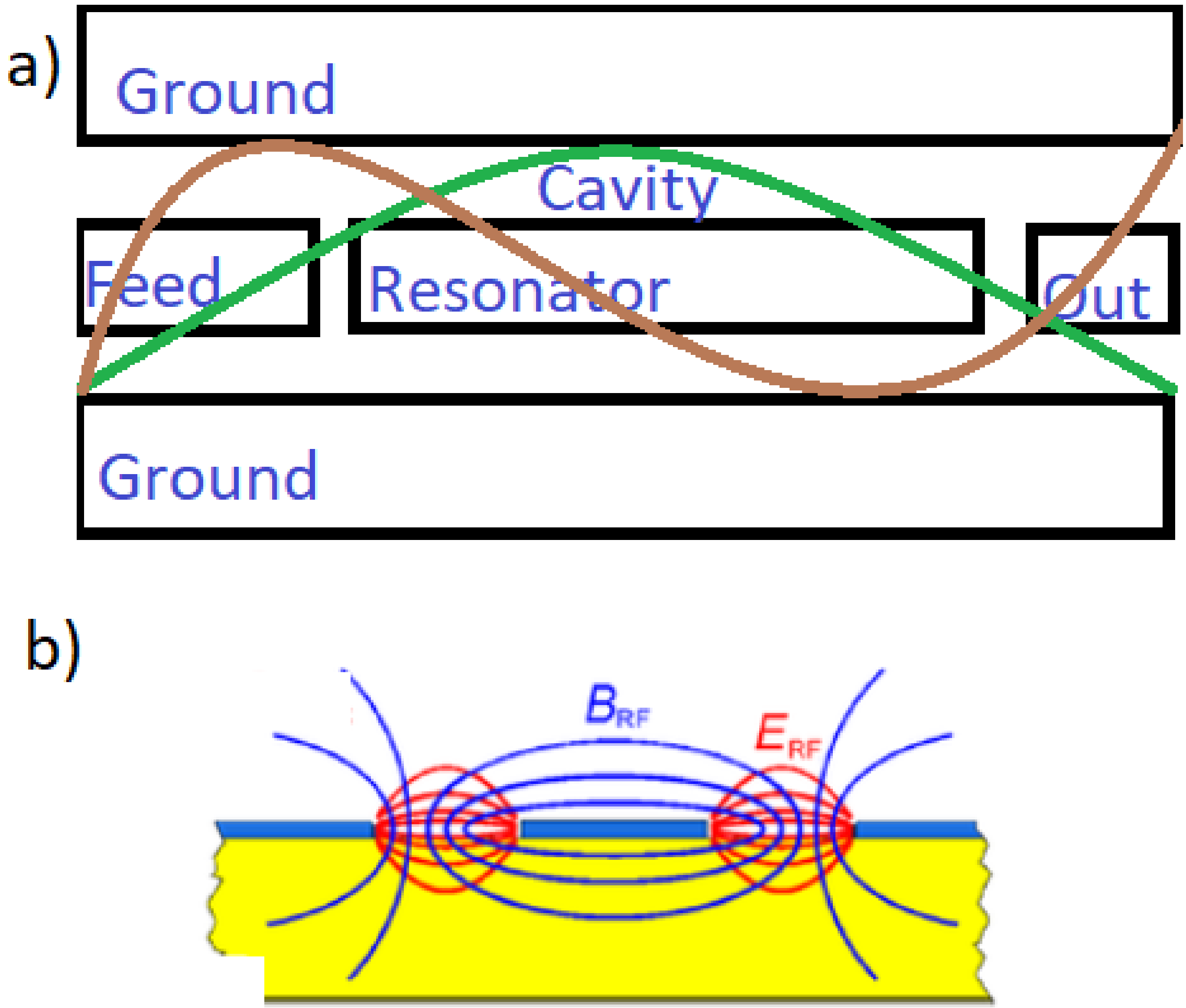

Figure 18: The top image (a) represents a generalized model for transmission lines. Here we notice a feed port which will excite our system, two parallel ground planes and a resonator which will produce resonant modes at specific frequencies illustrated by the sinusoidal lines. The cavity is the area between the resonator and ground planes. In the lower section (b) was extracted from www.researchgate.com [3], it shows a perpendicular cut to the resonator. On top the left and right squares represent ground planes. The middle rectangle represents the resonator, the circular field around it B_{RF} in blue represents the magnetic field. The lines extending from ground to the resonator represent the E_{RF} electric field

3.3.1 Original Wave guide Simulation

The model consists of a box filled with air and a silicon chip with the circuit elements on it. The circuit elements are defined as perfect electric conductors. Although this is not the same as a superconductor, it is enough for the simulation at hand. Although in reality the ressonator is in quantum regime, kept at the fundamental energy level and tuned to produce an average of one photon in the cavity. For these purposes we will neglect this while trying to preserve the dissipationless properties of the superconductor. Furthermore superconductors expel all magnetic field. This was also brought into question, the overall reason for neglecting the magnetic properties is the fact that the field of interest is eletric, the coupling occurs via the island's electric dipole moment and the electric field generated by the filament. Since the magnetic field is proportional to the electric field $\vec{E} = c\vec{B}$, c being the speed of light. Magnetic fields generated are so small, they will be neglected until further evidence to do otherwise. The key functionality focused on is the superconducting state property of transmitting an electric signal without losses. Therefore a perfect conductor is a reasonable approximation of a superconductor for this case. This would not be the case if the magnetic or quantum mechanical properties of superconductors were of interest.

Another point is the surrounding, it is possible to create an enviroment where the electromagnetic waves irradiated from the filament meet no boundaries. Another possibility is to place the circuit in a metal box, which seems to be an adequate aproximation to the experiment in which a samples are tested in a metalic cavities. Therefore in all transmission lines the outer boundaries were treated as perfect conductors. None of the outer boundaries are in contact with the chip where the circuit is drawn. It is an isolatd system. The length of center filament is 24 mm and the expected resonating frequency is 6.044GHz, which is the value obtained from A. Wallraff [28].

The solution to Equation 79 is probed by inputing frequencies which are the only variables neccessary to calculate the electromagnetic fields distributed through out the model. Restraints, can be applied to volumes (domains) and surfaces (boundaries). In other words these represent the boundary conditions for our PDE. For the domains a material is selected, Equation 79 differentiates one material from another due to their charecteristic pearmeability (μ_r), permittivity(ϵ_r) and conductivity (σ). For the outter domain the material assigned was air with ($\mu_r = 1$, $\epsilon_r = 1$ and $\sigma = 0$), the inner chip created with ($\mu_r = 1$, $\epsilon_r = 11.7$ and $\sigma = 0$) in order to emulate a dieletric, particularly silicon.

Furthermore the surface of the chip has a circuit drawn on it. The filament, ground plates and all other conducting surfaces were modeled as PECs. In addition to this the ground planes needed to be connected to the terminal. The top end of the terminal applies the voltage difference while the bottom end has V=0. This was achieved using the terminal properties shown on Figure 16.

3.3.2 Simplified Wave guide Simulation

The circuit we wish to simulate has a complex geometry. The original circuits has many small structures compared to the whole, there are also many turns which can cause errors due to poor mesh selection. To overcome this and separate the difficulties of mathematical modeling to geometry and design problem, we started with a model that has all the components of the original model, with the exception of the windy turns atributed to the original filament. This did make the process easier, as the success in this model turned into confidence to make the other model work. Furthermore there was the fundamental question, what are the turns for? There was speculation on weather it was just to fit the resonators in the chips, or if there were other reason.

The model was preset to 24 mm resonator length. The capacitive coupling is accomplished with an L shaped break in the PEC conducting strip. Along the filament runs a paralel ground plane separated by a non conducting gap (0.005[mm]) . The capacitor has a gap between plates of .002 [mm], The filament has a width of .01[mm].

The simplified wave guide was created to serve as a parameter to a more complex design. One wave guide consists of a capacitively coupled resonator to two lumped ports. Along side the strip line there are two ground planes these serve to direct the electric and magnetic field, this can be seen on Figure 18. Another attempt was made to model the wave guide from ref [28]. This wave guide has the same physics as the simplified model except it has a more complex geometry with turns. The simplified model was very useful due to faster simulation times and less troublesome geometry. It is coiled in a way that it fits in a 30 mm^2 silicon chip. The simplified version has the full 24mm and only .5 mm in width.

3.3.3 S-Parameters

S-parameters give insight as to how much of the signal is reflected or absorbed. S-parameters form a matrix of coefficients to describe signals sent from one port to another. On Figure 20 (a) there is an illustration which shows for example the S_{11} parameter which is the reflection coeficient. S_{21} on the other hand is the transmission coeficient. Since port 2 is off S_{12} and S_{22} equal zero. As for the smith-chart, it shows how well the impedance of your circuit is matched. When Re(z) = 1 (middle blue circle), the circuit is critically coupled and the feed port is transmitting maximum energy to the resonator.

For the purpose of this work only port one will be stimulated. Therefore we will have measurements for the reflected signal S_{11} and Transmited S_{12}. The other two matrix entries are empty.

$$M = \begin{bmatrix} S_{11} & S_{12} \\ S_{21} & S_{22} \end{bmatrix}$$

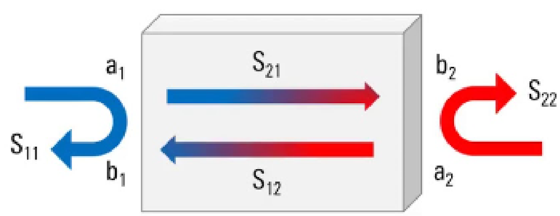

Figure 19: Illustration of S-Parameters [21]

3.3.4 Smith-Chart

When dealing with direct currents impedance matching is easier because resistance is a fixed real number. With alternating current the resistance gains an imaginary term related to the phase and how this phase propagates within the circuit. The impedance is given by Equation 80 which is a complex number. The imaginary part X is called reactance, it is derived from the circuits inductance and capacitance, $X = \omega L + 1/\omega C$. The real part of the impedance is the resistance. The key property of this chart is to enable impedance matching. For critical coupling the normalized reactance and resistance must be equal to 1. This point of critical coupling is exactly at the center of the chart seen on the left side of Figure 20.

$$Z = (R + iX) \tag{80}$$

Mathematically, it is known as a Möbius transformation which is given by the expression:

$$f = \frac{a + ib}{c + di}. \tag{81}$$

Where i is the complex variable and a,b, c and d are complex constants satisfying ad-bc ≠ 0. Möbius transformations is a general group of transformations to the common Cartesian coordinates. These can involve complicated combinations of translations, dilations, rotations and inversions. The Smith-Chart is a parabolic Möbius transformations such that z= (Γ + 1)/(-Γ + 1), a graphical representation can seen on the right side of Figure 20. A complex number Γ is ploted using the relationship afore mentioned, in the original coordinates horizontal axis represents the real part of Γ and the vertical axis corresponds to the imaginary part. The transformation to these axes causes progressive circles where the real part of z is constant, and the imaginary part is constant along parallel lines which originate at the far right of the chart seen on the left side of Figure 20. This chart makes it possible to visualize ressonant modes which gives new insight into the problem.

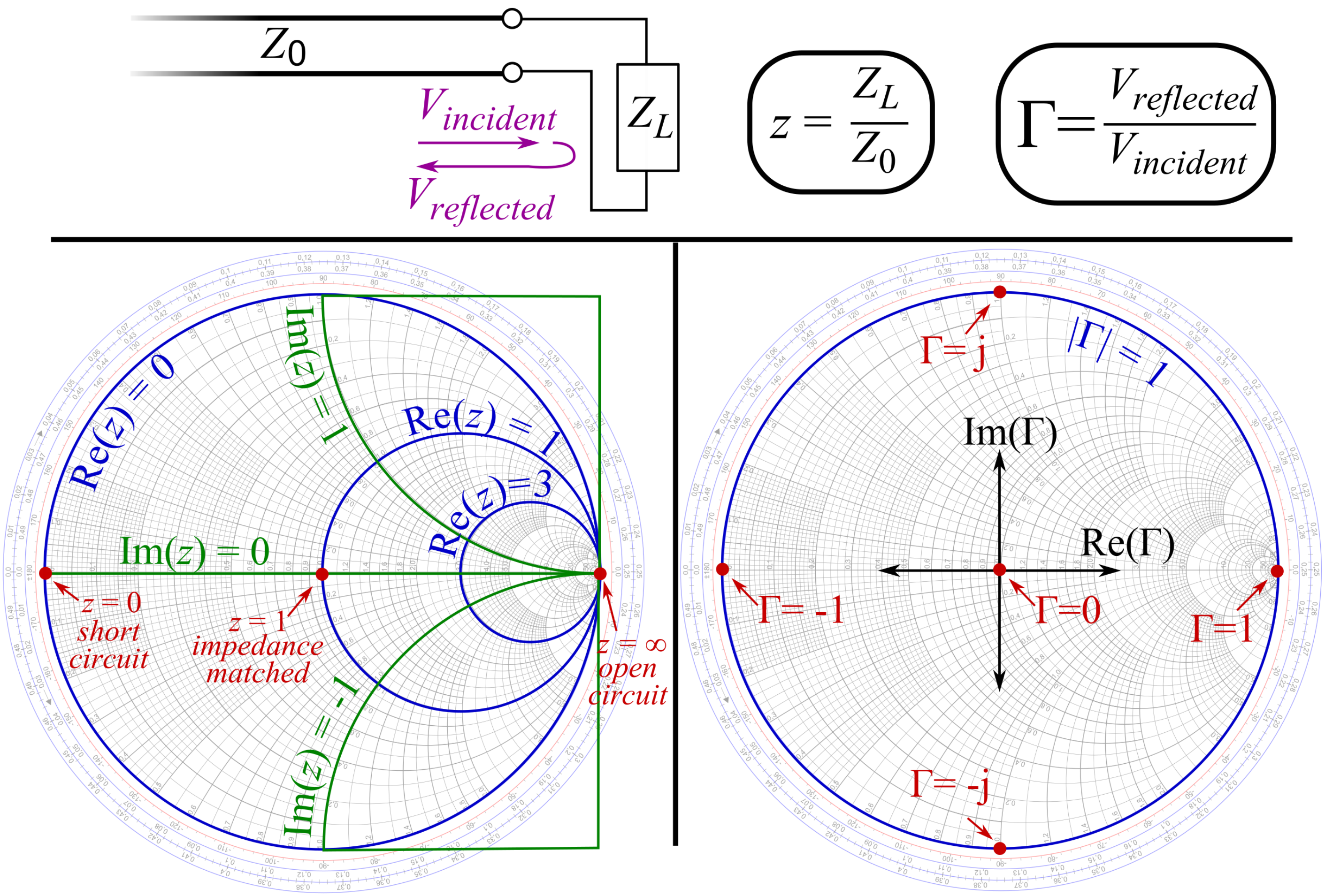

Figure 20: Smith-Chart reading guide[24]. The Im(z) lines correspond to imaginary parts of the impedance while the Re(z) represent the real part of the impedance. Smith-Chart via parabolic Möbius transformations of the type z= (Γ + 1)/(-Γ + 1).

3.3.5 Quality Factors

The quality factor is a way of measuring how much energy is lost by the resonator. High quality factors are needed for quantum computers, the long lifetime of the photon in the cavity ensures it will live long enough to interact with the qubit and enchange energy many times before the surrounding noise interferes. There are multiple ways for supercondcuting ressonator to dissipate energy.

$$Q = \omega \frac{average\ energy\ stored}{energyloss/second} = \frac{f_0}{\delta f} \tag{82}$$

During a cycle of the experiment seen in A. Wallraff, et al [28], the cavity is populated with one photon in average which is left to interact with the qubit, the cavity qubit coupling consists in the exchange of energy between cavity and qubit, therefore high Q factors are needed to ensure coupling will be observed.

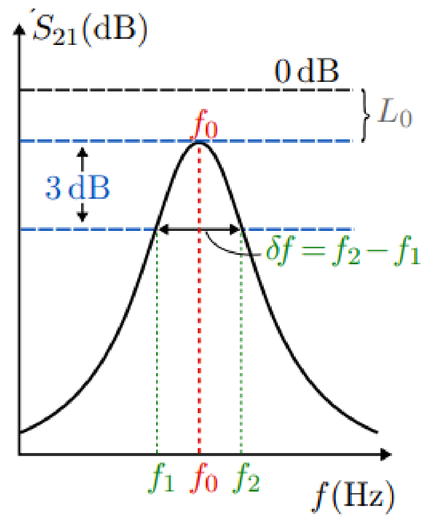

The transmission through a

resonator depending on the frequency.

Figure 21

There are many known processes through which a superconducting ressonator dissapates energy. For example, the fact that quasi particles (electrons) still exist in superconductors creates resistive dissipation. There can also be losses through the interaction of the ressonators electric field with the dipole moments in the dielectric, causing dielectric losses. This is just to exemplify factors that can contribute to a lower Q factor [25].

COMSOL Multiphysics can calculate the quality factor of a given mode of a ressonator. To do this, the eigenfrequency study of the Electromagnetic Waves package. For a given ressonator mode, COMSOL will calculate its Q factor.

3.4 Dipole perturbation in resonant cavity

This approach hopes to simulate how the small dipole moment of the cooper island affects the cavity. The concept is to insert a fixed dipole moment in the cavity. With this we hoped to gain insight into measurement analysis. This was not trivial due to the constraints that come with the physics in the Electromagnetic wave package (frequency domain) - COMSOL Multiphysics. This interface does not allow the introduction of a static electric field as an initial condition. To get around this, we have chosen to set up a terminal, in order to manually stimulate a tiny region in the cavity with an electric field. The next step was to place it in the cavity, in the model the cavity is the space between the resonator filament and the ground plane. The plan is then to find resonant modes of the resonator. Then study this model with the artificial dipole pointing up, down and off. For now this models aims to qualitatively illustrate the effects of a small perturbation in the cavity. In other words, the idea is to observe differences from bare to dressed cavity.

It should be noted however that adding a third port to our model, makes the S-parameter matrix 3x3 and due to the problem set up, the S-parameters are not automatically calculated. We do have access to parameters such as port impedance, which sheds some light on the matter.

3.5 Coupling a parallel LC circuit

This semiclassical approach is useful for analyzing the behavior of a charge qubit with distinct inductance L_J and capacitance C_J. An antenna like structure is placed in a cavity only the face is defined as a lumped element with inductance L_J and capacitance C_J. And this ressonating circuit can be coupled to the waveguide, and this system behaves in a similar way to our experiment, where a qubit is coupled to the waveguide. Furthermore the quantum properties of this system can be calculated using the model from the article, "Black-box superconducting circuit quantification", Simon E. Nigg, et al. of Yale University (USA)[19]. Published in 2012 this article shows how simulations made in the

HFSS program were able to correctly map the low energy levels of a cavity system coupled to an LC circuit.

In this model the qubit is modeled as having a fixed inductance L_J and capacitance C_J, the anarmonicity of the qubit is viewed as a perturbation and can be calculated via $E_{nl} = -\Theta_0^2\phi^4/(24E_J)$ being that $\Theta_0 = \hbar/2e$. The capacitance is determined via Charging Energy $C_J = e^2/(2E_C)$ and inductance is related to the Josephson Energy $L_J = -\Theta_0^2/E_J$.

This is work in progress, however it is definitely where the potential for the COMSOL software to aid laboratory production of qubits rests. This is a means of predicting qubit lifetimes and how it will effectively interact with the cavity, by the state dependent ressonating frequency shift.

3.6 Math module - Partial Differential Equations (PDE) - COMSOL Multiphysics

A quantum mechanical aproach to the simulation of Josephson Junctions would be considering three dimensional domains and applying the Hamiltonian for a Cooper pair, it's possible to calculate the energy levels it could possibly occupy. The ultimate goal would be to observe the Josephson Equations effect through these simulations. To conceive this model the partial differential equations section of the Math module from COMSOL Multiphysics was chosen. We will show here how the coefficients where used to produce Schrodinger's equation. Essencialy applying this equation will result in an spatial wave function. From which i will calculate the probability density $|\Psi^2|$.

The equation desired is the Schrodinger equation (Eq. 7) for a non relativistic particle. The PDE provides the general form PDE seen on Equation 83.

$$\lambda^2 e_a\Psi - \lambda d_a\Psi + \nabla\cdot(-c\nabla\Psi - \alpha\Psi + \gamma) + \beta\cdot\nabla\Psi + a\Psi = f \tag{83}$$

By using $e_a = 0$, $\alpha = 0$, $\gamma = 0$, $\beta = 0$, $f = 0$

$$-\lambda d_a\Psi - c\nabla^2\Psi + a\Psi = 0 \tag{84}$$

Next we take $d_a = 1$, $c = \hbar^2/2m$, $a = V$

$$-\lambda\Psi + \frac{-\hbar^2}{2m}\nabla^2\Psi + V\Psi = 0 \tag{85}$$

This equation was applied to a circle with 3 barriers as can be seen in the Figure 22. What differentiates the barrier from the super conductor is the value of the Potential V. In the superconducting material $V = 0$ in the barriers it has the value of $V = 6,2415 \times 10^{-7} eV$. The other boundary condition is imposed to confine the cooper pairs to the ring, this is done via Dirichlet boundary condition applied to the all external boundaries. This boundary condition sets Ψ to a fixed value, in this case 0. The ring is the micrometer scale with an inner radius of $14\mu m$ and outer radius of $16\mu m$, further more the height is $2\mu m$. Next using the eigenvalue study, we calculate values for lambda which represents the energy. We also get values for Ψ, by plotting $|\Psi^2|$ we get a probability density of our Cooper pair for a determined λ or energy level. We can also calculate Equation 15 to find the super current density probability.

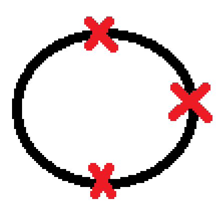

Figure 22: In this image we have an illustration to represent the three dimensional ring which we will attempt to model. The Potential Barriers are depicted by the red X symbol.

4 Results and Discussion

The process of creating quantum circuits is usually done with thin film deposition technology and lithography. The process of creating qubits will be done in two steps: first the transmission line is created, and then the qubit is built on a second deposition process. The ideal goal of the simulations is to forecast new better devices, at this point we are still far from that. This work aims to produce similar results to the ones observed in experiment, to serve as a basis for future model projections. Therefore we want to understand what is it that creates high quality cavities. The next step would be to simulate the cavity-qubit interaction, we are still in the preliminary process of this step and these results will be seen in section 4.3. In the Section 4.2 there is another method of simulating this interaction, however with less moving parts.

In Section 4.4 the Partial Differential Equations module was used to attempt to recover the josephson relations. Now I think this was not the best method solving this problem. However the model seems to sucessfully model the spatial probabilty density of a cooper pair in a ring with 3 barriers representing the JJs.

In Figure 23, we illustrate the principles. In Figure 23 (A) we show the first step which is the cavity which is discussed in section 4.1. Figure 23 (B) and (C) correspond to sections 4.3 and 4.2 respectively.

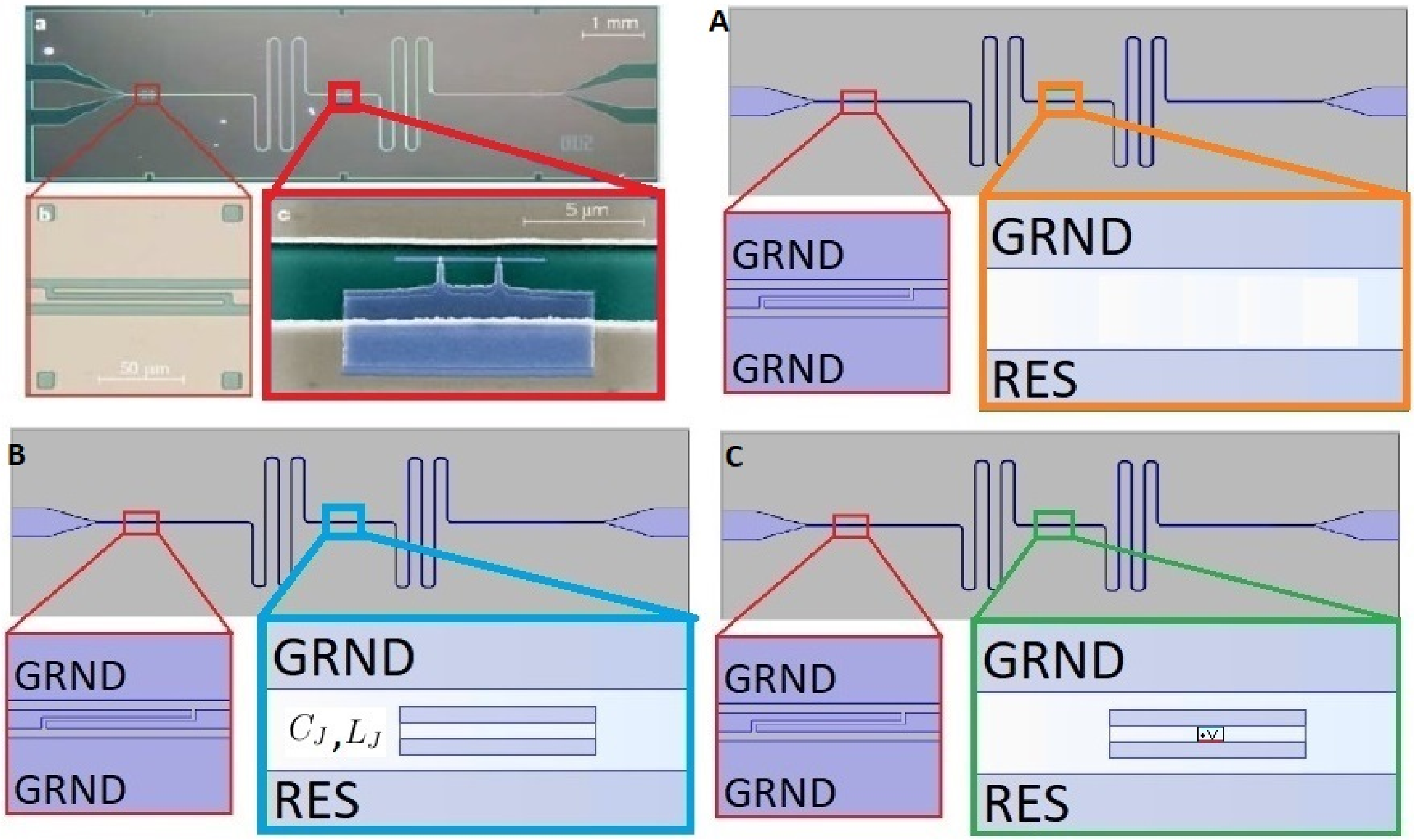

Figure 23: On the top left side is an image of the original circuit extracted from from the article published in Nature magazine by A. Wallraf, et al [28]. On the top right we have the bare cavity simulation. On the bottom left is the geometric representation of the coupled LC circuit, similarly on the bottom right a terminal was placed instead of the lumped element.

4.1 Transmission Line Resonator

This collection of results on transmission lines show the efforts made to simulate a transmission line described in the article published by A. Wallraff, et al [28]. This was done in two different parts. The original geometry often presented convergence problems due to its heteregeneous geometry. Therefore a simplified geometry was created to overcome this difficulty. The simplified model proved useful for testing new configurations. This is because the original circuit requires on average a longer simulation times. The main tools for characterization of the transmission line are the refractive and transmission indexes which will be presented here. These graphs point out the frequencies that represent cavity modes. Through these results we want to understand how these modes work, what makes a cavity useful for quantum computing and how can these simulations aid us in this goal.

4.1.1 Original Wave guide Simulation

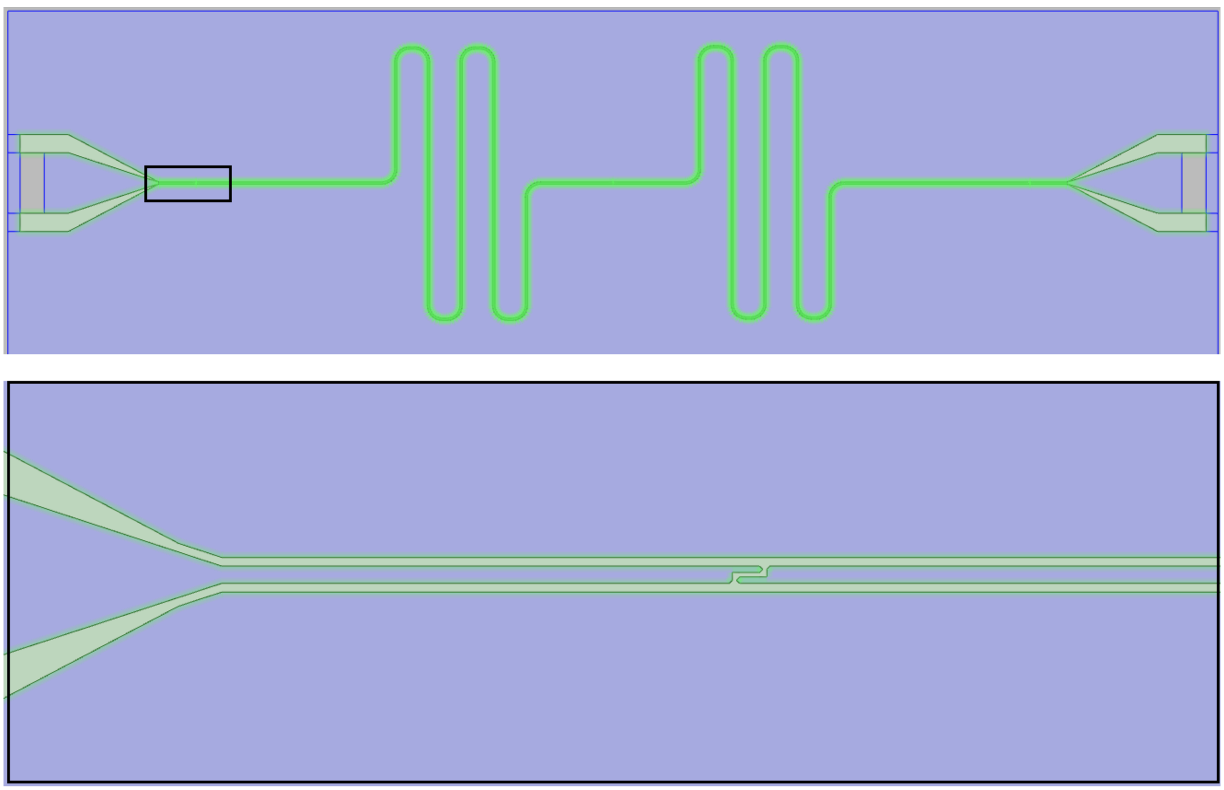

Figure 24: The blue surfaces indicate PEC boundaries, here it is shown how the parallel ground planes were connected to the ground end of the terminal via a PEC surface extending from the terminal to the paralel plates running along the filament. Note grey areas are not perfectly conducting and display material properties of Silicone which the whole chip is made of. It should also be noted that are no other conducting surfaces on the sides or bottom of the chip. All conducting surfaces in the circuit can be seen on this image. The gray box which surrounds the chip in all directions is a chamber with permittivity and permeability equal to air.

Through the information gathered in this work, hopes to have accomplished the goal of setting up a transmission line model similar to the one used in the experiment presented by A. Wallraff, et al [28].

The substrate has the properties of silicone, that is $\epsilon_r = 11$ &, $\mu_r = 1$ as for the conductivity $\sigma = 10^{-12}$ [S/m] which is nearly equal to zero. The fillament was made out be 24 [mm] long.

4.1.2 Lumped Port Set Up

The port design is not trivial, the currents extending along the port do influence the modes in the dieletric. Therefore the port must be placed in such a way that it does not cause fields that disturb the natural modes of the resonator. To my best knowledge, these interactions will not help the task at hand. It would seem controversial to design a ressonator to have interference caused by the input cable. Some of the results displayed here however, were done with an alternate port set up. This set up

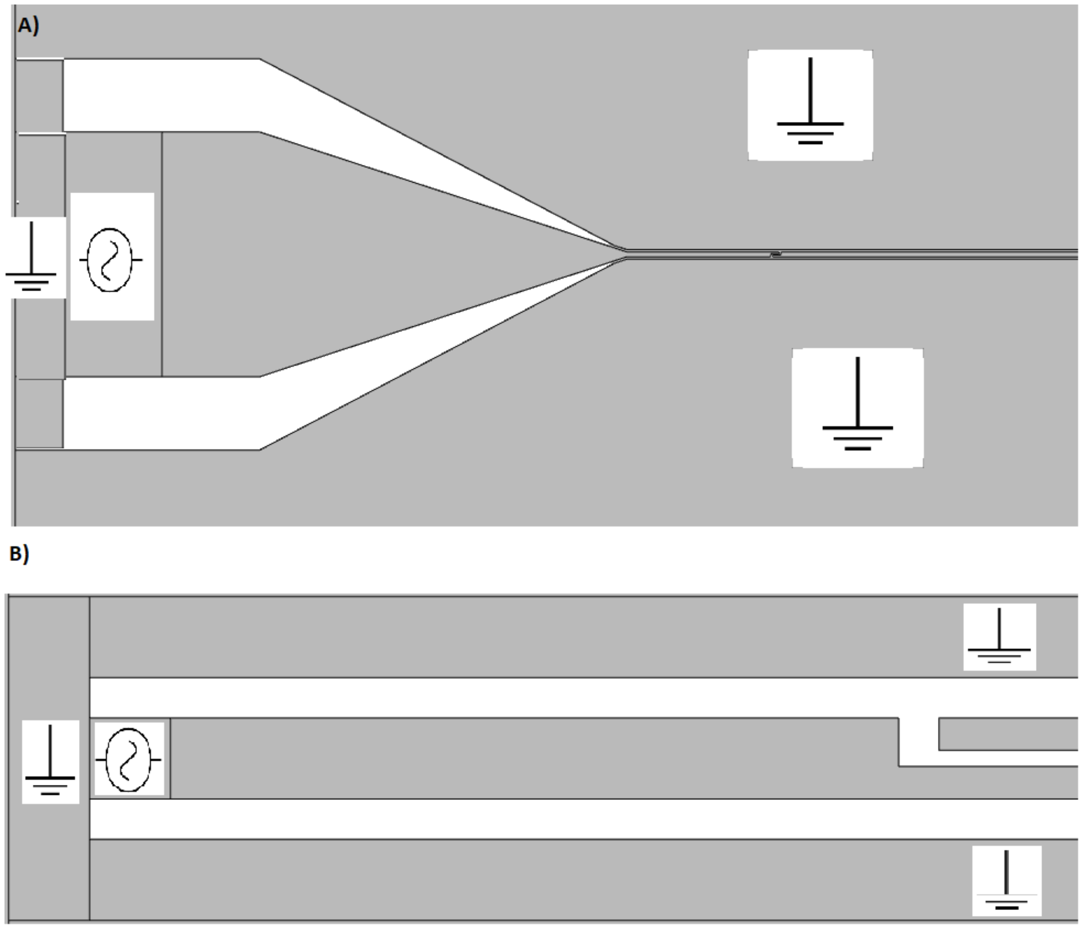

Figure 25: This image shows how the port was set up. The circle-inscribed "s" is the symbol for input AC applied to the circuit. The port was set up to have oscilating voltage on the right side, and ground on the left. The conductive boundaries extend the surface kept at 0 [V] to run along the ressonator as seen in the image. Both the Original design (A) and the simplified circuit (B) have the same set up.

4.1.3 Original Wave Guide Simulation - S - parameter

In this section, I will expose a collection of results, the first being what to the best of my knowledge is the most faithful to the original model. From the frequency domain study, the S-parameter graph is displayed on Figure 26. Next the Eigenfrequencies calculated with their respective Q-factors. In the following sub sections I will show other relevant results which corroborated to this final result.

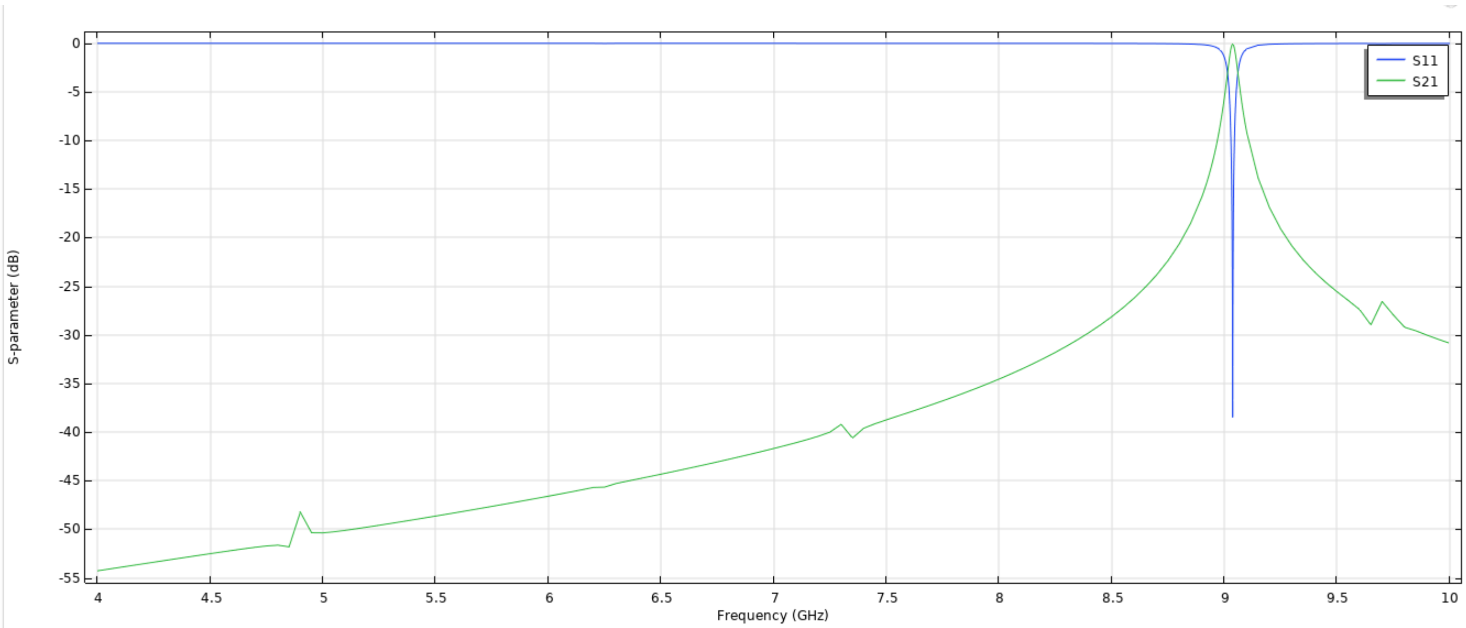

Figure 26: S parameter from 4 - 8.6 GHz with 125 MHz intervals, 8.6 - 9.1 GHz 1MHz interval and 9.1-10 GHz with 125 MHz intervals

Eigenfrequency (GHz)	Quality factor (1)
2.4420	5.1109E5
3.1385+0.0026977i	581.71
4.8919	2.8719E5
6.2467+0.0044182i	706.93
7.3269	1.4502E5
9.0370+0.023210i	194.68
9.6785+0.0068941i	701.94
9.7772	1.4533E5
10.892+0.0088471i	615.54
12.202+1.8895E-4i	32287
12.548+0.0075634i	829.52
14.666	90256

Figure 27: Quality factor distribution

4.1.4 Original Wave Guide Simulation with resonance near 6.044 GHz

This mode of the strong circuit was found as the effects of varying permeability and permittivity had on the resonant modes. It should be noted that this used a different port set up. The port is on the side of the chip, however for the overall configuration is the same, just placed in different place geometrically.

The length of center filament is 24 mm and the resonating frequency of 6.039GHz. The electric field at resonating frequency can be seen in Figure 28. The substrate permeability and permittivity were arbitrarily chosen and the value was $\epsilon_r = 50$ &, $\mu_r = 50$ as for the conductivity $\sigma = 0$ S/m.

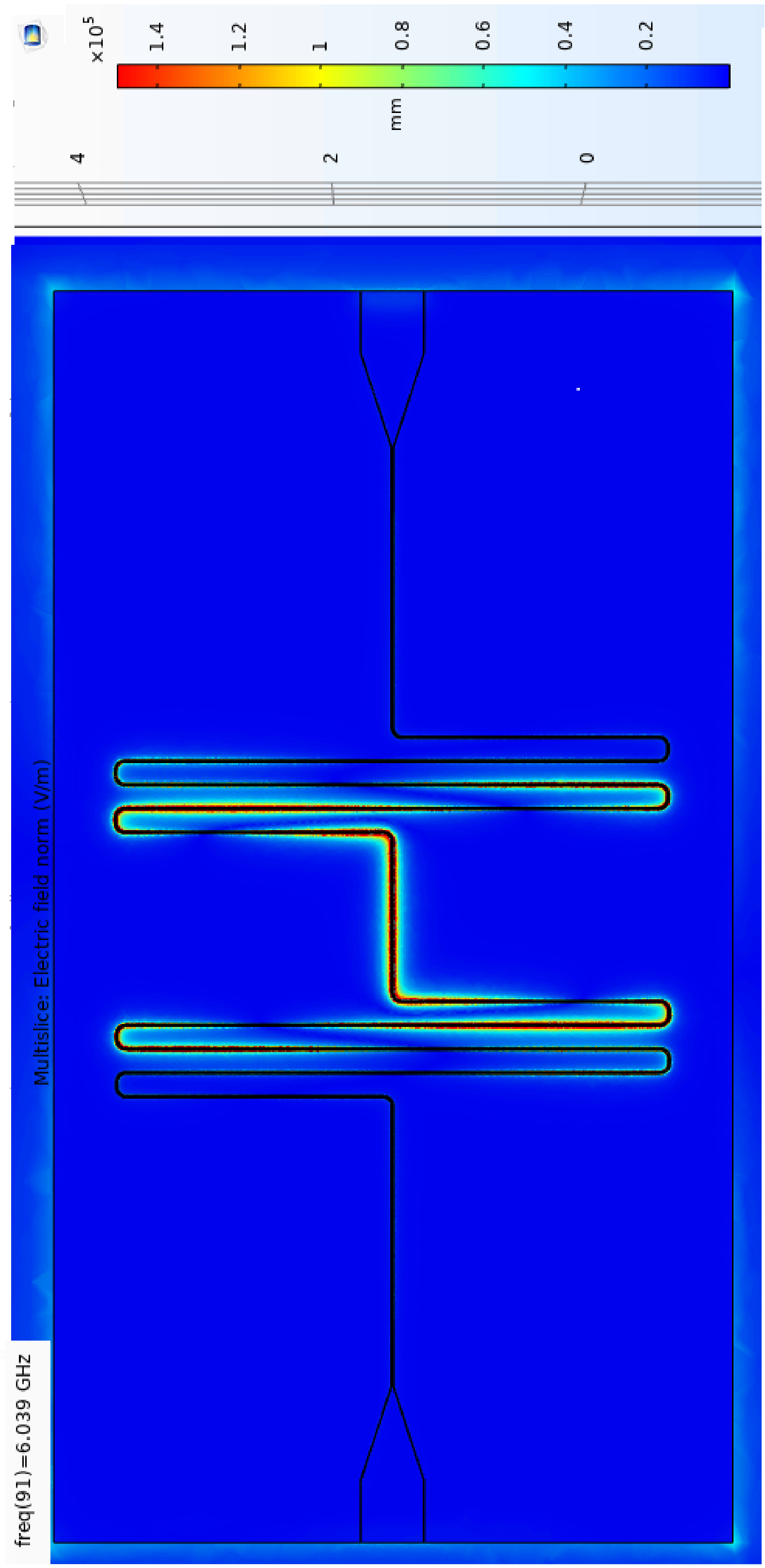

Figure 28: The electric field of the wave guide simulation on COMSOL Multiphysics resonating at 6.039 GHz. The scale is V/m.

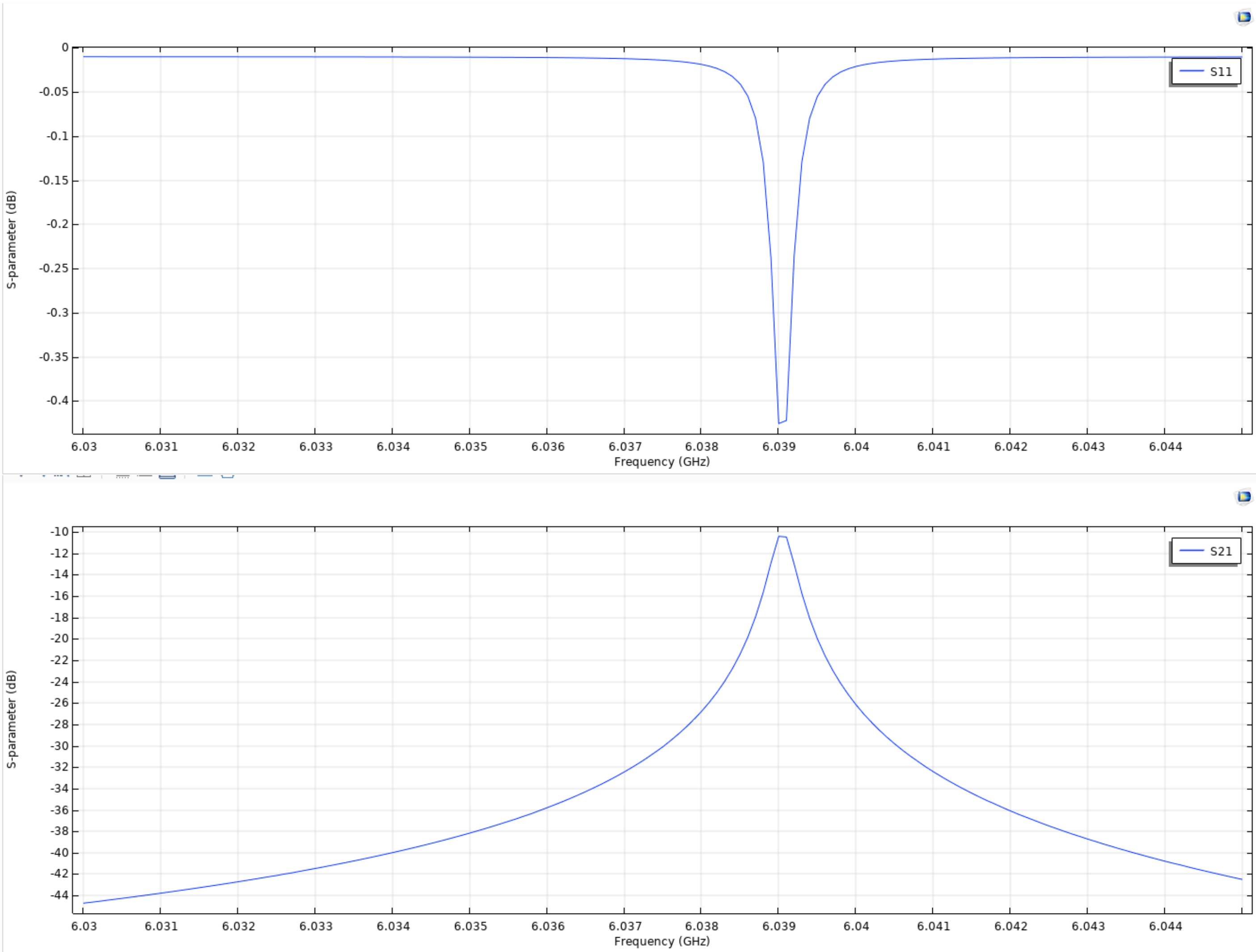

Figure 29: The top graph shows the magnitude of the S_{12} parameter which is a transmission index. The peak of S_{12} is directly related to the characteristic resonance frequency.The bottom graph shows the magnitude of the S_{11} parameter which is a reflection index. It was plotted separately from the S_{12} due to the large difference in scale. In this graph the cavity is empty, and it is resonating in the same 6.039 GHz which is close to the 6.044 GHz as in the article [28]

By reading the smith chart, its obvious that this transmission line is not critically coupled. Additional attempts are being conducted to have this improved.

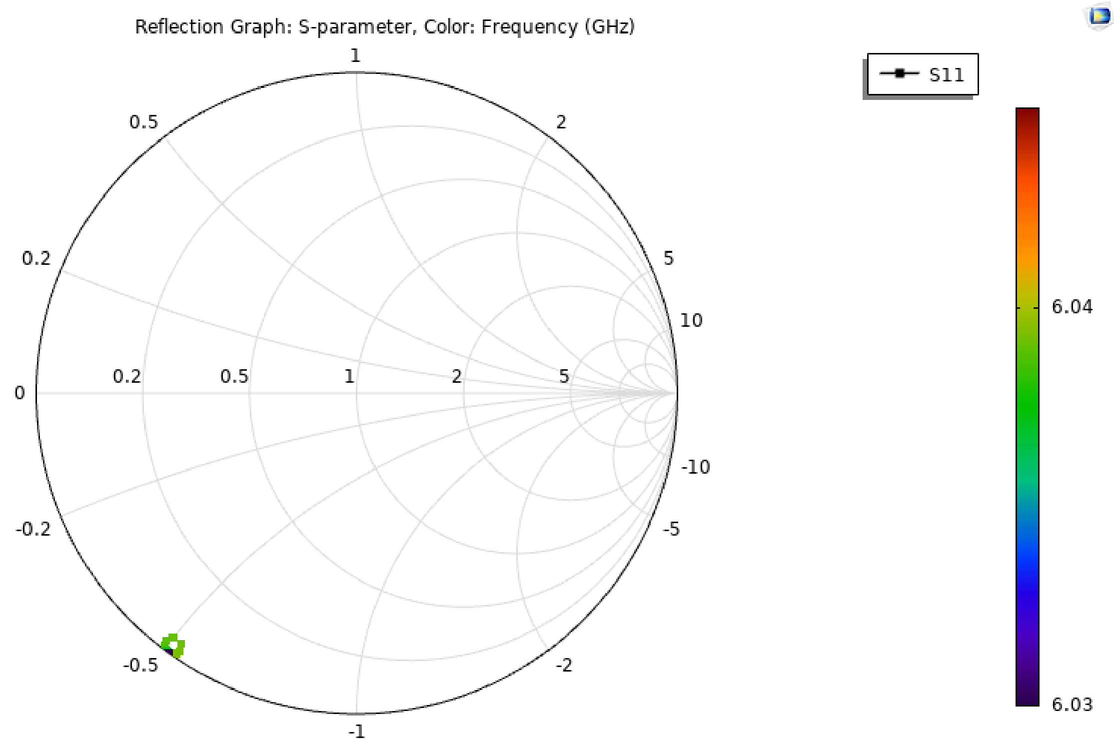

Figure 30: This smith chart is of a simplified model transmission line whose resonance mode is 6,045 GHz.

4.1.5 Manipulating resonant modes

As the results presented in Section 4.1.1 did not present the desired resonant mode, the goal became to understand what could be done to achieve this. Several modifications were made to the geometry, boundary conditions and material properties. The focus was to produce a resonant wave guide at the frequency of 6.044GHz. However, after a certain effort to obtain this result, the importance of the values of permeability and permittivity of the substrate was discovered. For simulations that resulted in Figure 34 the values $\epsilon_r = 11$ &, $\mu_r = 1$. If we think of mechanical waves such as sound, stroking the chord of a guitar in a swimming pool would be the analogue to operate the resonator with a substrate of low permittivity and permeability. In Figure 31 we can see how signal absorption and reflection changes when we gradually increase the permeability and permittivity of the medium. Thus enabling a way to control the vibrational modes of the transmission lines.

The graphs seen in Figure 31 represent a study conducted in the reference circuit citestrong, to determine the effect of substrate permeability and permittivity on the absorption index S_{12} and the reflection index S_{11}. They were tested (0/0, 20/20, 50/50, 80/80, 300/300), the results are shown in the following chart. As we can see as permeability is increased permittivity, the absorption index and the number of normal modes are increased on average. In this image the original circuit was swept from 5,000 to 7,000 GHz with intervals of 10 MHz. For (0/0, 300/300) the solution did not converge.

80/80

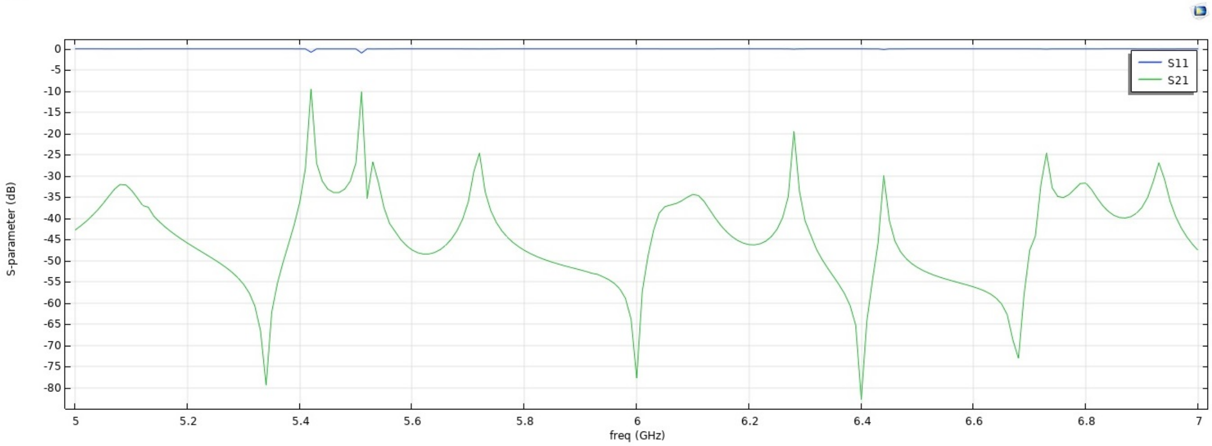

50/50

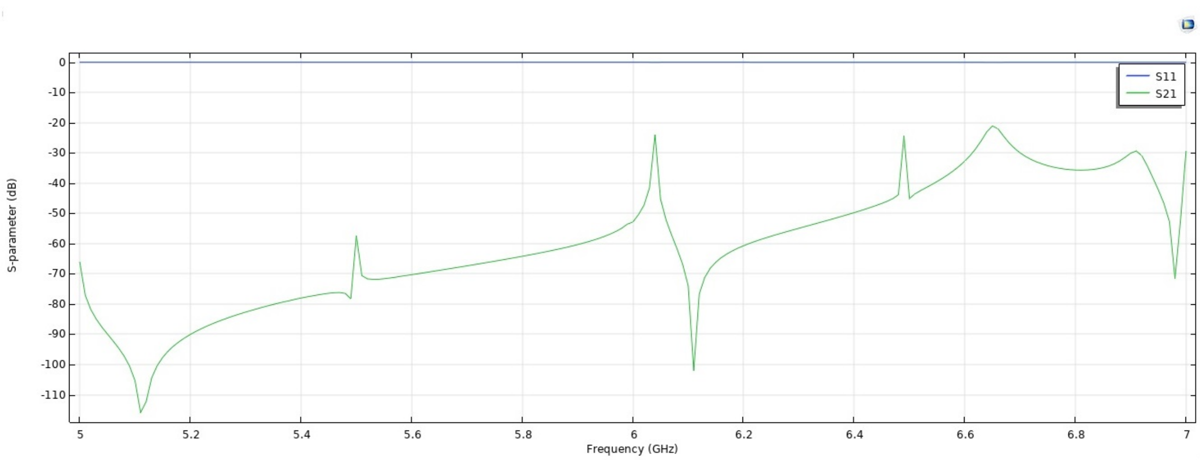

20/20

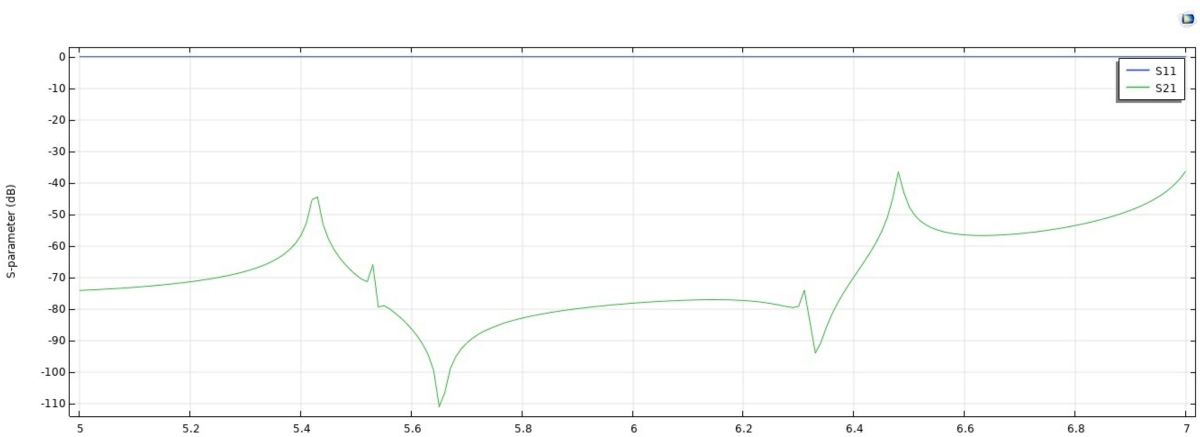

Figure 31: Permeability and permittivity of the substrate with values (0/0, 20/20, 50/50, 80/80, 300/300), and in the charts are the absorption indexes S_{12} and in the reflection index S_{11}. Spectrometry was made from 5 to 7 GHz ranging .01 GHz.

4.1.6 Simplified Wave guide Simulation 24mm silicone substrate

This result comes from the simplified model which to the best of my knowledge presents the correct conditions as presented by A. Wallraff, et al [28]. The substrate has the properties of silicone, that is $\epsilon_r = 11$ &, $\mu_r = 1$ as for the conductivity $\sigma = 10^{-12}$ [S/m] which is nearly equal to zero. There is one visible critically coupled mode present, at 5.6855 GHz. We notice this due to the fact it reaches 100% power output. By comparing this model to the latter we find that the curves in the original circuit induce magnetic fields witch act against the currents and therefore don't allow as much power to be absorbed.

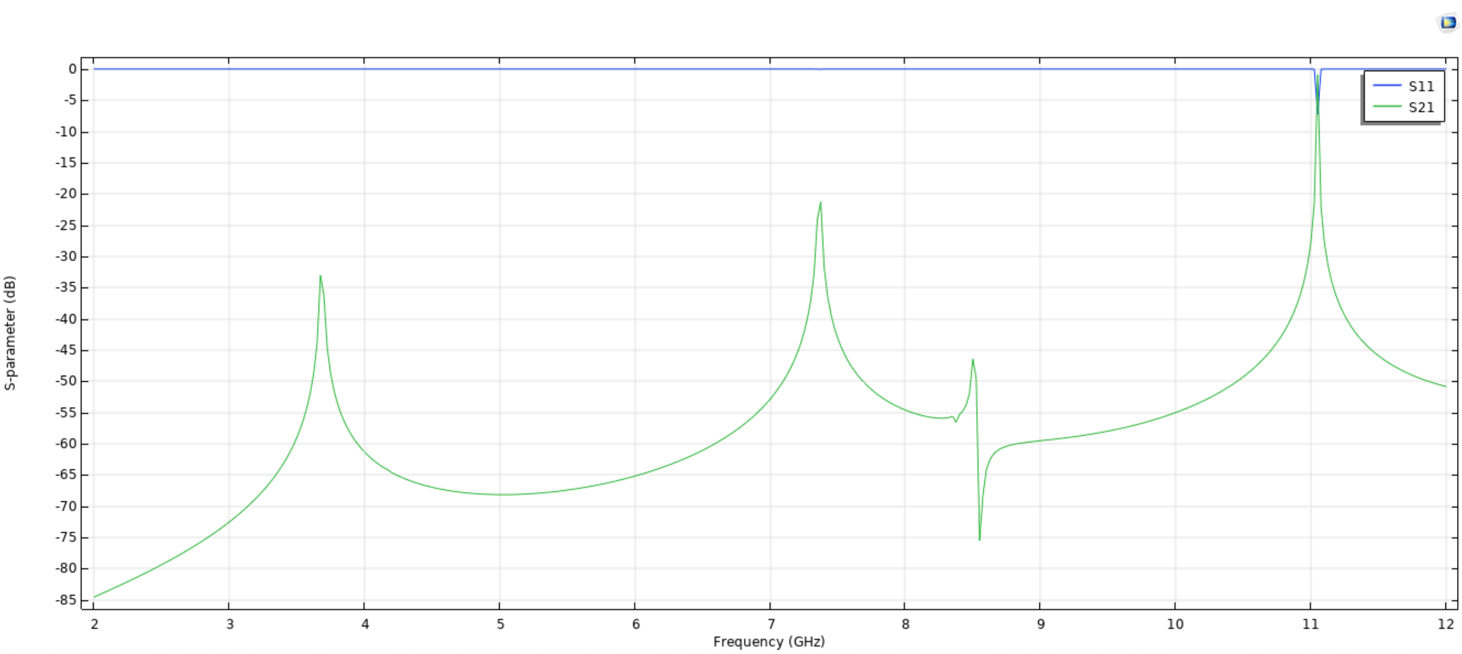

Figure 32: S parameter from 2 - 12 GHz with 10 MHz intervals.

In Figure 33 we have the magnetic and electric fields for a plane perpendicular to the resonator. This image can be compared to the Figure 18 (bottom).

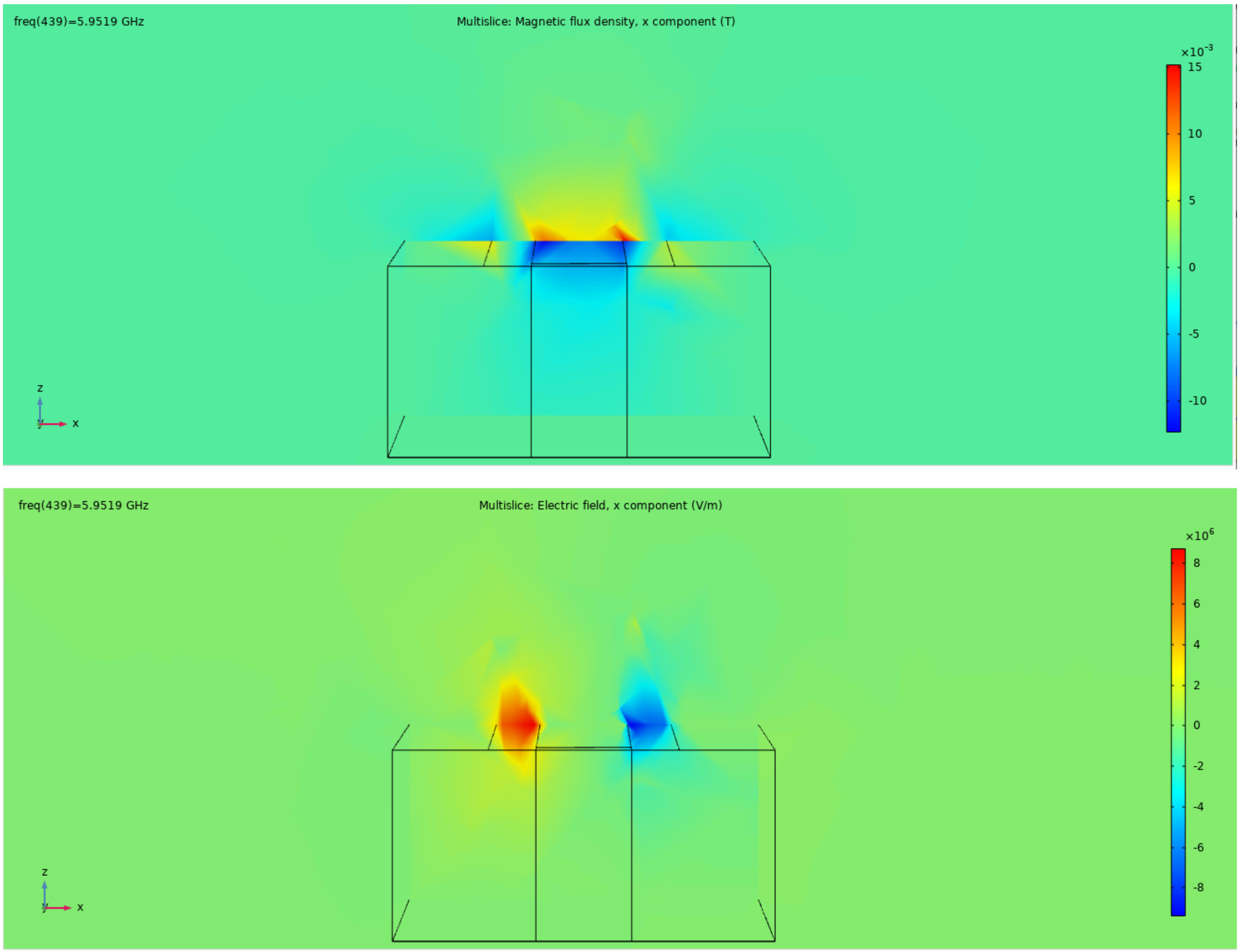

Figure 33: This image shows electromagnetic field in the direction perpendicular to resonator. The top image being the electric field and the bottom the magnetic field at resonant frequency.

4.1.7 Simplified wave guide simulation with resonance near 6.044 GHz

For the simplified circuit the resonator length was varied to achieve resonance at 6.045 GHz. At first the filament had 24 mm, a study was done to sweep the range from 4 to 8 GHz. By varying the length of the filament the closest resonance mode was moved onto the desired frequency of 6.045 GHz, and the final length is $l = 19,611[mm]$. As can be seen in Figure 34. This chart has resolutions ranging, first been swept from 6.030 to 6.042 ranging from 100 KHz, followed from 6.0420 to 6.046 ranging from 20 KHz, and last from 6.046 to 6.060 ranging from 100 KHz.

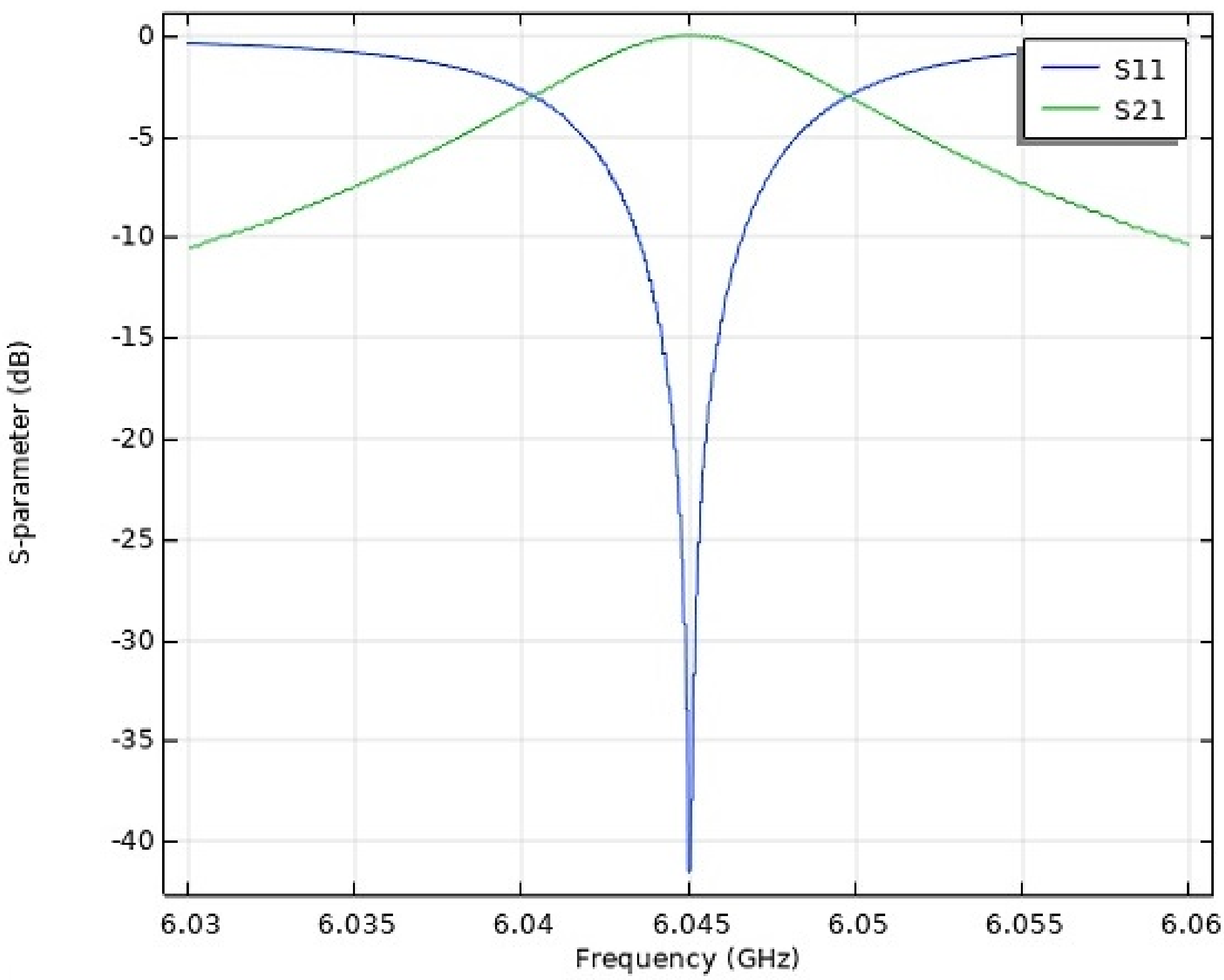

Figure 34: This plot is of a simplified model transmission line whose resonance mode is 6,045 GHz. On the y-axis we have the magnitude in dB and on the x axis the frequencies.

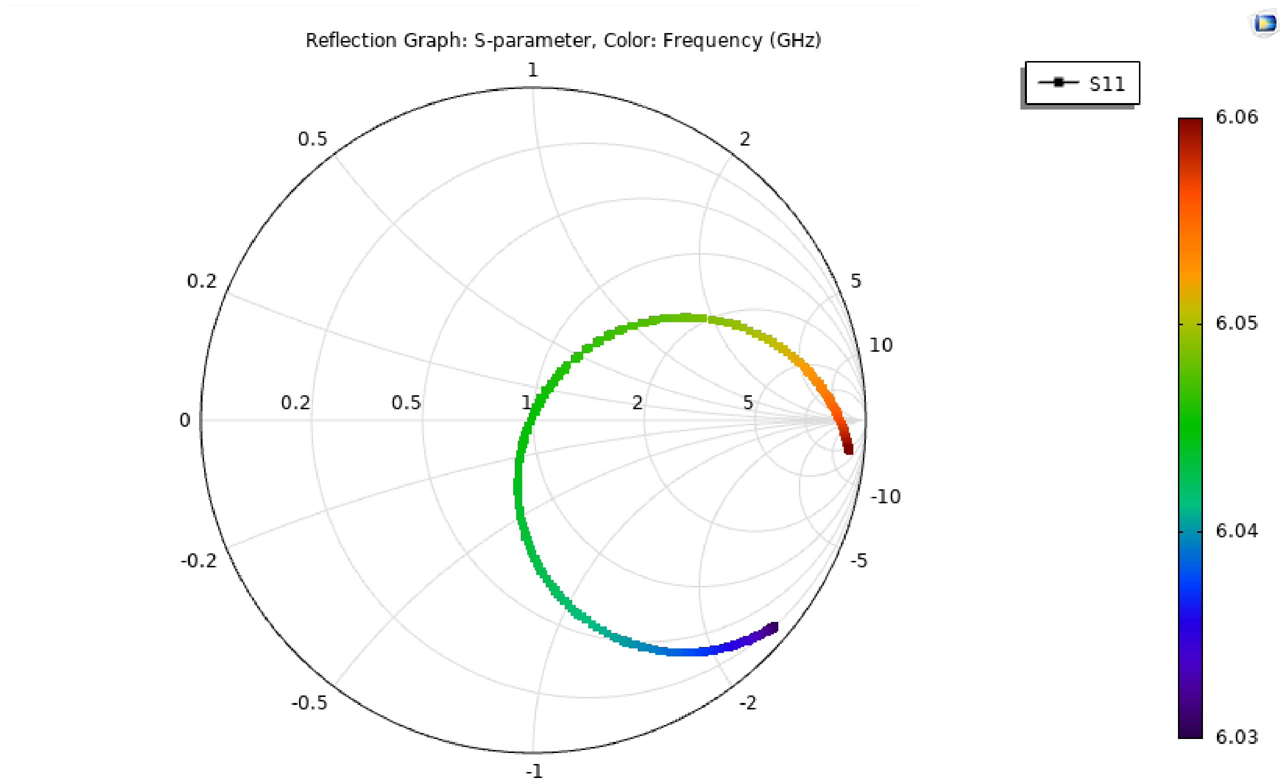

Figure 35: This Smith-chart is of a simplified model transmission line whose resonance mode is 6,045 GHz. This shows that our transmission line is close to being critically coupled to the feed.

4.2 Dipole Cavity Coupling

The measurement of superconducting qubits is achieved throught a transmission measurement of the resonator [28]. The goal of this simulation is to show that there are measurable changes in the signals read which could show what the state of the qubit is. Althought in the real experiment energy in the ressonator must be meticulously controled as to not disturb the system. We aim here to have a qualitative evaluation of the problem.

First it was necessary to show that it was possible to polarize an object. I did this in a separate model, this can be seen in the Image 36. Next a two dimensional version of this was created and placed in the cavity, next the already know resonant mode was swept for different polarizations.

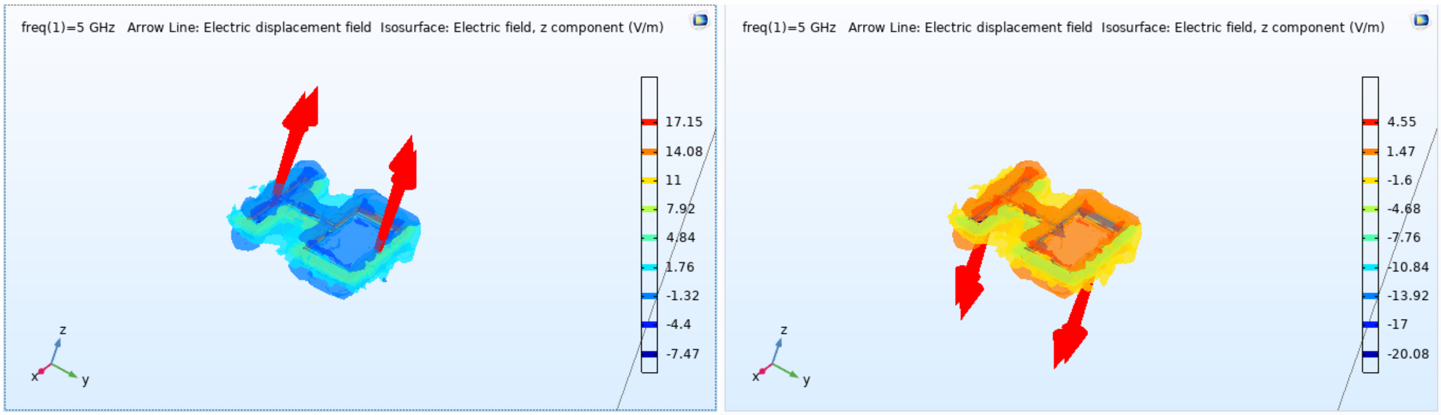

Figure 36: This image is of a polarized dielectric simulated in the RF module. The frequency applied to the object is the same, but the phase difference is equal to π. The electric displacement Field is represented by arrow graph. This serves to qualitatively illustrate the successful reproduction of a polarized object. The isosurface graph was used to map the electric field in the Z direction (V/m). On the left the phase of the port = 0 and on the right it is equal to π [28]

An intresting observation is that the small port has little effect on the field around it, this is evidence that the system is being treated as a perturbation, this can be seen in the Figure 36. This happens because the port power output depends on its size, more study needs to be made to approximate this to realistic value. As can be seen on Figure 38 (bottom) the electric field around the qubit is basically the same for both, demonstrating that this port is a perturbation. The two bars running parallel to the resonator are PECs they serve as the a mediator of the electric field. allowing the interaction between cavity and lumped Port. Also on Figure 38 we can see that we successfully alter the impedance of port one. The impedance is a measure of resistance, and here through this model we show that 10 μm dipole will affect a 24 mm long resonator. This allows for reading of the qubit state through the overall system impedance, this is an analog to quantum non demolition process of state detection. In the figure 38 , when ϕ = 0 the qubit is in phase with the resonator and the fields are orientated in the same direction. When the port is off there is a measurable decrease in phase, and by placing the qubit orientation opposite to the resonator, a bigger drop in the phase is observed.

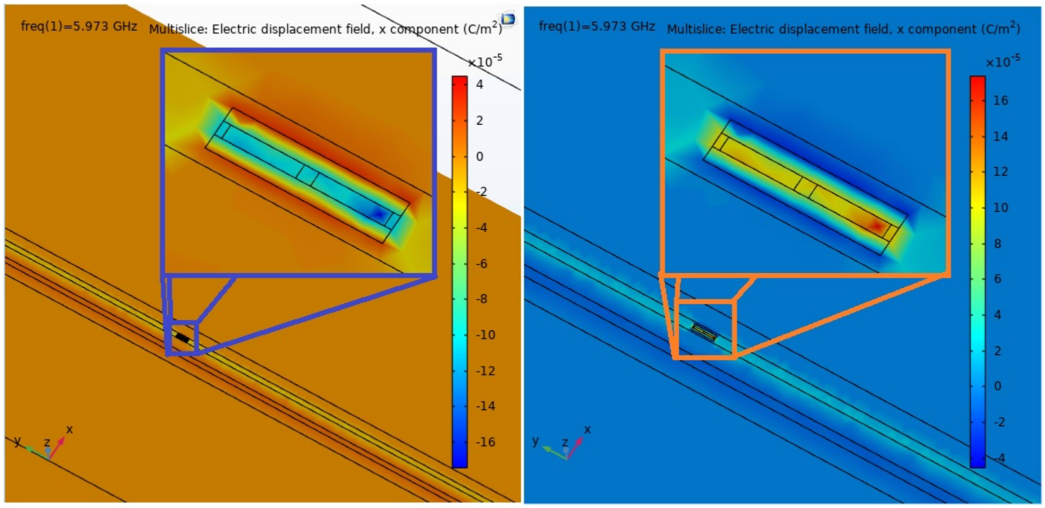

Figure 37

When ϕ = 0 the dipole is in phase with resonator, when $\phi = \pi$ the dipole is out of phase with resonator. In the simulations it was verified that phase of the impedance changed significantly for each particular case, as can be seen in the Figure 38. These results are are only qualitative as the energy scales from the experiment need to be compared to the ones used here for validation.

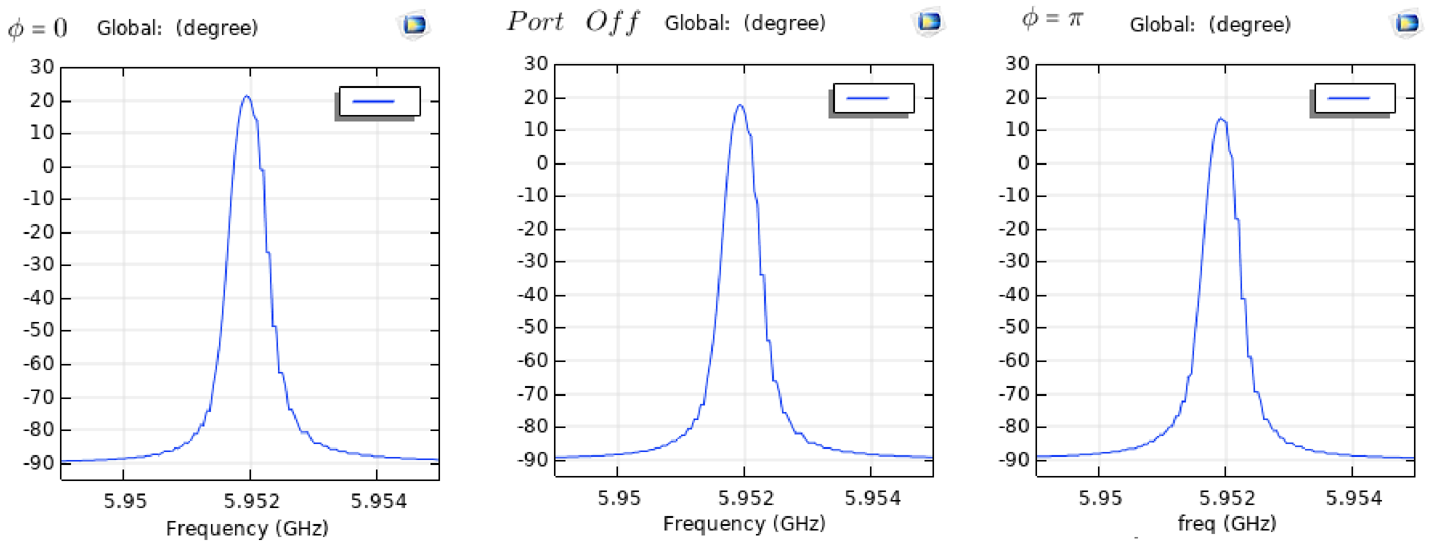

$$\uparrow \quad \phi = 0 \quad - - - > \quad Phase\ of\ the\ port\ impedance = 23.1\ degrees$$
$$\varnothing \quad Port\ Off \quad - - - > \quad Phase\ of\ the\ port\ impedance = 19.4\ degrees$$
$$\downarrow \quad \phi = \pi \quad - - > \quad Phase\ of\ the\ port\ impedance = 15.2\ degrees$$

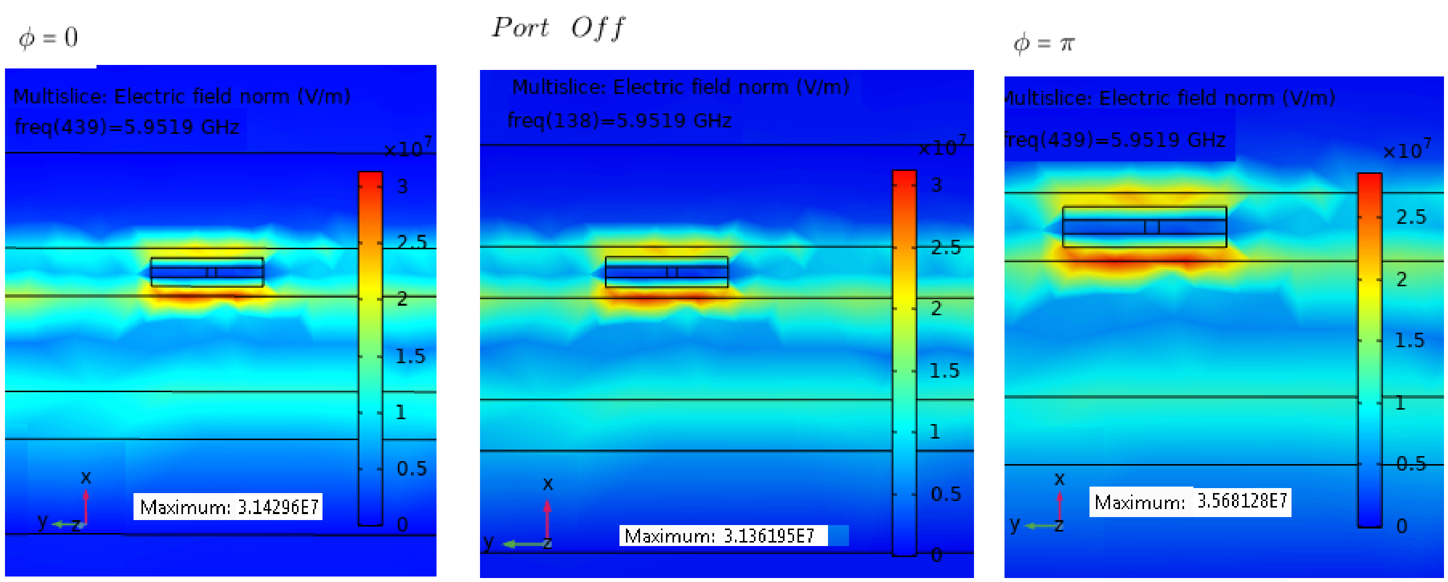

Figure 38: This graph was done by scanning the simplified line transmission, from 5.948 to 5.956 GHz ranging from 500 KHz. In the chart, we can see the impedance phase in degrees. We can see that it changes slightly for each configuration.

We can compare these results with the ones presented in the article by A. Wallraff, et al [28].

The results we hopped to reproduced are displayed in the Figure 39. There is a predicted resonant frequency shift. There is a technicality involving calculating the resonant frequency and using more then 2 ports in a model which prevented the calculation of the resonant frequency. However a shift in the phase of the impedance implies there might be a change in the resonant frequency. So this would be a next step to this model.

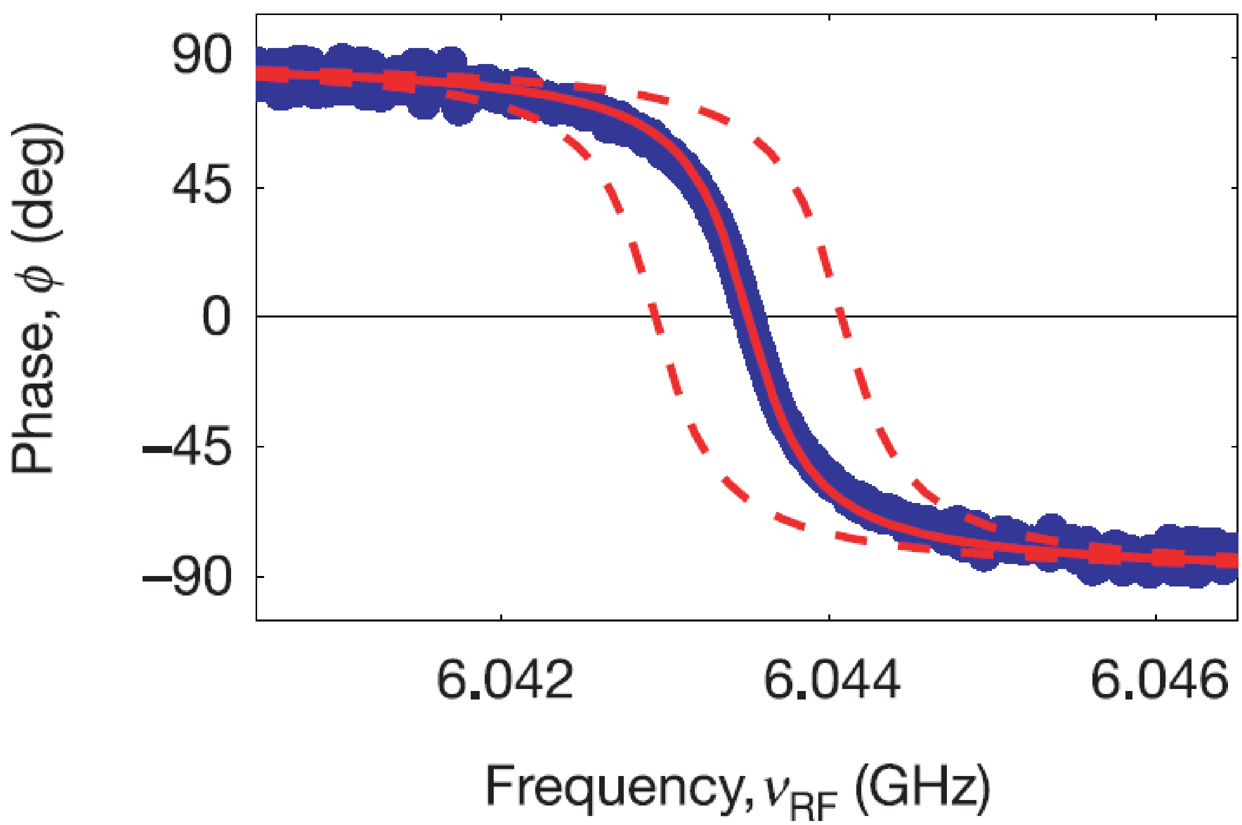

Figure 39: These results were extracted and adapted from the article by A. Wallraff, et al [28]. Here we see a graph a with experimental results in blue, a solid red line for the fit and dashed red lines represent predicted results.

4.3 Coupling a Parallel LC Circuit

The attempt to couple an LC circuit the cavity has the potential to be a useful tool for laboratory day-to-day. Through this it is possible to estimate the impedance of the antenna cavity system. The inverse of impedance is an equation given by the Equation 86. Y(c) is the inverse of the impedance of the antenna cavity system that is calculated by COMSOL Multiphysics. The roots of the imaginary part of the Equation 86 it is possible to calculate the Hamiltonian of low energies. This step is in progress but it is now possible to draw important conclusions of the graphic in Figure 40, and this result is an important milestone in progress.

$$Y(\omega) = i\omega C_J + \frac{i}{\omega L_J} + Y(c) \tag{86}$$

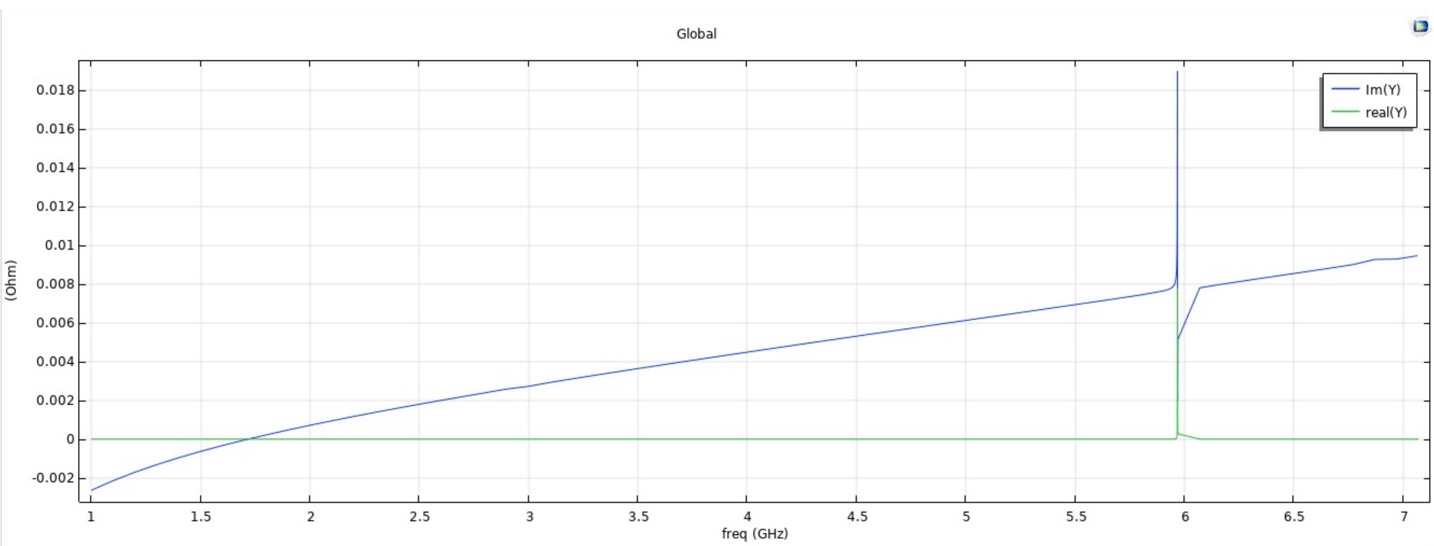

Figure 40: Graph of the imaginary and real parts of the impedance inverse.

In the graph seen in Figure 40 it is possible to extract the modes that cause the excitation between the fundamental level and the first excited level of the qubit. That in this graph we have $\nu_{01} = 1.717$ GHz and the first cavity mode $\nu_c = 5.968$ GHz. From this simulation it is also possible to calculate the quality factor of the cavity, which in turn allows to estimate the coherence times of the qubit. In addition, the qubit anarmonicity can also be calculated. These are work in progress.

4.4 Math Module - Partial Differential Equations (PDE) - COMSOL Multiphysics

In this model Equation 85 was applied to a circle with 3 barriers as can be seen in the Figure 41.

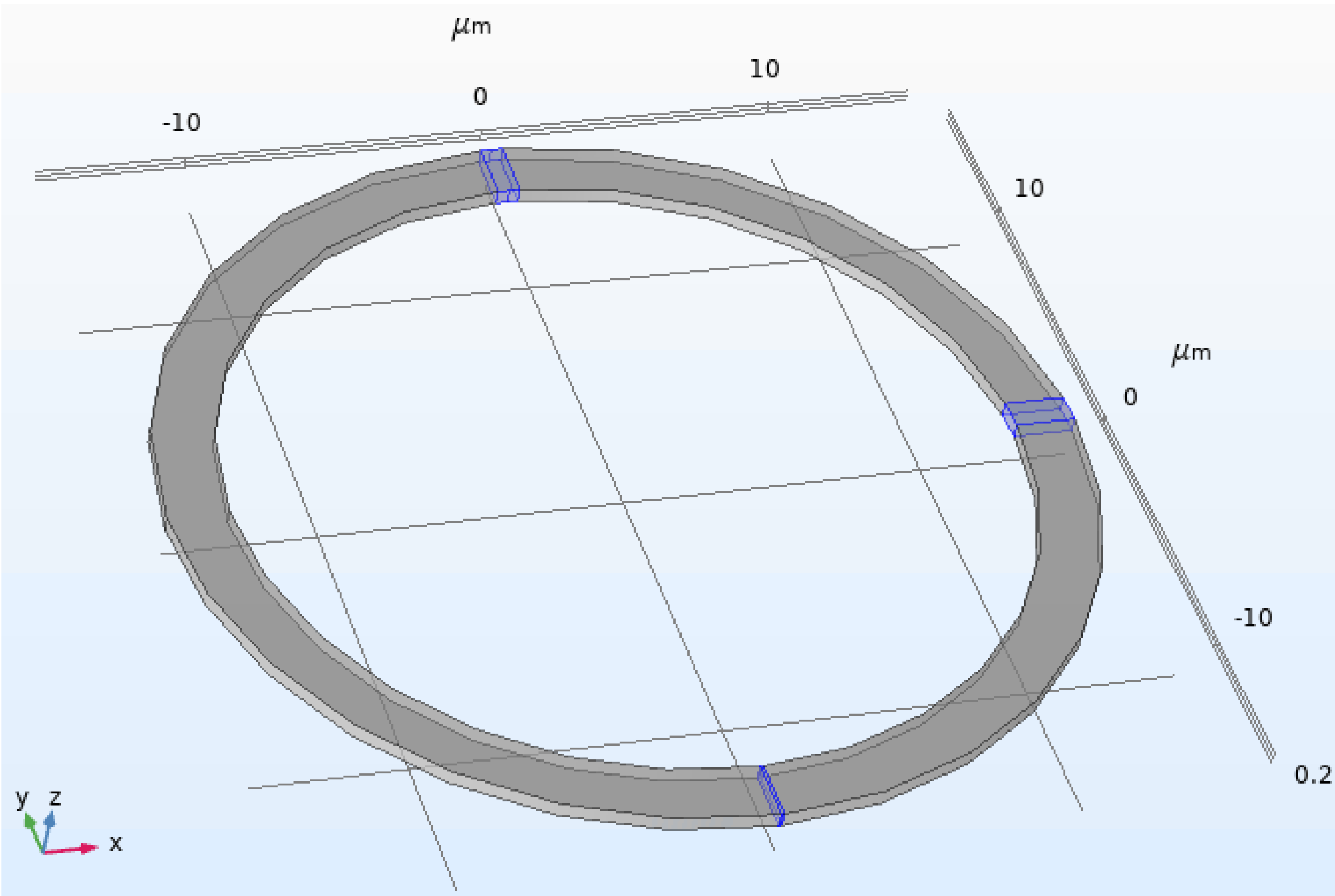

Figure 41: In this image we have a three dimensional perspective of the superconducting ring of the geometry used in the PDE interface. The selected domains in blue have $V \neq 0$.

The barriers have widths of 1.00 μm, 0.75 μm and 0.012 μm. And the calculated energy values are seen in Equation 87. Furthermore $|\psi(x, y, z)^2|$ is plotted on the Figure 42. This gives us the position probability for the center of mass of the Cooper pair.

$$
\begin{aligned}
\lambda_0 &= \quad 204.960 \;\; MHz \\
\lambda_1 &= \quad 205.293 \;\; MHz \quad ; \quad \Delta_{01} = 0.333 MHz \\
\lambda_2 &= \quad 205.946 \;\; MHz \quad ; \quad \Delta_{12} = 0.653 MHz \\
\lambda_3 &= \quad 206.408 \;\; MHz \quad ; \quad \Delta_{23} = 0.462 MHz
\end{aligned}
\tag{87}
$$

$$
\begin{aligned}
-i\hbar\lambda_0 &= \quad -2.1615E-26 \;\; J \\
-i\hbar\lambda_1 &= \quad -2.165E-26 \;\; J \quad ; \quad \Delta_{01} = 3.5117E-29J \\
-i\hbar\lambda_2 &= \quad -2.1718E-26 \;\; J \quad ; \quad \Delta_{12} = 6.8864E-29J \\
-i\hbar\lambda_3 &= \quad -2.1767E-26 \;\; J \quad ; \quad \Delta_{23} = 4.8721E-29J
\end{aligned}
\tag{88}
$$

This model shows anharmonic properties as the energy levels are not evenly spaced out. This can be see by different Δ values in figure 87 in MHz or Figure 88 in Joules. Furthermore we can study perturbations in the Hamiltonian such as a sinusoidal potential applied over the ring. The action of the electric field either flushes the superconducting particle to the far left or far right as can be seen in the Figure 43.

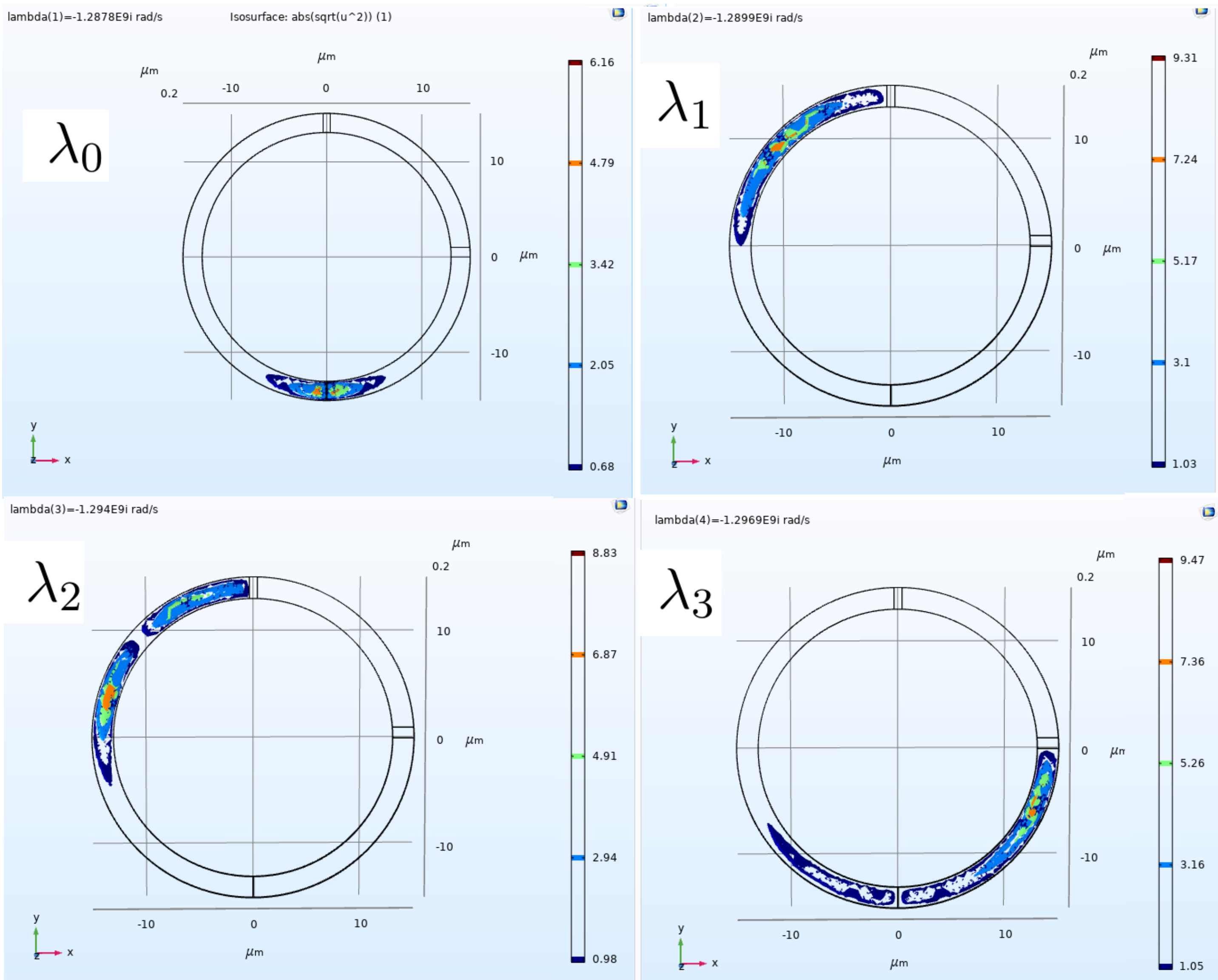

Figure 42: In this image we have a three dimensional plot of the position probability of the Cooper pair. Then function is not normalized so the values for $|\psi(x, y, z)^2|$ are merely qualitative. Nonetheless the higher value of $|\psi(x, y, z)^2|$ does indicate a higher probability. The first 4 energy levels are plotted.

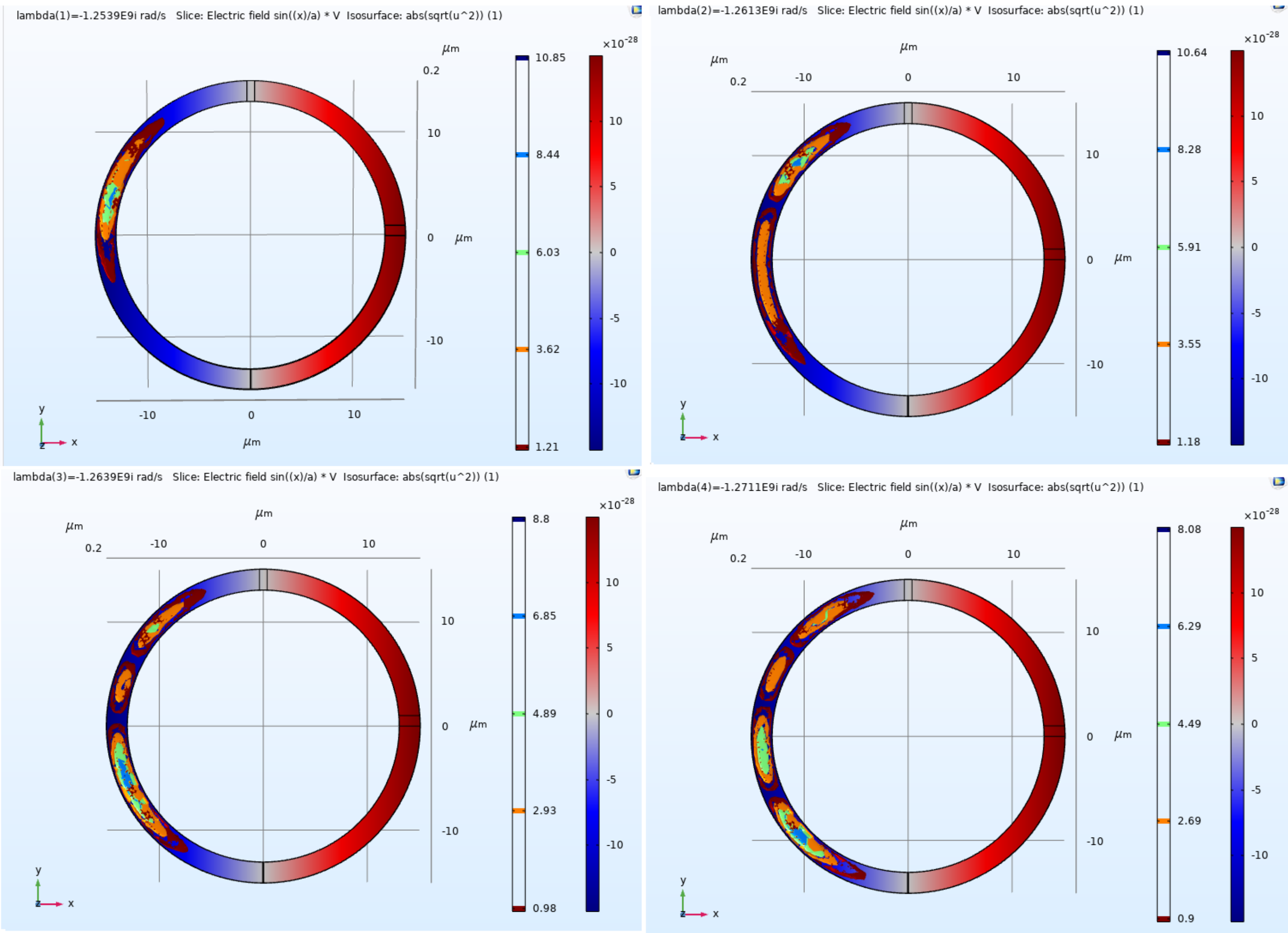

Figure 43: In this image we have a three dimensional plot of the position probability of the Cooper pair. With an sinusoidal electric field applied over the ring, the right side positive and the left negative. The first 4 energy levels are plotted from top to bottom.

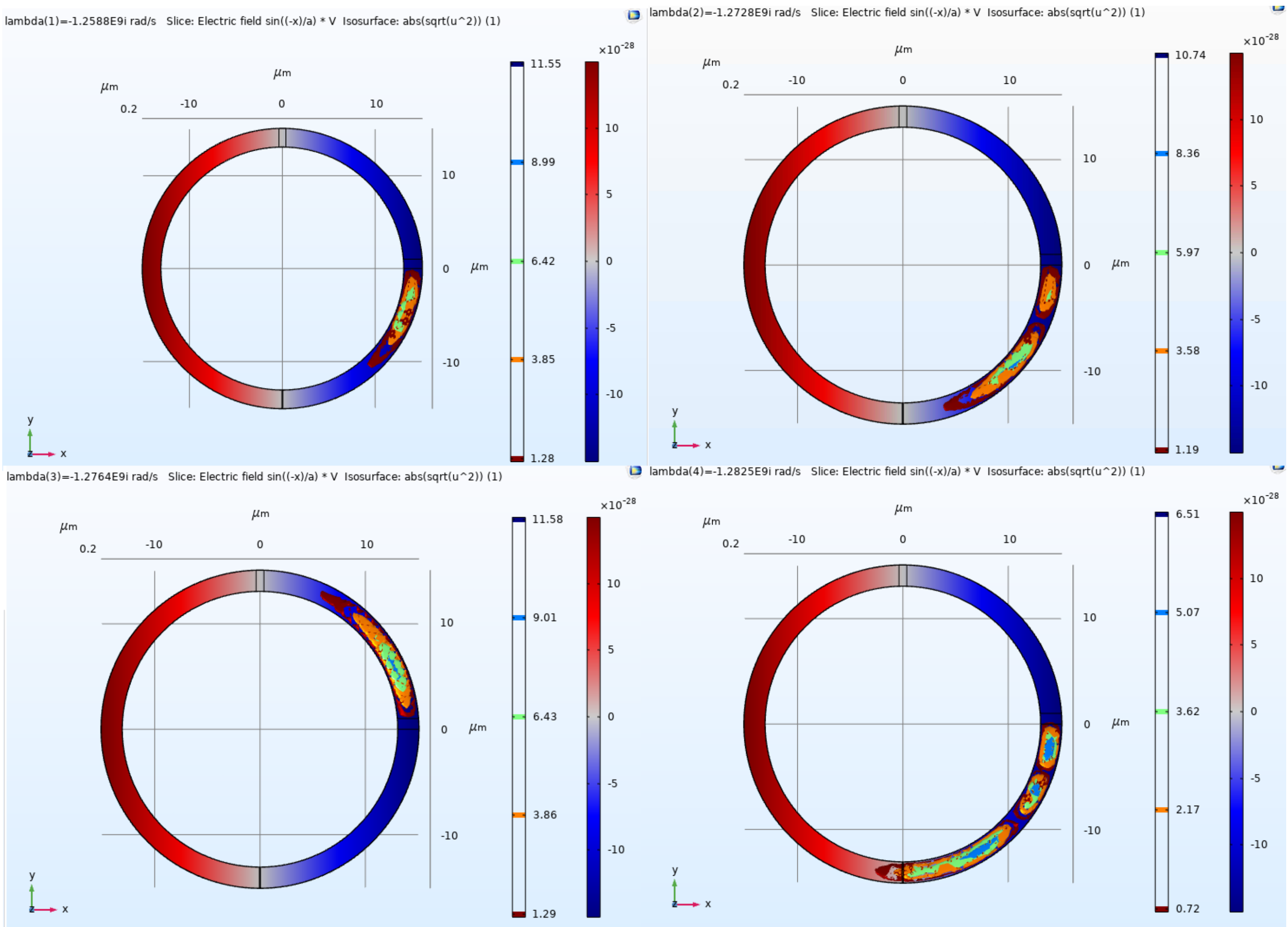

Figure 44: In this image we have a three dimensional plot of the position probability of the Cooper pair. With an sinusoidal electric field applied over the ring, the right side positive and the left negative. The first 4 energy levels are plotted from top to bottom.

The equation 15 was used to plot the current density probability seen on figure 45.

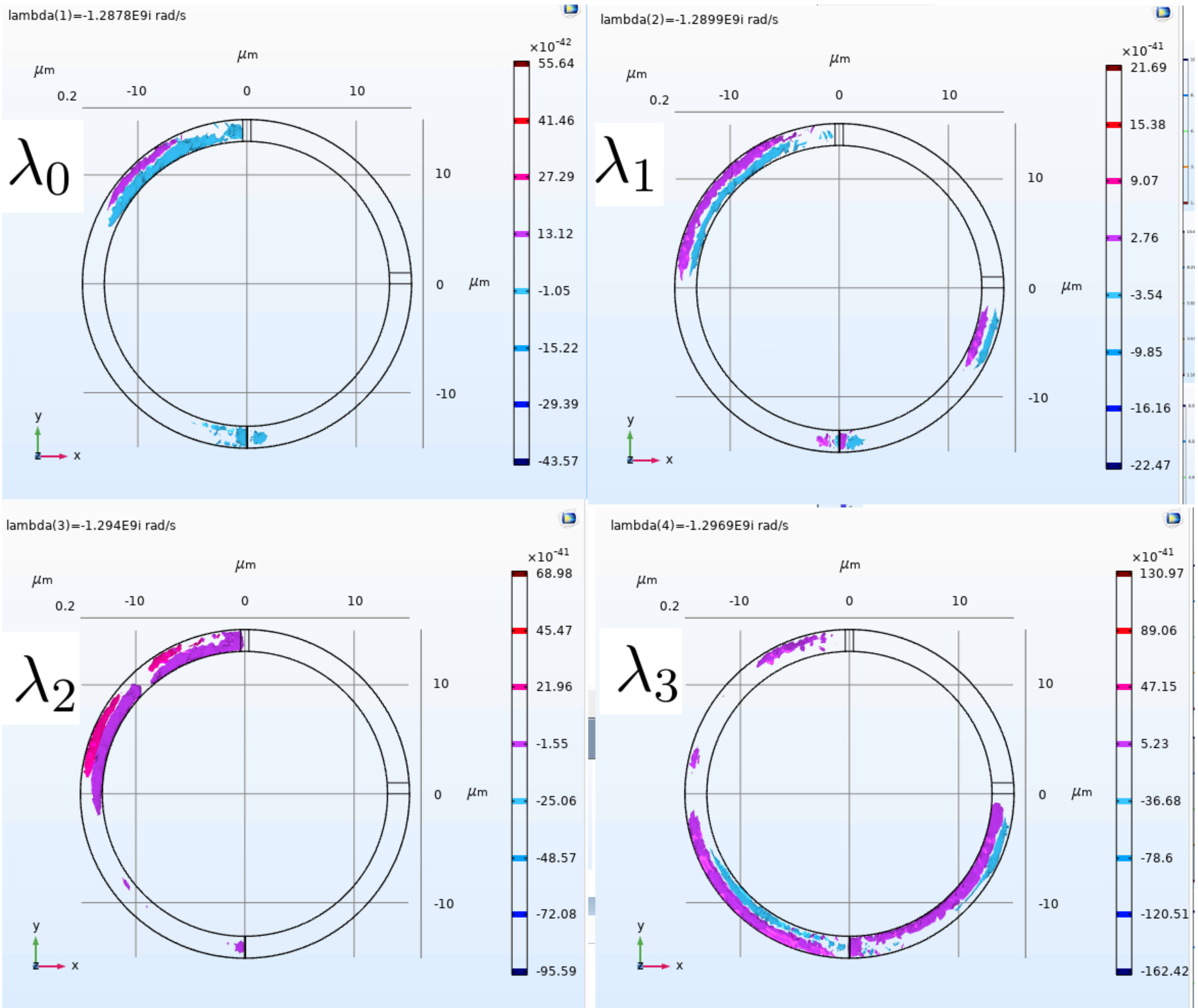

Figure 45: In this image we have a three dimensional plot of the current density probability in $A * m$. The first 4 energy levels are plotted.

5 Conclusion

The results presented in in Section 4 show that COMSOL Multiphysics is a tool that could successfully aid the production of quantum electrical circuits with coupled qubits. Simulations ease the understanding of concepts and enables sharing of these concepts with others, this promotes debate and the overall project evolution. Furthermore through the use of some more quantitative simulations such as the ones regarding transmission line ressonators, COMSOL could enable a measurable advantage in the production of prototypes.

The process of recreating the experiment from scratch, demands criterious judgement on what are the variables that can affect the overall result. This enables to create a deeper understanding of a problem empirically, starting at the basic undestanding and moving on forward to understanding how more complicated interactions can come to happen. First we discussed how we could find cavity modes using COMSOL Multiphysics and next introduced ways of manipulating these modes. This leads me to believe that having laboratory results could help to tune these models to experimental data. This would enable the projection of new circuits with optimized characteristics. The qualitative results aid the overall understanding of the phenomena and simplifies the physics, but going a step a further to help save time and effort in the quest for a reliable qubit is the ultimate goal.

References

[1] Frank Arute et al. “Quantum supremacy using a programmable superconducting processor”. In: *Nature* 574.7779 (Oct. 2019), pp. 505–510. ISSN: 1476-4687. DOI: 10.1038/s41586-019-1666-5. URL: https://doi.org/10.1038/s41586-019-1666-5.

[2] P. Cappallaro. *MIT xPRO Program: Quantum Computing Fundamentals lecture*. Aug. 2019.

[3] Conrad Clauß et al. “Broadband electron spin resonance from 500 MHz to 40 GHz using superconducting coplanar waveguides”. In: *Applied Physics Letters* 102 (Sept. 2012). DOI: 10.1063/1.4802956.

[4] COMSOL. *RF Module User’s Guid*. 2012.

[5] *D-wave*. https://www.dwavesys.com/tutorials/background-reading-series/quantum-computing-primer\#main. Accessed: 2020-03-06.

[6] Bascom S. Deaver and William M. Fairbank. “Experimental Evidence for Quantized Flux in Superconducting Cylinders”. In: *Phys. Rev. Lett.* 7 (2 July 1961), pp. 43–46. DOI: 10.1103/PhysRevLett.7.43. URL: https://link.aps.org/doi/10.1103/PhysRevLett.7.43.

[7] Daniel Esteve, Michel H. Devoret, and John M. Martinis. “Effect of an arbitrary dissipative circuit on the quantum energy levels and tunneling of a Josephson junction”. In: *Phys. Rev. B* 34 (1 July 1986), pp. 158–163. DOI: 10.1103/PhysRevB.34.158. URL: https://link.aps.org/doi/10.1103/PhysRevB.34.158.

[8] Richard P. Feynman. “There’s Plenty of Room at the Bottom”. In: *Feynman and Computation: Exploring the Limits of Computers*. USA: Perseus Books, 1999, pp. 63–76. ISBN: 0738200573.

[9] Rudolf Gross and Achim Marx. “Applied Superconductivity : Josephson Effect and Superconducting Electronics”. In: 2009.

[10] Lov K. Grover. *A fast quantum mechanical algorithm for database search*. 1996. arXiv: quant-ph/9605043 [quant-ph].

[11] Xiu Gu et al. "Microwave photonics with superconducting quantum circuits". In: *Physics Reports* 718-719 (Nov. 2017), pp. 1–102. ISSN: 0370-1573. DOI: 10.1016/j.physrep.2017.10.002. URL: http://dx.doi.org/10.1016/j.physrep.2017.10.002.

[12] Serge Haroche. "Nobel Lecture: Controlling photons in a box and exploring the quantum to classical boundary". In: *Rev. Mod. Phys.* 85 (3 July 2013), pp. 1083–1102. DOI: 10.1103/RevModPhys.85.1083. URL: https://link.aps.org/doi/10.1103/RevModPhys.85.1083.

[13] B.D. Josephson. "Possible new effects in superconductive tunnelling". In: *Physics Letters* 1.7 (1962), pp. 251–253. ISSN: 0031-9163. DOI: https://doi.org/10.1016/0031-9163(62)91369-0. URL: http://www.sciencedirect.com/science/article/pii/0031916362913690.

[14] Jens Koch et al. "Charge-insensitive qubit design derived from the Cooper pair box". In: *Phys. Rev. A* 76 (4 Oct. 2007), p. 042319. DOI: 10.1103/PhysRevA.76.042319. URL: https://link.aps.org/doi/10.1103/PhysRevA.76.042319.

[15] P. Krantz et al. "A quantum engineer's guide to superconducting qubits". In: *Applied Physics Reviews* 6.2 (June 2019), p. 021318. ISSN: 1931-9401. DOI: 10.1063/1.5089550. URL: http://dx.doi.org/10.1063/1.5089550.

[16] M. T. Levinsen et al. "An inverse ac Josephson effect voltage standard". In: *Applied Physics Letters* 31.11 (1977), pp. 776–778. DOI: 10.1063/1.89520. eprint: https://doi.org/10.1063/1.89520. URL: https://doi.org/10.1063/1.89520.

[17] F. London. "On the Problem of the Molecular Theory of Superconductivity". In: *Phys. Rev.* 74 (5 Sept. 1948), pp. 562–573. DOI: 10.1103/PhysRev.74.562. URL: https://link.aps.org/doi/10.1103/PhysRev.74.562.

[18] John M. Martinis and Kevin Osborne. *Superconducting Qubits and the Physics of Josephson Junctions*. 2004. arXiv: cond-mat/0402415 [cond-mat.supr-con].

[19] Simon E. Nigg et al. "Black-Box Superconducting Circuit Quantization". In: *Physical Review Letters* 108.24 (June 2012). ISSN: 1079-7114. DOI: 10.1103/physrevlett.108.240502. URL: http://dx.doi.org/10.1103/PhysRevLett.108.240502.

[20] Sandip Pakvasa. *The Stern-Gerlach Experiment and the Electron Spin*. 2018. arXiv: 1805.09412 [physics.hist-ph].

[21] *S-parameter*. https://www.youtube.com/watch?v=BijMGKbTOWk. Accessed: 2020-03-06.

[22] V. M. Schäfer et al. "Fast quantum logic gates with trapped-ion qubits". In: *Nature* 555.7694 (Mar. 2018), pp. 75–78. ISSN: 1476-4687. DOI: 10.1038/nature25737. URL: http://dx.doi.org/10.1038/nature25737.

[23] Peter W. Shor. "Polynomial-Time Algorithms for Prime Factorization and Discrete Logarithms on a Quantum Computer". In: *SIAM J.Sci.Statist.Comput. 26 (1997) 1484* (1996). DOI: 10.1137/S0097539795293172. URL: https://arxiv.org/abs/quant-ph/9508027.

[24] *smith chart*. https://www.digikey.com/en/articles/techzone/2014/mar/the-smith-chart-an-ancient-graphical-tool-still-vital-in-rf-design. Accessed: 2020-03-06.

[25] Philipp Summer. "Characterization of superconducting coplanar waveguide resonators at millikelvin temperatures". In: 2014.

[26] R. J. Thompson, G. Rempe, and H. J. Kimble. "Observation of normal-mode splitting for an atom in an optical cavity". In: *Phys. Rev. Lett.* 68 (8 Feb. 1992), pp. 1132–1135. DOI: 10.1103/PhysRevLett.68.1132. URL: https://link.aps.org/doi/10.1103/PhysRevLett.68.1132.

[27] A. M. Turing. "On Computable Numbers, with an Application to the Entscheidungsproblem". In: *Proceedings of the London Mathematical Society* s2-42.1 (Jan. 1937), pp. 230–265. ISSN: 0024-6115. DOI: 10.1112/plms/s2-42.1.230. URL: https://doi.org/10.1112/plms/s2-42.1.230.

[28] A. Wallraff et al. "Strong coupling of a single photon to a superconducting qubit using circuit quantum electrodynamics". In: *Nature* 431.7005 (Sept. 2004), pp. 162–167. ISSN: 1476-4687. DOI: 10.1038/nature02851. URL: https://doi.org/10.1038/nature02851.

[29] David J. Wineland. "Nobel Lecture: Superposition, entanglement, and raising Schrödinger's cat". In: *Rev. Mod. Phys.* 85 (3 July 2013), pp. 1103–1114. DOI: 10.1103/RevModPhys.85.1103. URL: https://link.aps.org/doi/10.1103/RevModPhys.85.1103.

[30] Manjin Zhong et al. "Optically addressable nuclear spins in a solid with a six-hour coherence time". In: *Nature* 517 (Jan. 2015), pp. 177–80. DOI: 10.1038/nature14025.